EXPERIMENTAL STUDY OF BOILING HEAT TRANSFER DURING WATER JET IMPINGEMENT ON A HOT STEEL PLATE

By

Ágúst Torfi Hauksson

B.Sc., University of Iceland, 1999

A THESIS SUBMITTED IN PARTIAL FULFILLMENT OF

THE REQUIREMENTS FOR THE DEGREE OF

MASTER OF APPLIED SCIENCE

in

THE FACULTY OF GRADUATE STUDIES

DEPARTMENT OF MECHANICAL ENGINEERING

We accept this thesis as conforming

to the required standard

THE UNIVERSITY OF BRITISH COLUMBIA

November 2001

In presenting this thesis in partial fulfilment of the requirements for an advanced degree at the University of British Columbia, I agree that the Library shall make it freely available for reference and study. I further agree that permission for extensive copying of this thesis for scholarly purposes may be granted by the head of my department or by his or her representatives. It is understood that copying or publication of this thesis for financial gain shall not be allowed without my written permission.

Department of MECHANICAL ENGINEERING

The University of British Columbia
Vancouver, Canada

Date 21. NOV. 2001

DE-6 (2/88)

ABSTRACT

The growth in demand for high-quality metallic alloys has placed greater emphasis on the predictability of cooling methods used in manufacturing processes. In particular, the production of tailored steel properties through controlled cooling on the runout table. This study focuses on some fundamental issues that influence heat transfer on a steel mill runout table. The purpose of the study is to develop an efficient experimental method and gather data at conditions as close as possible to industrial conditions. Surface and internal temperatures are measured during transient cooling of a flat, upward facing fixed steel surface cooled by a highly subcooled single circular free surface jet of water. A numerical model is used to calculate the surface heat flux using the measured temperatures. Local boiling and cooling curves are presented at stagnation and several streamwise distances from the stagnation point. The effect of water flow rate and subcooling on the overall heat transfer with special emphasis on critical heat flux is discussed. Progression of the re-wetting front is studied as well as the instantly cooled zone around stagnation.

TABLE OF CONTENTS

LIST OF FIGURES

LIST OF TABLES

ACKNOWLEDGMENTS

Thanks to: Dr. D. Fraser, Dr. I. V. Samarasekera, Dr. V. Prodanovic, Dr. D. McAdam, Dr. M. Gadala and Dr. M. Militzer.

For help with experiments, thanks to: Pat Wenman, Gary Lockhart, Ross McLeod, Carl Ng, Grant Caffery, Pierre Constantineau and Erin Young.

For keeping me sane during this project, thanks to: Eva Hlín Dereksdóttir, Hildur Ingvarsdóttir, Ólafur Arnar Jónsson, Sveinbjörg Sveinbjörnsdóttir, Davíð Óskarsson, Eko guitars, General Motors, GNU snowboards and last but not least my parents Haukur Ágústsson and Hilda Torfadóttir.

1

INTRODUCTION

Around 200 million metric tons of steel are hot rolled worldwide annually, in hot strip mills, into flat products. Coils of prescribed gauge and properties are manufactured from a slap of known chemical composition. The mill process usually follows a continuous casting facility. The run out table and the down coiler come as the last step of the rolling process.

On the run out table the steel strip travels on motorized steel rollers placed at appropriate distances, around 18 in apart, to limit bending of the strip. The runout table can be as long as 150 meters. Cooling banks are typically placed at both the top and bottom of the moving strip. The cooling bank consist of headers that supply water to arrays of jets, water curtains, laminar tubes or aspirated sprays depending on the specific mill configuration [1].

The finishing temperature in controlled hot rolling lies in the range 800-950 °C and the coiling temperature is within the range of 510-750 °C [2]. The cooling takes place on the run out table. Water is supplied from large water tanks. Pressure to the nozzles is accomplished by either pumping the water from water tanks placed below the run out table or by the use of gravity from tanks above. Fairly constant pressure is required to secure sufficient and stable water flow. After use, the water is usually filtered, pumped back into the water tanks and recirculated. Usually no coolers or heaters are in the water tanks and the water is supplied at room temperature (18 - 40 °C). The bottom headers are usually located less than 100 mm below the moving strip and the top ones at least 1200 mm above the table so that excessive bending of the strip will not damage the headers.

Controlling the cooling on the run out table is very important as the cooling rate of the steel strip governs the final mechanical properties of the product. Knowledge of heat transfer in the strip is crucial in order to control the cooling and obtain the desired uniform properties in the product [3].

The purpose of the present study is to gain more knowledge on the heat transfer between the steel strip and the supplied water. This was done by experimentally studying the transient heat transfer between a steel plate in the as rolled condition and an impinging water jet with an industrial scale geometry and conditions. Heat fluxes were calculated using temperature measurements. The initial size of the impingement zone and the progression of rewetting front on the surface were estimated using temperature measurements and visual observations.

In this research transient water jet impingement cooling of an upward facing fixed surface was studied. An experimental procedure was developed to measure temperatures. Parameters as close as possible to industrial parameters were used.

2

LITERATURE REVIEW

Jet impingement heat transfer is of great importance in the steel industry. The mechanical properties of the final product can be adjusted by controlling the microstructure through controlled cooling. The governing mode of heat transfer on a typical steel mill run out table is water cooling, usually jet impingement. Less dominant modes of heat transfer are free and forced convection to air and radiation to the surroundings.

A lot of theoretical and experimental work has been done on boiling heat transfer in the last half century. This is described in a few critical reviews [4][5][6][7]. Run out table jet impingement cooling is a highly transient process. Very limited research has been done on transient problems at industrial or near industrial conditions.

A schematic view of a metal strip on a run out table with surface and bottom water jets and guide rolls can be seen in Figure 2-1.

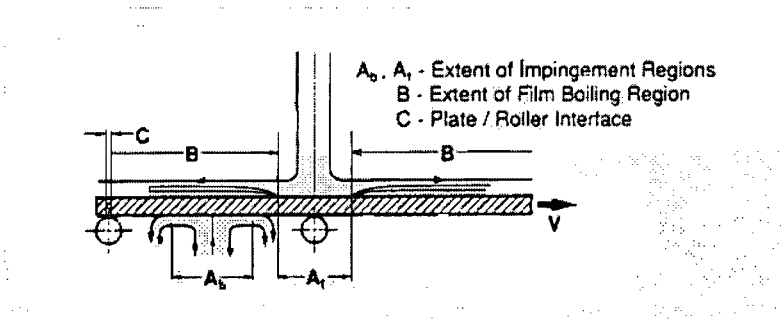

FIGURE 2-1 Strip with guide rolls and impinging jets [29]

In the following sections the current literature on hydrodynamics and thermodynamics of liquid jet impingement will be reviewed.

2.1 HYDRODYNAMICS OF JET IMPINGEMENT

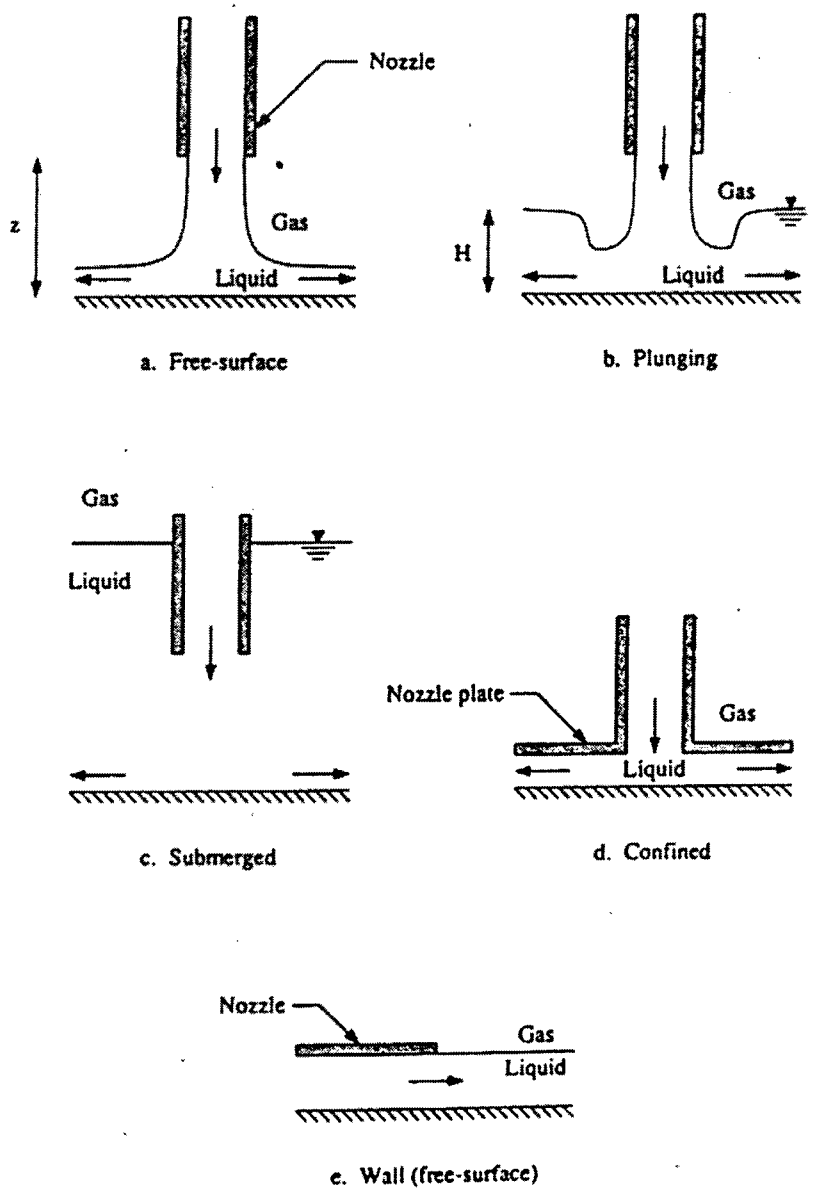

FIGURE 2-2 Jet configurations [6]

Jet impingement can, hydrodynamically, be divided into five categories: free surface jets, plunging jets, submerged jets, confined jets and wall jets. These configurations are all shown in Figure 2-2. Furthermore, impinging jets can be classified by their shape, whether the

jet is oriented normally or obliquely with respect to the impingement surface or whether the impingement surface is flat, convex or concave. A free surface jet, Figure 2-2 (a), is where the liquid travels relatively undisturbed from the nozzle to the impingement surface. This is the case for a water jet injected into air impinging on an unconstrained flat surface. Unconstrained meaning that the water can flow off the edges and hence, does not pool on the surface. On an industrial runout table there can be either free surface or plunging jets depending on the configuration. Usually the moving metal strip on a steel mill runout table is cooled by an array of water jets. Jets in the first row act as free surface jets but further down stream a layer of water is formed on top of the plate and the jets act as plunging jets. As the thickness of the water layer increases the effect of impingement decreases. For maximum heat transfer all the jets should be free surface types.

Figure 2-3 shows the inviscid pressure and velocity distributions for a free surface planar jet with uniform velocity profile along with the varying flow regimes. The stagnation region has the same size and shape as the jet and a combination of the stagnation and acceleration regions are referred to as the impingement region or impingement zone. At the stagnation point the streamwise velocity is zero and then increases rapidly within the stagnation and acceleration regions. In the parallel laminar flow region outside the acceleration zone the velocity approaches the velocity of the jet and the thickness of the liquid layer decreases with increasing distance from stagnation along the surface. Further downstream the flow becomes turbulent and the streamwise velocity decreases while the liquid film thickness increases. Liu et al. [8] developed a correlation for the size of the laminar flow region as given by Equation (1). The equation defines the radius of the impingement zone and the location of transition from laminar to turbulent flow for a free surface liquid jet.

$$1.57 < \frac{r}{d_{ji}/2} < r_t = 600 \cdot \left(\frac{v_{ji} \cdot d_{ji}}{\nu}\right)^{-0.422} \quad (1)$$

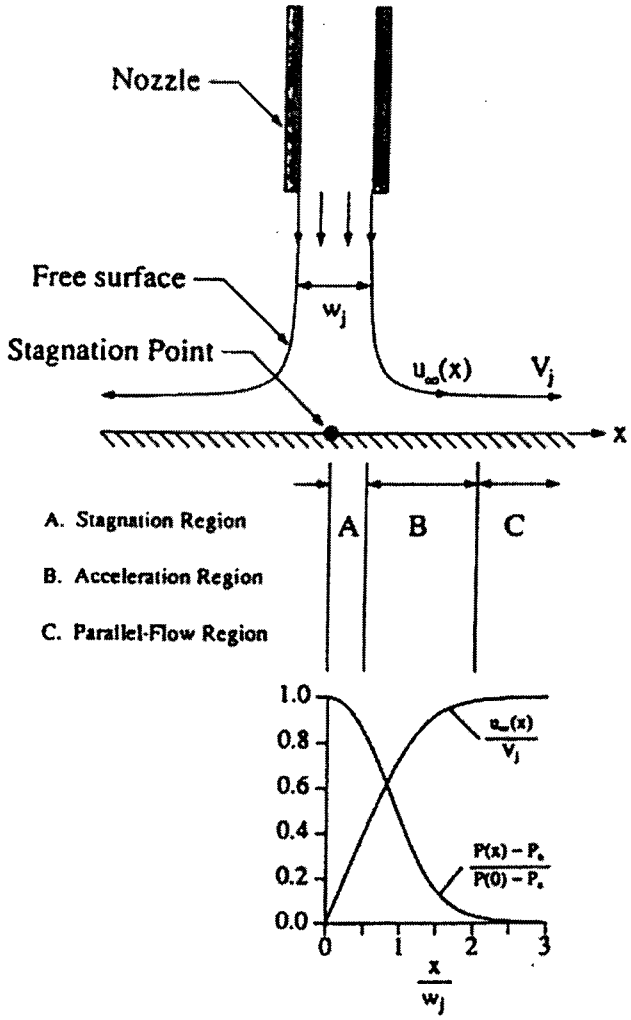

FIGURE 2-3 Inviscid pressure and velocity profile and flow regions for a planar jet with uniform velocity profile [6]

Where r is radial distance from stagnation, d_{ji} is diameter of jet at impingement, v_{ji} is jet velocity at impingement and ν is kinematic viscosity.

The effect of gravity on the jet velocity at the impingement surface is significant if nozzle to surface distance is relatively large. Equation (2) gives a good approximation of the impingement velocity as a function of exit velocity and nozzle height.

$$v_{ji} = \sqrt{v_j \pm 2 \cdot g \cdot H} \tag{2}$$

Where v_{ji} is jet velocity at impingement, v_j is jet velocity at nozzle exit, g is gravitational acceleration and H is plate to nozzle height.

The + sign applies to downward flow increasing the velocity at impingement from the exit velocity of the jet. The effect of gravitational acceleration on downward facing free surface jet results in thinning and stretching of the water column. These effects satisfy continuity and are commonly neglected in most jet impingement literature.

Unlike the velocity, the pressure is at its maximum at the stagnation point and decreases to the pressure of the ambient with increasing streamwise distance. In the parallel laminar flow region, as mentioned earlier, the streamwise velocity is essentially the same as that of the jet and the hydrodynamic effect of impingement is no longer realized in the flow, [6]. Ochi et al. [9] measured the velocity and pressure along a surface of a plate impinged by a circular jet of water. They defined the impingement zone as the zone where the streamwise velocity is in proportion to the distance from the stagnation point. By using a 10 mm jet and a jet velocity of 3 m/s they found the impingement zone to be bound by $r/d_j \leqq 1.28$. It should be noted that this number is somewhat larger than presented earlier in Equation (1). Liu [39] experimentally found that the boundary of the thermodynamic impingement zone, (zone of constant heat flux) for a circular jet ranged from 1.67 to 2.11 times the diameter of the circular water jet. The size of the thermodynamic impingement zone does not have to be the same as the size of the hydrodynamic one as defined earlier.

The pressure distribution also determines the local saturation conditions of the liquid along the surface. Variations in the saturation temperature of the liquid T_{sat} cause variations in the degree of local subcooling, ΔT_{sub}, and wall superheat, ΔT_{sat}. Most publications reviewed here neglect this effect and use saturation conditions based on the ambient pressure. For the parameters used in the current study this effect causes up to a 5°C increase in the saturation temperature at stagnation (highest pressure location).

2.2 HEAT TRANSFER.

A considerable amount of work has been done on jet impingement heat transfer during the last few decades. Knowledge on submerged gas jets is of significance for cooling electronics, drying of paper and cooling critical parts of high temperature turbines to name a few, [25][26]. Numerical models have been developed to model the heat transfer in boiling and during jet impingement [27][28][29][30][31]. A lot of research on free surface jets has also been done and has been critically reviewed, [6][23].

2.2.1 Jet impingement and boiling curves

Jet impingement boiling heat transfer is a complicated phenomenon. The modes of heat transfer depend on velocity, temperatures of the liquid and impinged surface as well as the physical properties of both liquid and solid. If the initial wall superheat is high enough one should see film boiling, transition boiling, nucleate boiling and finally convective heat transfer (once the wall has cooled down below the boiling temperature). To be able to visualize the process, some knowledge of the modes of heat transfer is necessary.

Figure 2-4 shows a saturated boiling curve on a log log scale. This shape of boiling curve is commonly seen in saturated pool boiling. The boiling curve for forced convective saturated subcooled boiling may look quite different but similar trends as are shown in Figure 2-4 will be seen. The dotted line from B to B' shows what happens in heat flux controlled systems where the heat flux is raised. In those cases the heat transfer mode changes directly from the point of maximum heat flux to film boiling. This will not be discussed in this review as it is not relevant in the current study.

Experimentally developed boiling curves for jet impingement boiling heat transfer at stagnation are shown in Figure 2-5. These figures show a trend similar to the one shown in Figure 2-4. Boiling at the stagnation point in jet impingement should behave as pool boiling as the velocity of the water along the surface of the plate is zero. As the water sub-cooling is

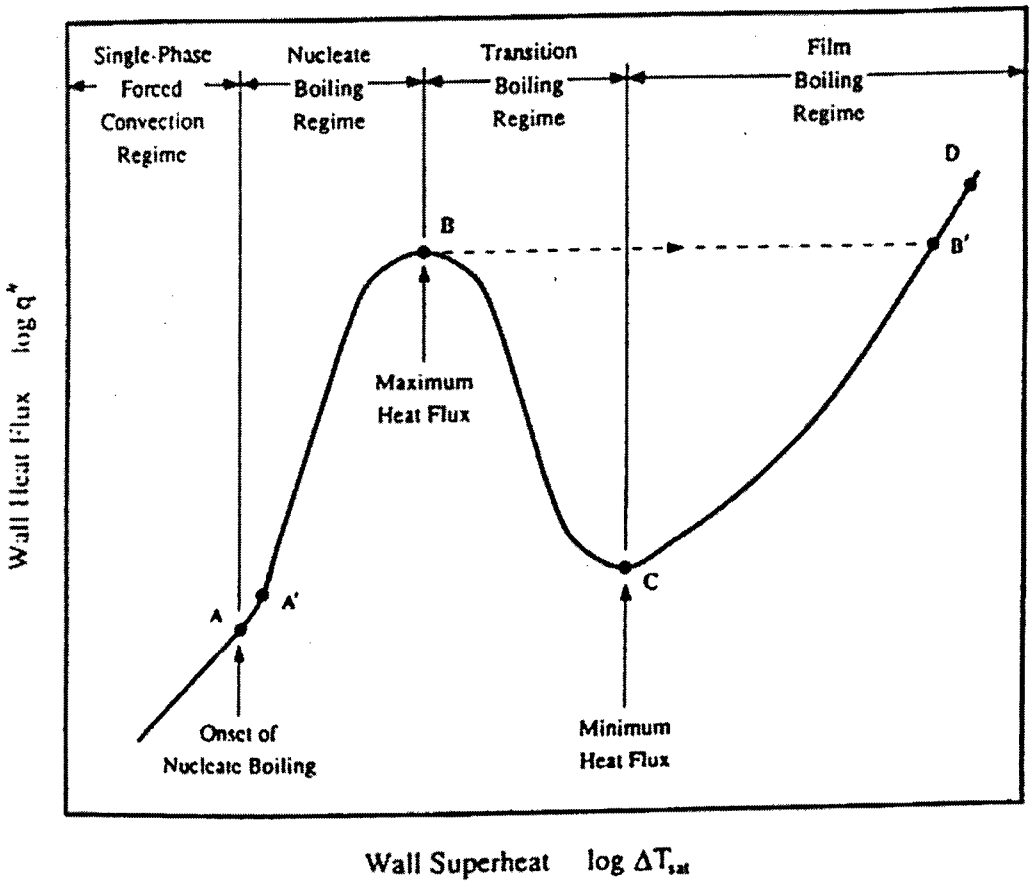

FIGURE 2-4 Boiling curve for saturated liquid [6]

increased the shape of the curve changes, a shoulder appears in the transition region and the point of minimum heat transfer, Leidenfrost point, is shifted to a higher temperature. For high sub-cooling, the point of minimum heat transfer is shifted outside the temperature range and no film boiling occurs. The phenomenon of a shift in the Leidenfrost point with changes in sub-cooling and jet velocity is discussed in Section 2.2.6 on page 28.

The effect of jet velocity can be seen in Figure 2-5 (b) which shows increasing heat flux with increasing jet velocity. The increase in heat flux with increasing jet velocity is partially due to an increase in ΔT_{sub} at stagnation, ΔT_{sub} increases due to higher pressure at stagnation, and also due to increased convective heat removal from the stagnation zone with increasing velocity. The shape of the curves is still the same and similar trends can be seen.

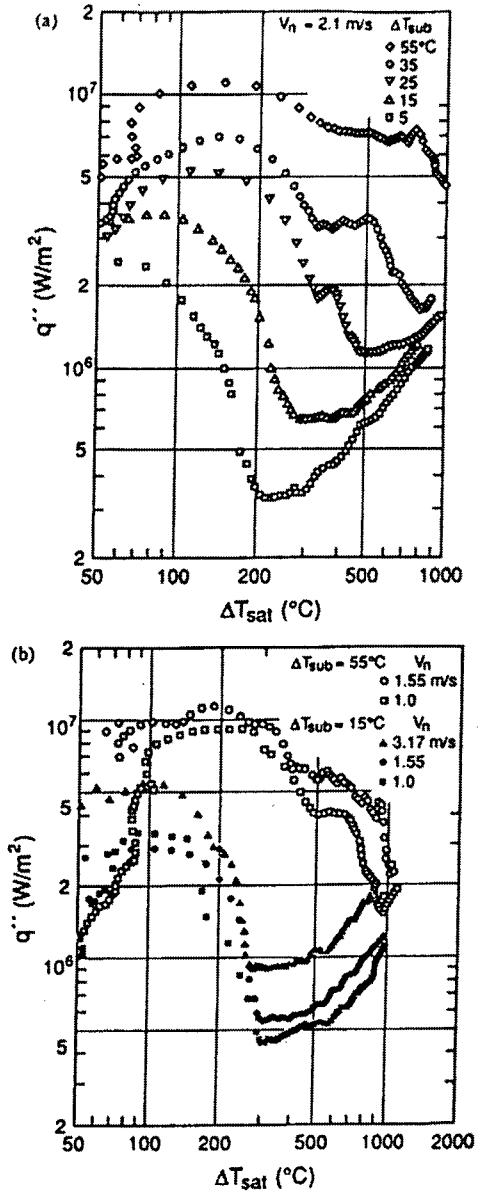

FIGURE 2-5 Experimentally developed boiling curves at the stagnation point for a planar, free surface jet of water showing the effects of (a) sub-cooling and (b) jet velocity, v_n [38]

Observations have also been made by Viskanta and Incropera [23] on jet impingement cooling for an industrial run out table and on a stationary plate by Kokado et al. [24]. Both studies found the varying modes of heat transfer to be consistent with the above discussed regimes. Figure 2-6 shows jet impingement and the various heat transfer regimes as observed by Viskanta et al. [23]. In region I, close to the nozzle, they observed single phase forced con-

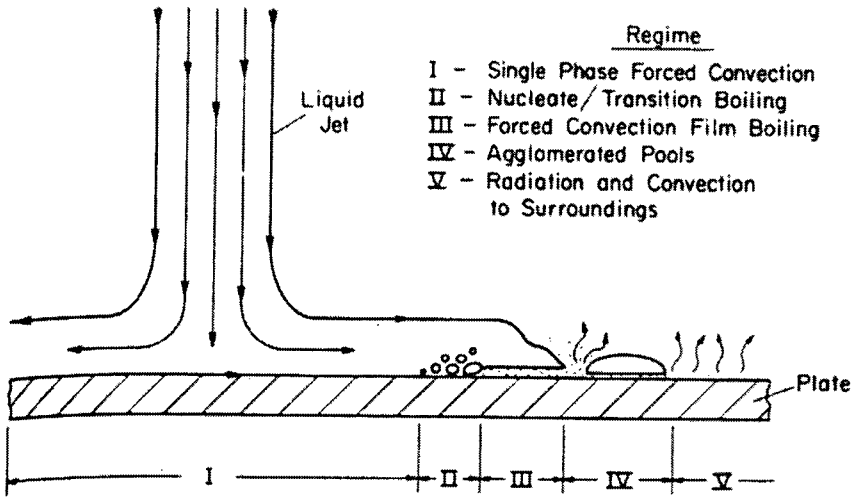

FIGURE 2-6 Heat transfer regimes adjacent to an impinging jet on a stationary plate (note: lengths for each regime are not necessarily to scale) [23]

vection. Further away from the center as the surface temperature increases the onset of nucleate boiling was observed and, further away from the jet, transition and film boiling.

2.2.2 Single phase convection

Convective single-phase heat transfer is the mode of heat transfer when there is no boiling. The wall temperature has to be lower than or equal to the saturation temperature of the liquid at given pressure, for single-phase convection to take place. In jet impingement heat transfer the single-phase convective heat transfer coefficient varies over the surface as the boundary layer develops and also due to hydrodynamic variations in the flow. Wolf et al. [14] reported that in single phase convection they found the heat transfer coefficient to be constant far enough downstream so that the effect of impingement in the flow is no longer realized. They found this to be outside a region bound by approximately three jet widths from stagnation. They also mentioned a zone of constant heat transfer coefficient close to stagnation.

Stevens and Webb [12] studied heat transfer in the non-boiling regime under a liquid jet, impinging normally on a flat surface with constant heat flux. The parameters varied were jet Reynolds number, nozzle to plate spacing and jet diameter. Although they presented differ-

ent correlations depending on jet diameter they concluded that the dependence of stagnation Nusselt number on jet Reynolds number could be described well by a power law, $Re^{1/3}$. Near constant heat transfer coefficients were found within a region bounded by $r/d_j < 0.75$. Such a constant heat transfer coefficient indicates that some thermodynamic impingement zone can be defined. This zone is not necessarily the same size as the hydrodynamic impingement zone defined earlier. This thermodynamic impingement zone was defined as the zone of constant heat transfer around the stagnation point. Nozzle to plate spacing was found to have a minor effect.

Wolf et al. [15] reported local non-boiling heat transfer measurements along the impingement surface of a uniformly heated surface for a circular free surface water jet. All their data was taken using a water temperature and heat flux of 25°C and 0.5 MW/m^2 respectively. The jet Reynolds number Re_j (= $v_j\, d_j$ / υ) investigated was in the range 23,000 to 46,000. They developed a correlation for the stagnation Nusselt number given by Equation (3) that correlated all their data within 33%. Properties were evaluated at the film temperature.

$$Nu_{stagnation} = 0.202 \cdot Re_{ji}^{0.620} \cdot Pr^{0.4} \tag{3}$$

Where

$$Nu_{stagnation} = \frac{h \cdot d_{ji}}{k}, Re_{ji} = \frac{v_{ji} \cdot d_{ji}}{\nu} \tag{4}$$

and h is the heat transfer coefficient, d_{ji} is jet diameter at impingement, k is conduction of water, v_{ji} is jet velocity at impingement and ν is kinematic viscosity.

Vader et al. [33] studied non boiling convective heat transfer to an impinging planar jet of water from a constant heat flux surface. They looked at effects of water temperature and jet velocity. Stagnation Nusselt numbers were found to be well correlated by Equation (5), valid for $2\text{x}10^4 < Re_{ji} < 9\text{x}10^4$ and $2.7 < Pr < 4.5$ and with properties evaluated at film temperature.

They found the effect of velocity on the heat transfer coefficient to be significant but the effect of water temperature was small until quite far downstream.

$$Nu_{stagnation} = 0.28 \cdot Re_{ji}^{0.58} \cdot Pr^{0.4} \quad (5)$$

Where

$$Re_{ji} = \frac{v_{ji} \cdot d_{ji}}{\nu} \quad (6)$$

and d_{ji} is jet diameter, v_{ji} is jet velocity and ν is kinematic viscosity.

Oliphant et al. [32] studied non boiling jet impingement heat transfer to a array of impinging jets and found the heat transfer to depend on velocity and array configuration. Their data were well correlated using correlations of the same form as Equation (3) and Equation (5) when spacing between nozzles was large. Their data also showed that the effect of nozzle to plate spacing was small.

Referring back to Figure 2-4 single-phase convection is the mode of heat transfer to the left of point A. The transition from single-phase convection to fully developed boiling takes place between points A and A'. Heat transfer in fully developed nucleate boiling is found to be independent of jet velocity. However at single-phase convection and partial boiling, point A to A', the dependence is clear with lower heat flux at lower jet velocities [10][14].

2.2.3 Nucleate boiling

If the wall temperature exceeds the saturation temperature of the liquid nucleate boiling occurs. At relatively low superheats, before the onset of nucleate boiling, superheated liquid rises to the surface where evaporation takes place. At the onset of nucleate boiling bubbles begin to form on, and detach from the hot surface, hence enhancing fluid circulation and increasing the heat transfer. The region between points A' and B on Figure 2-4 represents fully developed nucleate boiling.

Katto and Monde [10] studied saturated jet impingement boiling heat transfer at stagnation. They found, for a jet velocity range of 5.3-6.0 m/s, the fully developed nucleate boiling curve to be roughly an extension of a saturated pool boiling curve to higher wall superheats and heat fluxes, independent of jet velocity. It has also been shown that this independence applies for lower velocities, as low as 0.67 m/s [11][13][18][34].

The effect of liquid subcooling on fully developed nucleate boiling in jet impingement has also been investigated. Monde and Katto [34] examined the effect of liquid subcooling in jet impingement at stagnation. They reported that their data deviated from the saturated results at low wall superheats. But at higher wall superheats the results were independent of subcooling giving the same result as for saturated boiling. They found that wall superheat is the effective driving force of heat transfer in fully developed nucleate boiling.

The effect of wall superheat on heat flux has, on the other hand, been shown to be significant. Miyasaka et al. [16] reported, for jet impingement at the stagnation point, a strong dependence of wall superheat on heat flux during fully developed nucleate boiling on a heated surface with constant water subcooling and jet velocity. They did not present a heat transfer correlation but stated that the jet boiling curves showed a similar tendency to pool boiling curves. They presented a correlation for pool boiling heat flux, given by Equation (7), that seems to fit their jet impingement data fairly well for wall superheats up to 60°C. Water subcooling was 85°C.

$$q''_{pool} = 79 \cdot \Delta T_{sat}^{3.0} \tag{7}$$

Where q''_{pool} is pool boiling heat flux and ΔT_{sat} is wall superheat.

Copeland [18] studied boiling heat transfer on a downward facing heated surface to an impinging upward facing jet of water. He found that the heat flux in fully developed nucleate boiling depended only on the wall superheat. The data were well correlated for wall superheats in the range of 8 to 31°C using Equation (8).

$$q''_{FNB} = 740 \cdot \Delta T_{sat}^{2.3} \quad (8)$$

Where q''_{FNB} is fully developed nucleate boiling heat flux and ΔT_{sat} is wall superheat.

Wolf et al. [14] studied local jet impingement boiling heat transfer using an adjustable constant heat flux upward facing surface and sub cooled water jet. They used a rectangular nozzle and a constant cooling water temperature of 50°C. They saw single phase convection, partial boiling and fully developed nucleate boiling at various locations on the heated surface. At lower jet velocities the onset of boiling was found to be at a lower heat flux. Also, there was no partial boiling observed close to the stagnation point. As the heat flux was increased the mode of heat transfer changed directly from single phase convection to fully developed nucleate boiling and no sign of partial boiling was found. At locations further away from the stagnation point a period of partial boiling was observed as the, adjustable, surface heat flux was increased. Finally, fully developed boiling occurred with further increases in the heat flux. They reported fully developed nucleate boiling over the entire surface at heat fluxes in the range of $1.74 < q < 2.71$ MW/m^2. At heat fluxes lower than 1.74 MW/m^2, no boiling was seen close to stagnation even though the surface temperature was higher than the saturation temperature of the cooling water. The effect of jet velocity on heat transfer was most apparent within the single phase and partial boiling regimes. In the fully developed boiling regime, the heat transfer was independent of jet velocity. They presented a correlation that correlated their data within 32%.

$$q''_{FNB} = 63.7 \cdot \Delta T_{sat}^{2.95} \quad (9)$$

Where q''_{FNB} is fully developed nucleate boiling heat flux and ΔT_{sat} is wall superheat.

Correlations having the same form as Equation (7) through Equation (9) have been presented by other researchers. Monde et al. [11] presented a correlation for saturated water that spanned wall superheats from 18 to 46°C, see Equation (10). Ishigai et al. [38] studied nucleate boiling during impingement using a subcooled planar jet of water and a upward facing

heated surface. Equation (11) correlated their data taken at steady state and using jet velocities of 1.0 and 2.1 m/s and a subcooling of 35°C.

$$q''_{FNB} = 450 \cdot \Delta T_{sat}^{2} \tag{10}$$

$$q''_{FNB} = 42 \cdot \Delta T_{sat}^{3.2} \tag{11}$$

Ruch and Holman (1975) presented a correlation, reviewed by Wolf et al. [6], for a Freon-113 jet impinging on a downward facing heated plate with wall superheat in the range from 17 to 44°C. Equation (12) gives the general form of their correlation.

$$q''_{FNB} = \left(\frac{1}{C_{sf}} \cdot \frac{c_{p_f} \cdot \Delta T_{sat}}{h_{fg}} \cdot \left(\frac{\mu_f \cdot c_{p_{fl}}}{k_f}\right)^{-1.7}\right)^{n} \cdot \left(\frac{g \cdot (\rho_f - \rho_g)}{\sigma}\right)^{0.5} \cdot \mu_f \cdot h_{fg} \tag{12}$$

Where C_{sf}, a constant dependent on the surface-fluid combination, and n were found to be 3.07 x 10^{-3} and 1.95 respectively.

Chen (1966) presented a correlation for convective boiling, reviewed by Collier [22]. His correlation is based on the assumption that the convective boiling can be described as a combination of the macroconvective mechanism, corresponding to the effect of fluid flow, and the microconvective mechanism corresponding to the boiling part of the heat transfer. In its general form the correlation can be expressed as Equation (13).

$$h_{tp} = h_{conv} + h_{boiling} \quad \text{or} \quad h_{tp} = h_{FC} \cdot F + h_{NB_{pool}} \cdot S \tag{13}$$

Where h_{tp}, h_{FC} and h_{NB} stand for two-phase, forced convective and nucleate boiling heat transfer coefficients, respectively. F is an enhancement factor accounting for the enhancement of heat transfer due to increased velocities in a two phase flow. S is a suppression factor that accounts for the suppression of nucleate boiling due to the flow. Chen gave the parameters F and S in a graphical form, see Collier [22]. He also suggested that h_{FC} and h_{NB} could be evaluated with the well known Dittus-Boelter correlation, see Equation (14), and Forster and Zuber correlation, see Equation (15), for forced convection and pool boiling, respectively.

$$h_{FC} = 0.023 \cdot Re_f^{0.8} \cdot Pr_f^{0.4} \left(\frac{k_f}{d_{pipe}} \right) \quad (14)$$

$$h_{NB_{pool}} = 0.00122 \cdot \left(\frac{k_f^{0.79} \cdot c_{p_f}^{0.45} \cdot \rho_f^{0.49}}{\sigma^{0.5} \cdot \mu_f^{0.29} \cdot h_{fg}^{0.24} \cdot \rho_g^{0.24}} \right) \cdot \Delta T_{sat}^{0.24} \cdot \Delta P_{sat}^{0.75} \quad (15)$$

Chen's correlation as presented above is valid for flow in pipes. His general form can adapted to other conditions and boiling modes.

Kumagai et al. [35] studied the transient cooling of a hot metal slab by an impinging jet during boiling heat transfer. The initial temperature of the slap was about 400 °C and it was cooled by a water jet from a rectangular nozzle 1 mm wide. They measured the heat flux at stagnation and at 8 locations down stream as far as 56 jet widths from stagnation. They found the heat flux in the fully developed nucleate boiling region to have little dependence on location although it was highest at stagnation, see Figure 2-7. They did not present a correlation for their data.

2.2.4 Critical heat flux

Point B on Figure 2-4 is the point of maximum heat flux or point of critical heat flux. At this point many large bubbles are formed and if the wall superheat is higher the mode of heat transfer is called transition boiling, which is discussed in Section 2.2.5. If surface heat flux is controlled but not the wall superheat the mode of heat transfer changes directly from boiling at the critical point to film boiling, in other words it follows the dotted line from point B to B´ on Figure 2-4. If wall superheat is increased beyond the point of critical heat flux the bubbles formed on the surface begin to coalescence on the surface and decrease significantly the area of liquid solid contact that again causes the heat flux to decrease. In temperature controlled situations the critical heat flux is hence unstable as any change in wall superheat results in a decrease in heat flux.

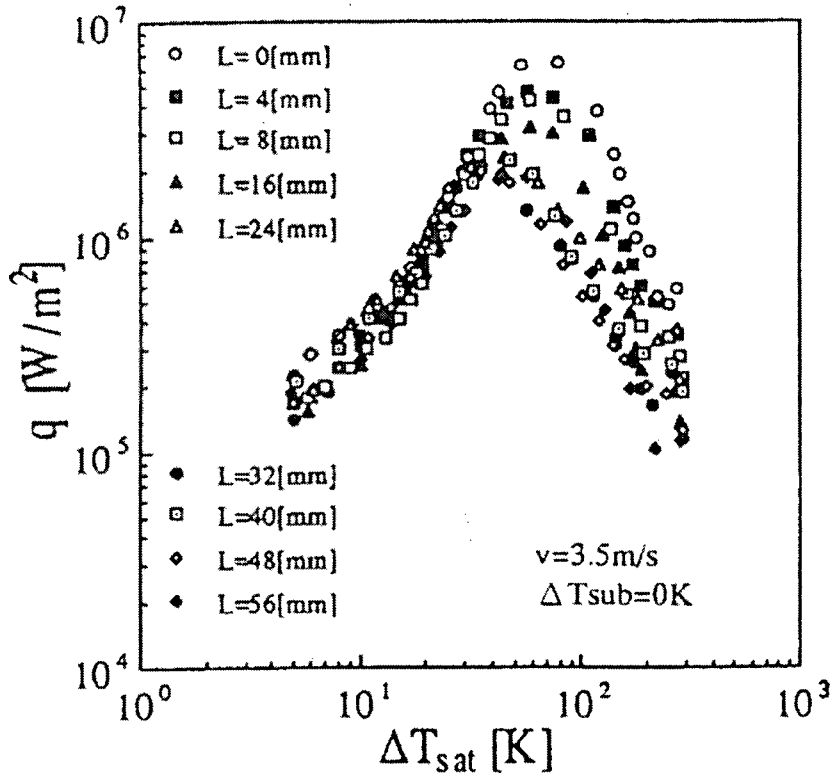

FIGURE 2-7 Boiling curves for saturated water jet impingement at various locations [35]

Several different regimes of critical heat flux have been reported but at atmospheric pressure a V-regime (variance of critical heat flux with respect to velocity) occurs for the majority of flow conditions. In such a regime the form of dependence on jet velocity is generally that the critical heat flux is proportional to $V_j^{1/3}$ [6].

Monde [11] presented a correlation given by Equation (16) that correlated data from a number of studies.

$$\frac{q''_{CHF}}{\rho_g \cdot h_{fg} \cdot v_{ji}} = 0.0757 \cdot \left(\frac{\rho_f}{\rho_g}\right)^{0.725} \cdot \left(\frac{\sigma}{\rho_g \cdot D_h \cdot v_{ji}^2}\right)^{1/3} \cdot \left(\frac{1}{1 + 0.00113(D_h/d_j)^2}\right) \qquad \textbf{(16)}$$

Where q''_{CHF} is the critical heat flux, ρ_g and ρ_f are densities of water in gas and liquid phase respectively, h_{fg} is enthalpy of evaporation, v_{ji} is jet velocity at impingement, σ is surface tension, D_h is heater diameter and d_j is jet diameter. The heater diameter D_h is the diame-

ter of the circular heated impingement surface in steady state studies. The correlation is valid for saturated water, jet velocities in the range of 0.3 to 15 m/s and D_h/d_j ratio up to 36.4.

Some more relevant work was done on jet impingement heat transfer with a sub-cooled free surface jet of water. Miyasaka et al. [16] studied critical heat flux at the stagnation point in sub cooled jet impingement boiling using a small downward facing heated surface. They investigated the effect of jet velocity in the range (1.5 m/s $< v_j <$ 15.3 m/s) and sub-cooling over the range (30°C $< \Delta T_{sub} <$ 85°C). The magnitude of the critical heat flux was found to depend on jet velocity and the degree of sub-cooling. The critical heat flux data was well correlated using Equation (17) through Equation (19). They defined the critical heat flux as being the heat flux at the beginning of the first transition region, see Figure 2-8. They presented the correlation in the form of a pool boiling critical heat flux correlation for both saturated liquid (sub-cooling = 0) and sub-cooled pool boiling critical heat flux. A multiplier was added to account for the jet velocity effects. Properties were taken at system pressure, generally atmospheric.

$$q''_{CHF} = q''_{\text{CHF, sub, pool}} \cdot (1 + 0.86 \cdot v_{ji}^{0.38}) \tag{17}$$

where

$$q''_{\text{CHF, sub, pool}} = q''_{\text{CHF, sub=0, pool}} \cdot \left(1 + 0.112\left(\frac{\rho_f}{\rho_g}\right)^{0.8}\left(\frac{c_{pf} \cdot \Delta T_{sub}}{h_{fg}}\right)^{1.13}\right) \tag{18}$$

and

$$q''_{\text{CHF, sub=0, pool}} = 0.16 \cdot h_{fg} \cdot \rho_g \cdot \left(\frac{\sigma \cdot g \cdot (\rho_f - \rho_g)}{\rho_g^2}\right)^{1/4} \tag{19}$$

Where v_{ji} is jet impingement velocity, ρ_f and ρ_g are densities of water and water vapor respectively, c_{pf} is specific heat of water, ΔT_{sub} is water sub-cooling, h_{fg} is enthalpy of evaporation, σ is surface tension and g is gravitational acceleration.

Ishigai and Mizuno [19] examined the effects of sub-cooling and jet velocity on the critical heat flux to a circular jet of water. Jet velocity and sub-cooling were in the ranges of (1.3 m/s $< v_j <$ 9.0 m/s) and ($45°C < \Delta T_{sub} < 80°C$) respectively. Correlation of the data was presented in dimensional form, see Equation (20). The correlation provided a good fit to their data but its use is limited to the range of their data as given above.

$$q''_{CHF} = 0.0142 \cdot 10^6 \cdot \left(\frac{v_{ji}}{d_j}\right)^{0.34} \cdot \Delta T_{sub}^{1.15} \tag{20}$$

Where d_j is jet diameter and v_{ji} and ΔT_{sub} are as defined earlier.

Miyasaka et al. [16] studied critical heat transfer from a heated surface to a planar free surface jet. They observed and hypothesized about the existence of two transition regions from fully developed nucleate boiling to the critical heat flux point. Their data are shown in Figure 2-8 and the two transition regions are quite clear. The line marked Eq.(1) on Figure 2-8 represents their correlation for fully developed nucleate pool boiling, given earlier by Equation (7), and lines marked Eq.(2) and Eq.(3) are correlations for the two transition regions they observed in pool boiling using the same heated surface and same degree of sub-cooling. The sub-cooling was 85°C. Comparing the jet impingement data and the pool boiling correlation curves it can be seen that the same trends occur in both cases. In the fully developed nucleate boiling region the correlation fits rather well, supporting the theory that in this region the heat flux is independent of jet velocity. In the two transition regions the trends are the same but the pool boiling correlations under estimate the heat flux in the impinging case. This is in agreement with Equation (17) through Equation (20) stating that critical heat flux is dependent on jet velocity. The correlations for the transition regions represented by lines Eq.(2) and Eq.(3) on Figure 2-8 are given by Equation (21) and Equation (22) respectively.

$$q''_{\text{sub=85, pool, 1}} = 690 \cdot 10^5 \cdot \Delta T_{sat}^{0.65} \tag{21}$$

$$q''_{\text{sub=85, pool, 2}} = 11.23 \cdot 10^6 \cdot \Delta T_{sat}^{0.12} \tag{22}$$

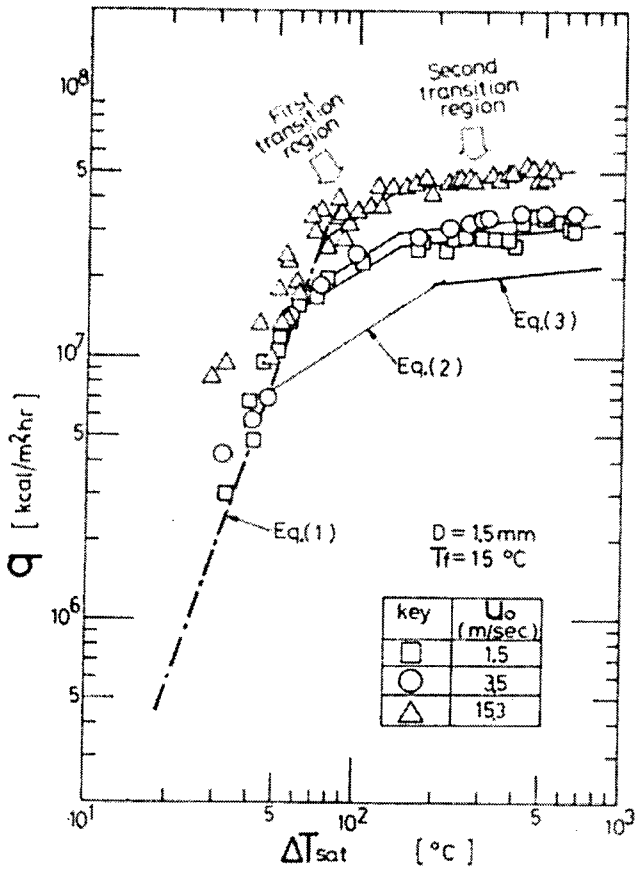

FIGURE 2-8 Subcooled impinging water jet boiling curve, U_0 is jet velocity [16]

Miyasaka et al. correlated the data in the first and second transition boiling regions for various subcooling and jet velocities. The correlations are given by Equation (23) for the first transition region and by Equation (24) for the second transition region.

$$q''_1 = q''_{\text{sub=85, pool, 1}} \cdot (1 + 0.66 \cdot v_{ji}^{0.32}) \cdot \chi \tag{23}$$

$$q''_2 = q''_{\text{sub=85, pool, 2}} \cdot (1 + 0.4 \cdot v_{ji}^{0.4}) \cdot \chi \tag{24}$$

where the parameter χ is to account for stagnation pressure and given by Equation (25).

$$\chi = \frac{\left(h_{fg}\cdot\rho_g\cdot\left(\frac{\sigma\cdot(\rho_f-\rho_g)}{\rho_g^2}\right)^{1/4}\cdot\left(1+0.112\left(\frac{\rho_f}{\rho_g}\right)^{0.8}\left(\frac{c_p\cdot\Delta T_{sub}}{h_{fg}}\right)^{1.13}\right)\right)_{P=P_a+\frac{1}{2}\cdot\rho_r\cdot v_{ji}^2}}{\left(h_{fg}\cdot\rho_g\cdot\left(\frac{\sigma\cdot(\rho_f-\rho_g)}{\rho_g^2}\right)^{1/4}\cdot\left(1+0.112\left(\frac{\rho_f}{\rho_g}\right)^{0.8}\left(\frac{c_p\cdot\Delta T_{sub}}{h_{fg}}\right)^{1.13}\right)\right)_{P=P_a,\,(\Delta T_{sub}=85°C)}} \quad (25)$$

Kumagai et al. [35] studied the transient cooling of a hot metal slab by an impinging jet during boiling heat transfer. They studied the effect of jet velocity and liquid sub-cooling on the critical heat flux. The critical heat flux increased with increased sub-cooling at all locations. The effect of jet velocity on the critical heat flux was also found to be significant particularly at higher heat fluxes and higher velocities. They also found that the region of impingement heat transfer grew radially faster with increasing velocity. At low velocity the critical heat flux for locations far away from stagnation was fairly uniform. As the velocity was increased, the effect of impingement reached further downstream from stagnation and hence increased the heat flux from that area. This effect was noticeable as far downstream as 16 jet diameters for a jet velocity of 3.5 m/s. They did not present a correlation for their data.

Ishigai et al. [38] studied both transient cooling and constant heat flux at the stagnation point for a surface during jet impingement. The surface was cooled, in the transient case, from an initial temperature of 1000°C. They studied the effect of sub-cooling and jet velocities in the ranges 5°C to 55°C and 1.0 m/s to 3.17 m/s respectively. On Figure 2-5, shown earlier, the boiling curves they found for various jet velocities and sub-cooling can be seen. Dependence of the critical heat flux on sub-cooling is clear with higher heat flux associated with increased sub-cooling. The effect of jet velocity is however not as clear. From Figure 2-5 (b) it can be seen that the heat flux increases with increasing jet velocity, especially at lower sub-cooling.

Similar curves as the ones found by Ishigai et al. [38] were found by Ochi et al. [9] as shown in Figure 2-9. They reported results indicating that the effect of water sub-cooling decreased as the sub-cooling increased, becoming very small around and above 65°C sub-cooling. Similar shifts in the point of minimum heat flux due to varying sub-cooling are shown in

Figure 2-9 as in Figure 2-5 (a) earlier. At low sub-cooling the curve has a similar shape as seen earlier in Figure 2-4 but as the sub-cooling is increased the curves become flatter. The nucleate, transition and film boiling regions are difficult to point out at high sub-cooling and finally the point of minimum heat transfer is shifted out of the temperature range and no film boiling is seen.

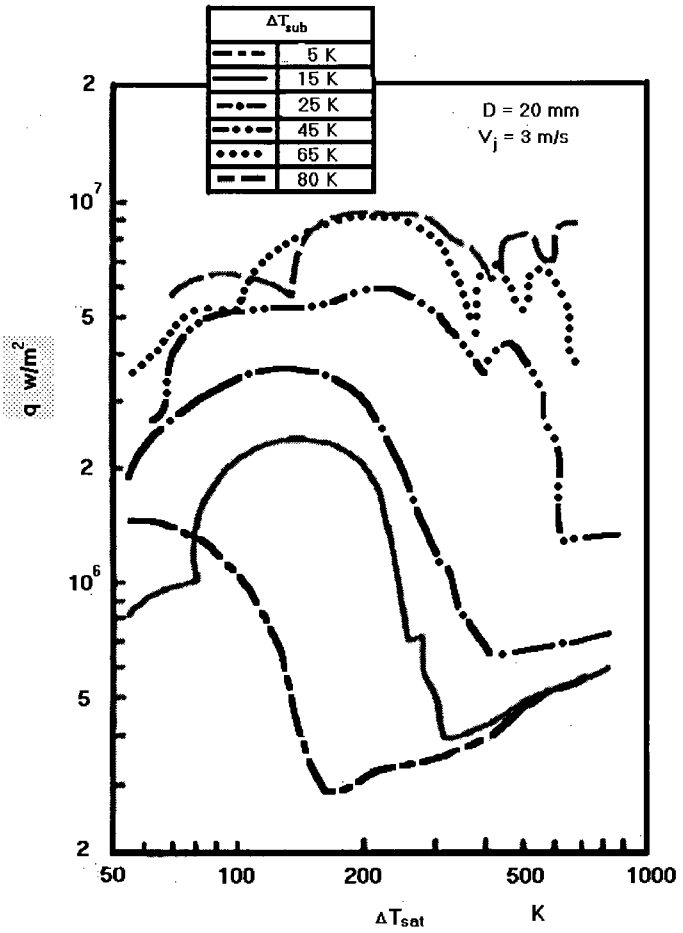

FIGURE 2-9 Boiling curves at the stagnation point for various sub-cooling [9]

Liu [39] made measurements during the transient cooling of a stationary steel plate cooled by water jet impingement using initial plate temperatures, cooling water temperatures and jet diameters as listed in Figure 2-10. He used the same apparatus as the current study. He found the critical heat flux to depend highly on initial plate temperature but found the cooling water temperature to have a very small effect in the impingement zone at the levels of sub-cooling tested.

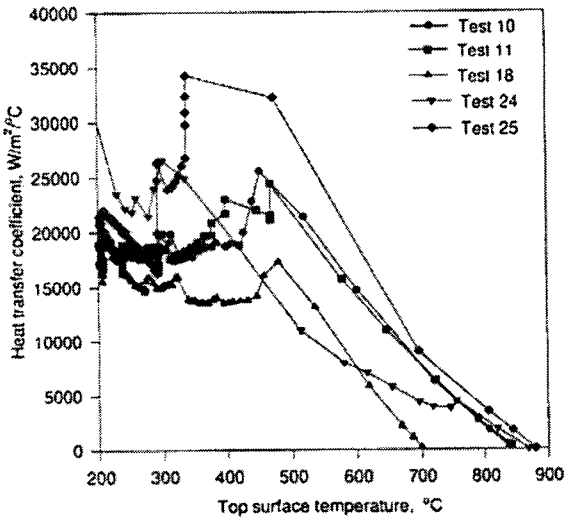

Test#	Steel	T_p, °C	T_w, °C	D, mm
10	DQSK	900	13	18.92
11	DQSK	900	30	18.92
18	DQSK	700	30	18.92
24	SS316L	900	30	18.92
25	DQSK	900	28	30.0

T_p: Initial plate temperature; T_w: Water temperature; D: water jet diameter

FIGURE 2-10 Boiling curves at stagnation [39]

The effect of nozzle to plate distance on critical heat flux was studied by Katto and Kunihiro [17]. They used a jet with saturated water impinging on a hot surface and found the nozzle to plate distance to have little effect on the critical heat flux. They looked at nozzle to plate distances in the range of 0.63 to 42 jet diameters.

2.2.5 Transition boiling

In transition boiling the vapor blankets formed by the coalescence of bubbles are unstable and collapse so the surface is intermittently wetted resulting in large fluctuations in surface temperature and heat flux. Transition boiling is partially nucleate boiling and partially unstable film boiling and is recognized as the least understood of all boiling regimes [5].

In the transition boiling region heat transfer decreases with increased wall superheat and reaches a minimum at the point of minimum heat transfer, shown earlier as point C on Figure 2-4. The zone around the point of minimum heat transfer is a zone of transition towards

film boiling. Point C, minimum heat transfer, is often called the Leidenfrost point. The Leidenfrost phenomenon is well known during pool boiling. This phenomenon can be observed by watching water droplets sizzle and dance around on a hot surface. It has been reported that in transition pool boiling, the heat flux appears to be higher during heating of a surface than during cooling at the same wall superheat [20]. Transition boiling heat transfer during cooling has been studied by various researchers and is more relevant in the current work and will hence be reviewed here.

Chen and Hsu [21] studied heat transfer during liquid contact in transition boiling and found that the heat flux is roughly equal to the critical heat flux that would be expected for water at the same temperature. The average heat flux during liquid contact was found to vary from 105 W/m^2 to 107 W/m^2 while water sub-cooling was varied from 0°C to 80°C and wall superheat from 50°C to 450°C. The heat flux during vapor contact was much lower and fluctuations in heat flux and surface temperature were commonly seen during transition boiling [22].

Ishigai et al. [38] studied transient and steady state boiling at the stagnation point during water jet impingement. Figure 2-5 shows their data for various jet velocities and subcooling. The boiling curves for low sub-cooling have a similar shape as the one for the saturated case in Figure 2-4 but at higher subcooling the shape is quite different. The curve is much flatter and a shoulder appears in the transition boiling region. The effect of cooling water subcooling in the transition region is apparent with higher heat flux as the subcooling is increased. The effect of jet velocity is not as strong but, at high subcooling, higher heat flux is seen at higher jet velocities. Figure 2-11 shows a more detailed view of one of their boiling curves for transient cooling. Here the shoulder in the transition boiling region is clear. According to their observations the surface was intermittently wetted in the transition boiling region, i.e. from point A to point D in Figure 2-11. The liquid solid contacts were repeated with a relatively low frequency in the region between points A and C. In the interval between points C and D the

liquid contact took place at a higher frequency and the contact area was observed to be nearly constant in size. Some of their steady state data is also shown in Figure 2-11. They observed that the slope of the boiling curve in the nucleate boiling region is much steeper in the steady state case than in the transient case. Same equipment was used in both steady state and transient experiments.

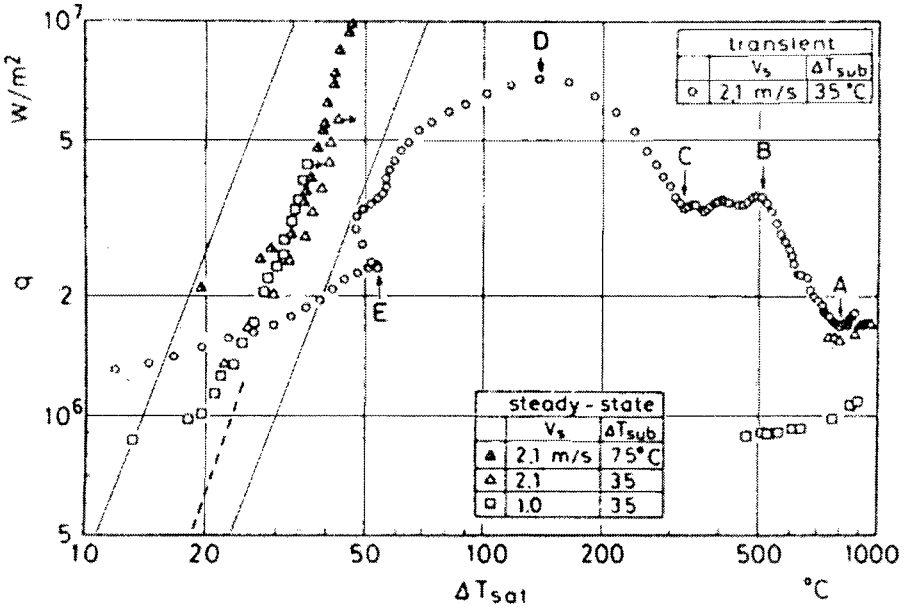

FIGURE 2-11 Sub cooled water jet impingement boiling curve with a shoulder in the transition boiling region [38]

Ochi et al. [9] did similar test as Ishigai et al. [38] and also observed a shoulder in the transition boiling region, see Figure 2-9, but did not speculate about why it appears. They also measured heat transfer at locations downstream from the stagnation point and found the heat transfer in all boiling regions to decrease as the distance from the stagnation point increased. This is in agreement with what Kumagai et al. [35] found. They used 0°C sub-cooling and found the heat flux in the transition region to decrease significantly with increased distance from the stagnation point, seen earlier in Figure 2-7.

Available correlations that correlate experimental data in the transition boiling region can be divided into two categories. Firstly there are correlations that are mathematical approximations of the boiling curve in the transition boiling region and secondly there are correlations that are based on the analysis of the physical mechanism of transition boiling. The correlations based on the physical mechanism are very complicated and their use requires knowledge of parameters such as the heating surface section occupied by vapor at a given time and wall liquid contact time. A mathematical form that has been suggested by various researchers to approximate the boiling curve is given by Equation (26) [5].

$$q'' = A \cdot \Delta T^{-m} \tag{26}$$

The parameters A and m have different values for each series of experimental data. These formulas approximate the boiling curve in the center part of the transition region but data points close to the points of minimum and maximum heat flux are ignored.

Kandlikar et al. [40] reviewed the form of correlations introduced by Berenson (1962) and given by Equation (27). These correlations are based on the assumption that transition boiling is a combination of unstable nucleate boiling and unstable film boiling.

$$q'' = F \cdot q''_f + (1 - F) \cdot q''_g \tag{27}$$

Where F is a parameter that denotes the proportion of the surface that is in liquid contact at a given moment and q''_f and q''_g are heat fluxes at liquid and vapor contact, respectively. Kandlikar et al. correlated pool boiling data from the literature for F and q''_f, given by Equation (28) and Equation (29), respectively. They found it reasonable to assume q''_g is equal to the minimum heat flux, q''_{MHF}.

$$F = e^{-2.2 \cdot \frac{\Delta T_{sat}}{\Delta T_{CHF}} + 2} \tag{28}$$

$$q_f = q_{CHF} \cdot \frac{1 - 0.18 \cdot \frac{q_{MHF}}{q_{CHF}}}{0.82 \cdot \frac{\Delta T_{sat}}{\Delta T_{CHF}}} \quad (29)$$

Where q_{CHF} and ΔT_{CHF} are the critical heat flux and wall superheat corresponding to the critical heat flux respectively.

2.2.6 Minimum heat flux

The transition from film to transition boiling takes place around the point of minimum heat transfer, commonly referred to as the Leidenfrost point. The location of this point has been studied by numerous researchers and correlations have been developed but non have been shown to apply for a variety of liquids [36]. Ishigai et al. [38] correlated the minimum heat flux for a plane jet of water, with jet velocity and sub-cooling in the ranges 0.65 m/s to 3.5 m/s and 5°C to 55°C respectively, using Equation (30). From Equation (30) it can be seen that minimum film boiling temperature (T_{min} = surface temperature at minimum heat transfer) increases with increasing jet velocity and sub-cooling.

$$q''_{min} = 5.40 \cdot 10^4 \cdot (1 + 0.527 \cdot \Delta T_{sub}) \cdot v_j^{0.607} \quad (30)$$

This is consistent with results presented by Ochi et al. [9]. The point of minimum heat transfer was observed to occur at a higher wall temperature as the subcooling was increased. The point of minimum heat flux finally shifted to a higher temperature than their initial plate temperatures of 900-1000°C and hence was no longer seen. They found this to be at sub-cooling greater than 65°C. They also investigated the effect of jet diameter on the minimum heat transfer. Their velocities, sub-cooling and nozzle diameters were in the ranges 2 m/s to 7 m/s, 5°C to 45°C and 5 mm to 20 mm respectively and correlation of the stagnation point data was presented as given by Equation (31).

$$q''_{min} = 3.18 \cdot 10^5 \cdot (1 + 0.383 \cdot \Delta T_{sub}) \cdot \left(\frac{v_{ji}}{d_{ji}}\right)^{0.828} \quad (31)$$

The same trends were observed by Kokado et al. [24] who also studied transient cooling of a hot plate from 900°C by a impinging water jet. They reported that at low subcooling no immediate wetting of the surface around the stagnation point was observed. At higher subcooling the region around the stagnation point darkened immediately indicating immediate liquid-solid contact. They found the maximum water temperature for immediate wetting to be 68°C. Liu and Wang [37] also made measurements that show the effect of subcooling and jet velocity on the point of minimum heat transfer and reported similar effects as discussed above.

2.2.7 Film boiling

In the film-boiling region, from point C on Figure 2-4 and up, the heat transfer from the surface to the liquid is across a vapor film. First the primary mode of heat transfer is forced convection within the vapor film but as the temperature is increased, radiation becomes a more dominant mode of heat transfer [6]. Reviews of research advances in film boiling have been published by Kalinin et al. [4] and Viskanta et al. [23].

Ishigai et al. [38] obtained film boiling data by cooling a steel plate from an initial temperature of approximately 1000°C by an impinging jet of water and taking measurements at stagnation, see Figure 2-5. They observed film boiling only at a lower subcooling than approximately 50°C. Their data shows that the sub-cooling and jet velocity have an effect on heat flux in jet impingement film boiling. Increasing subcooling increases the heat flux especially in the vicinity of the point of minimum heat flux but the effect is less apparent at higher wall superheats and becoming very small at 900°C superheat. Heat flux also increases with higher jet velocities, the boiling curve has a similar shape but is shifted to higher heat fluxes as jet velocity is increased.

Ochi et al. [9] heated a stainless steel plate up to 1100°C and cooled it with an impinging water jet. They looked at the effect of jet diameter, sub-cooling and jet velocity. They also looked at heat transfer at locations outside the stagnation area. The same behavior as observed by Ishigai et al. [38] was seen on the effect of sub-cooling and jet velocity. They also found the

heat transfer to increase as the jet diameter was decreased for all heat transfer modes. This is believed to be due to the radial velocity gradient of the water on the impingement surface as it becomes larger. The heat fluxes at locations down stream from stagnation were lower than those at stagnation due to a thinner water film thickness and increasing water temperature.

Liu and Wang [37] studied film boiling heat transfer for water jet impingement. Both the theoretical analysis and experimental investigation were performed for the jet stagnation zone. The theoretical analysis gave, for highly sub cooled water, a correlation for wall heat flux in the film boiling region Equation (32).

$$q''_w = 1.414 \cdot \frac{Re_j^{1/2} \cdot Pr_f^{1/6} \cdot (k_f \cdot k_g \cdot \Delta T_{sub} \cdot \Delta T_{sat})^{1/2}}{d_j} \quad (32)$$

In their experimental investigation they investigated, among other things, the effect of sub-cooling and jet velocity using a constant jet diameter of 10 mm and cooling a thin stainless steel plate from an initial temperature of 1000°C. Figure 2-12 shows their experimental data compared to the predicted values using theoretical analysis. The solid correlation lines, marked with temperature and velocity values, were found using Equation (32). The dashed lines were found using another correlation for lower sub-cooling, not presented here. The curves with markers on them are the experimental cooling curves. For relatively low sub-cooling the experimental data were qualitatively coincident with the calculated values but at higher sub-cooling the experimental values were considerably higher than predicted. This was thought to be because the vapor layer is thinner, thus allowing greater heat transfer. It can be seen from the experimental curves that subcooling and jet velocity have a strong effect on the heat flux in film boiling. The effect of velocity was similar to what was presented by Ishigai et al. [38], Figure 2-5, where the curve shifts upwards with increasing velocity.

Zumbrunnen, Viskanta and Incropera [47] analytically studied film boiling on a moving plate and found the plate motion to have significant effect on heat transfer. Plate motion was especially important when the plate motion greatly exceeds the liquid velocity.

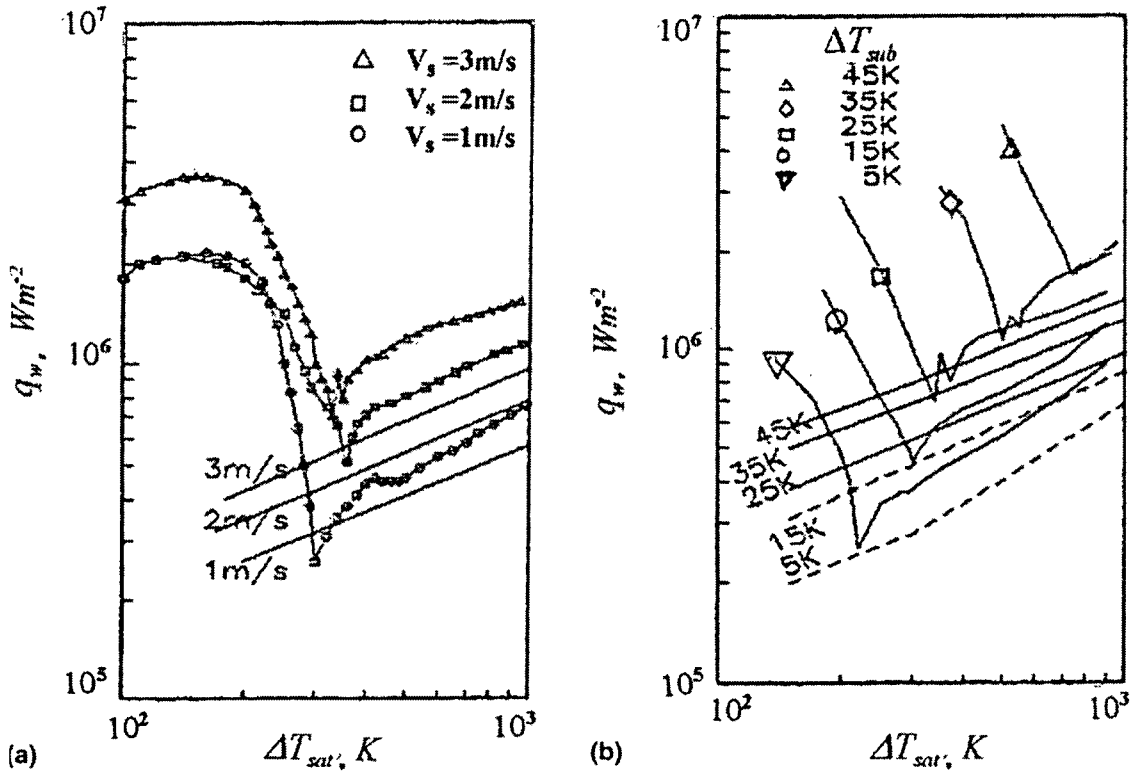

FIGURE 2-12 Jet impingement experimental data compared to predicted values in the film boiling region: (a) for subcooling of 25°C and (b) for impinging velocity of 3 m/s [37]

3

EXPERIMENTAL PROCEDURES AND APPARATUS

Much prior research in this field was done using surfaces that are constantly heated while being impinged by a liquid jet. This method is convenient as it allows the researcher to investigate the problem at steady state. Usually the heating is accomplished by passing an electric current through a metal plate [12][14][15][16][32][41]. Other methods have also been used to heat the surface such as attaching heating elements on the back surface of the test plate [21][34]. Some work has also been done using transient methods when the test plate is heated up prior to the test and then cooled using an impinging jet. The most common way to do this, is either to heat the plate in a furnace and than move the plate under the nozzle for cooling [2][24][39], or heat it in the same way as described above for constant heating and turn the heating off before cooling is started [9][37][38].

Various methods have been used to measure the temperature of the impinged surface and finding the heat flux. The most common method is to attach one or more thermocouples on the reverse side of the test plate, opposite to the impinging jet, and then calculating the surface temperature. The surface temperature and heat flux is then found using an inverse heat conduction model or by solving the steady state energy equation to find the surface temperature and heat flux [2][9][12][14][15][24][37][38]. Some researchers have also installed thermocouples inside their test plates to get an estimate of the temperature gradient. Some have then used that temperature gradient to estimate the surface temperature and heat flux

[32][34][35]. Non of the reviewed researchers reported direct measurements of surface temperature, or heat flux, during jet impingement.

In the following sections the current experimental equipment, method of instrumentation and experimental procedure will be described in detail.

3.1 EQUIPMENT

All measurements in the present study were made using a run out table cooling facility located in the high head room laboratory in the Advanced Materials Process Engineering Laboratories (AMPEL) in the Brimacombe building at UBC. A schematic view of the facility can be seen in Figure 3-1.

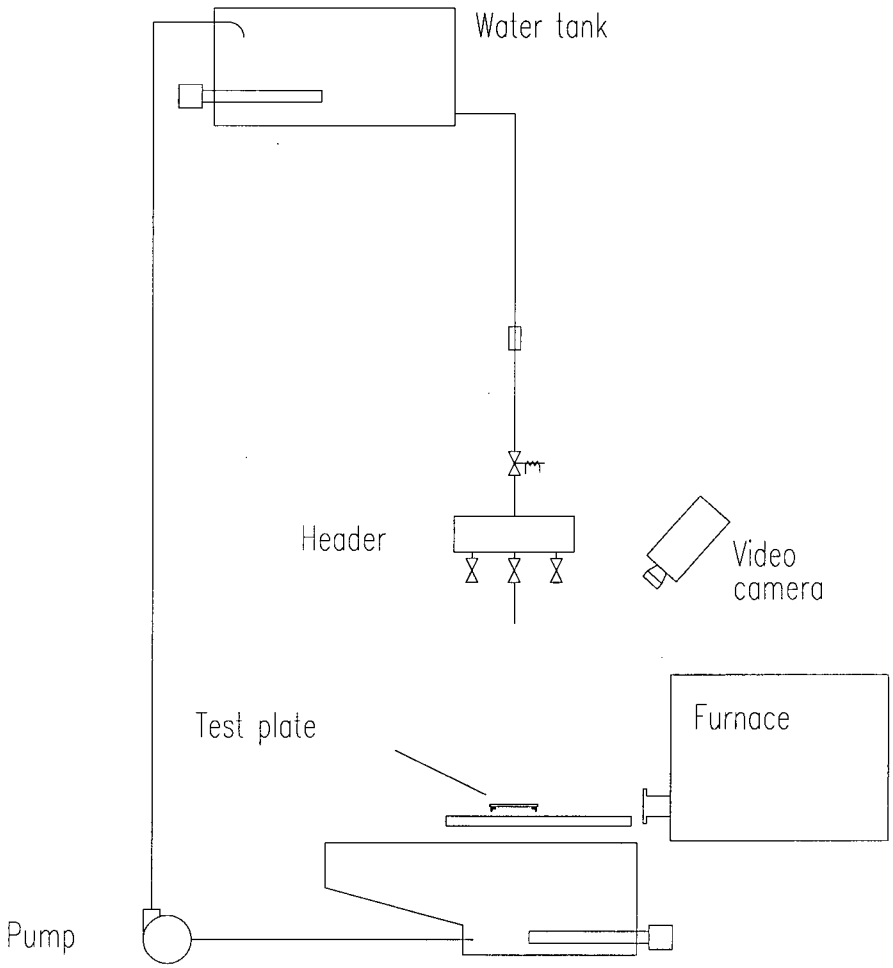

FIGURE 3-1 Schematic view of the UBC run out table test facility

The facility is industrial scale and consists of a large water tank located at the top of a 6.5 m high tower, containment water tank, flow control valves, water pump, nozzle header and furnace. Measurements are made by heating an instrumented plate in the furnace and by later, cooling it with water jets using industrial scale headers. The nozzles in the header can easily be changed. There can be up to three nozzles at a time and spacing between nozzles is adjustable from 50 to 90 mm. Height of the nozzles above the hot plate can be adjusted from 0.6 m to 2 m. Total water flow is adjustable to a maximum of 138 l/min, depending on number of nozzles and nozzle diameter. The water can be heated to 50°C using a heater in the overhead and containment water tanks. Temperature meters are located in the water tanks and control the water heaters. A float switch operated water pump brings the cooling water from a reserve below the hot plate up, to the overhead water tank keeping the water level in the tank constant and hence the flow rate. The water flow is controlled by hand operated adjustable valve below the header. Flow rates can be obtained using a digital flow meter for high flow rates or a bucket and stopwatch for flow rates outside the operating range of the digital flow meter. Water flow can be turned on and off using an electrically operated valve. A special S-shaped tube, not shown on Figure 3-1, can be used to direct the water flow away from the hot plate while the flow in the nozzle is developing. This ensures that the water jet will be fully developed once it hits the plate. The furnace, made by Lindberg/Blue M. (240 V, 25 A, 5.8 kW, 60 Hz), can heat plate samples up to 1200 °C and is filled and pressurized with nitrogen gas to prevent oxidation during heating. It has a working space capable of heating plates of size up to 280x280x10 mm.

The measurements made for this research were all done using only one nozzle. The nozzle was located so that the water jet hit the centre of the test plate. The nozzle used was a carefully cut commercial 304 stainless steel pipe with a mean inner diameter of approximately 19 mm. Nozzle to plate distance was kept constant throughout the study at 150 cm. The effect of cooling water temperature and flow rate was investigated in the range from 30°C to 50°C and 15 l/min to 45 l/min respectively.

Two kinds of steel plates were used during the research. The steel grades used were DQSK (Drawing Quality Special Killed) carbon steel and SS316 stainless steel. The chemical composition of the steels is shown in Table 3-1.

TABLE 3-1 Chemical composition of steels used in wt%

Alloy	C	Mn	P	S	Si	Al	Cr	Ni	Mo	N
DQSK	0.06	0.24	0.005	0.011	0.006	0.041				0.0035
SS316	0.06	1.86					19.2	11.3	2.67	

Each plate was only used once as the plates bent, warped and oxided during the cooling process. In all runs the plate bent towards the impinging nozzle, and was slightly convex at the end of the cooling process. This bending was small and hence its effect on heat transfer and flow rates were neglected. All plates were used in the as rolled condition but cleaned with methanol before heating. No polishing of the plate surface was done.

The first measurements were made using DQSK steel, which experienced a phase change in the temperature range used and properties of DQSK steel are not well documented. In order to minimize uncertainties associated with the phase change, later tests were done using a SS316 stainless steel. Properties of SS316 steel are well documented and accurate data is available stating its conductivity, density and thermal capacity. Special attention was given to accurate predictions of the conductivity with respect to its dependence on temperature.

A Canon video camera was used to film every run. These pictures were used for comparison with measured results when estimating the initial size of the impingement zone as well as the progression of the re-wetting front during cooling. The video was also used to see how well centred the water jet was on the plate and to document if any non-symmetry in the cooling pattern was present.

3.2 INSTRUMENTATION

3.2.1 Intrinsic thermocouples

Thermocouples were used to measure the temperature inside and on the surface of the test plate. Traditionally a thermocouple is formed by joining together the two dissimilar metal wires in a bead at the end of the wires. That junction gives a unique voltage at a given temperature and so the voltage reading of the thermocouple represents the temperature of the junction. On the other hand, an intrinsic thermocouple is formed when two dissimilar metal wires are attached to the test piece separately but still very close to each other. The test piece now acts as the junction and the reading of the thermocouple gives the temperature of the surface area at the attachment point. This method eliminates the thermal mass of the junction and hence decreases the response time to zero. These two wires are then connected to a data acquisition system that converts the voltage value to a temperature value using a known relation for each given thermocouple type.

Thermocouples of Type K (Omega 304-K-Mo-1.5mm) were used for this study. Their operating range spans temperatures as high as 1150°C. Type K thermocouples are constructed of Chromel-Alumel wires and have an error of approximately 0.75% when used at temperature higher than 277°C and approximately 2°C at lower temperatures [42]. Each thermocouple wire is around 0.002" in diameter and the wires are lead through an insulating metal coat, filled with alumina insulation. The metal coat has an outer diameter of approximately 1/16". A schematic view of the wires, the protective coat and insulation can be seen in Figure 3-2.

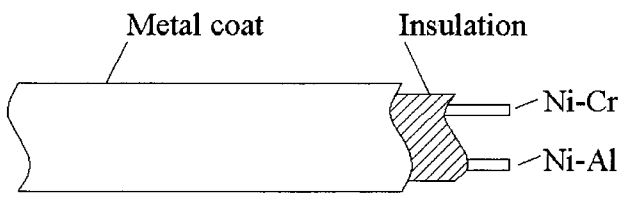

FIGURE 3-2 Schematic view of a thermocouple

A total of 16 thermocouples were used for each run. A PC operated data acquisition system powered by an InstruNet software package was used to sample the temperatures at a frequency of 100 Hz. Additional measurements were done using a higher frequency, as high as 600 Hz, using fewer thermocouples, to take a closer look at interesting phenomenons during cooling in the impingement zone and to determine the required sampling rate.

3.2.2 Thermocouple installation

The 16 thermocouples used in each run were installed inside and on the surface of the plate. Measurements were made at eight locations on the test plate, where each location was a combination of two thermocouples. Figure 3-3 shows a schematic view of the novel method

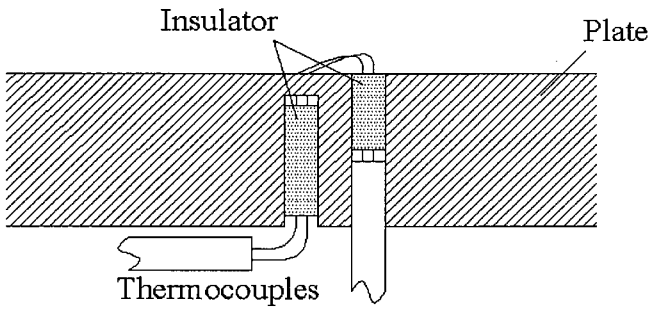

FIGURE 3-3 Installation of thermocouples

developed for installation of the two thermocouples at one measurement location. At each location two 1/16" diameter holes are drilled in the plate at a distance of 1/8" apart, measured from center to center. One hole is drilled all the way through, the other one, a flat-bottom hole, was drilled to a distance of approximately 0.04" from the surface. This distance was measured accurately with a micrometer to within ± 0.0001". One thermocouple is located in the bottom of the flat bottom hole and the other one on the surface of the plate right on top of the other one. The radial distance from the center of the plate to the center of each flat bottom hole is the location of each thermocouple as shown in Figure 3-4.

The locations of measurement were evenly distributed with one thermocouple combination in the center and the others located at 5/8" increments radially outward from the center. These locations were not in line but lay on rays from the center with one thermocouple on each ray. This was done to limit the possible influence of flow disturbance, caused by a poorly installed surface thermocouple, on other thermocouples downstream. Having all the thermocouples on one ray was tested and the small flow disturbances around some surface thermocouples lead to non symmetric cooling and hence created some undesired error. Using the symmetry of the plate and the fact that the center of the water jet is located in the center of the plate, this gives the same result as having the thermocouples on a straight line. Figure 3-4 gives a schematic view of the locations of measurement on the plate. This layout was used while gathering all the data for this study and was identical for all the plates.

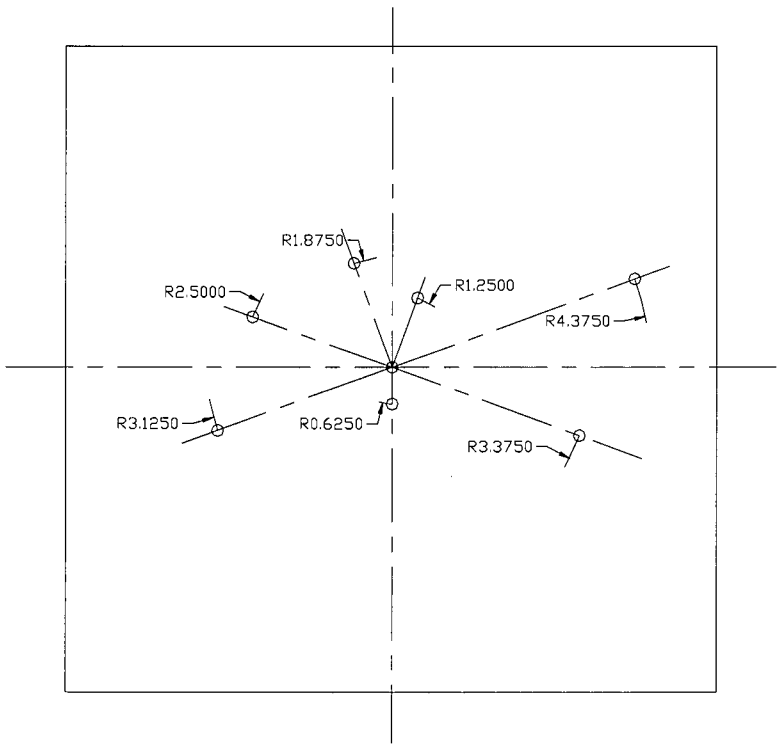

FIGURE 3-4 Locations of measurement on test plate

The surface thermocouple wires were spot welded separately on the surface above each flat-bottom hole. The thermocouple insulation coat was fixed in the hole going through the plate and the two thermocouple wires were led along the surface and spot welded at the point

of measurement. Great care has to be exercised in doing this, as the wires may not touch the plate anywhere but at the spot weld. Any contact between the wires and the plate can result in a premature connection and hence a wrong point of measurement. To limit flow disturbance as much as possible the insulation coat of the thermocouples was fixed at about half way through the hole. The thermocouple wires were than led through an alumina insulator with 1/16" diameter and two holes through it having a diameter slightly larger than the one of the thermocouple wires. This kept the wires separated and insulated from each other and the plate. The ends of this insulator were straight. By adjusting the length of the insulator properly, its upper end could be leveled with the surface of the plate, thereby limiting the effect of the hole on the water flow along the surface. The hole drilled through the plate was downstream from the flat-bottom one and hence downstream from the point of measurement to limit the effect of material removal and flow disturbance as much as possible. The wires were then spot welded separately, separated by a distance of approximately 1 mm, on the surface above the flat bottom hole. Special care was taken while spot welding the surface thermocouples as poor installation could result in flow disturbance or in poor performance of the thermocouple.

The internal thermocouple wires were spot welded separately to the bottom of the flat-bottom hole. This was done by placing an insulator, like the one used for the surface thermocouple, with two holes of the same diameter as the two thermocouples wires and an outside diameter of 1/16", in the hole. The wires were then thread through the holes in the insulator with a charged capacitor connected, one pole to the wire and one to the plate. When the wire was very close to the bottom of the hole the capacitor discharged with a spark between the wire and the plate. This spark melted the end of the thermocouple wire so, if moved rapidly down, it spot welded itself to the bottom of the hole. Great care has to be taken while installing these thermocouples so the spot-welds hold throughout the test. It is also important that the two wires do not get in contact with each other and thereby create a premature junction and a false reading.

This installation gave two intrinsic thermocouples one on top of the other and separated by a known distance. This setup made the surface act like a heat flux gage. The two temperature measurements can then be used to evaluate the temperature gradient at that location and hence, the heat flux using Equation (33).

$$q'' = k(T)\frac{dT}{dx} \tag{33}$$

Where q'' is heat flux per unit area, $k(T)$ is conductivity of steel as a function of temperature and dT/dx is the temperature gradient at the plate surface.

The thermocouple wires were fed from the plate to the data acquisition system through a pipe that was attached to the plate using steel angles. This pipe also acted as a handle on the plate to remove it from the furnace. The pipe was attached on the end of the plate and insulation was used to limit heat transfer from the holding bracket to the plate during cooling. A schematic view of the attachment is shown in Figure 3-5. Error due to this attachment is assumed to be negligible.

This method of installing the thermocouples has not been used previously in a similar kind of study. Most previous studies on transient boiling jet impingement heat transfer made use of thermocouples mounted on the back face of a test piece or below a plug inserted in the test piece. Kumagai et al. [35] recorded the temperature inside a metal slab during jet impingement by inserting thermocouples into the slab at varying depths. They extrapolated the internal temperature values to get the surface temperature. Their temperature range was 400°C to 100°C and they did not mention the method of installation or if intrinsic thermocouples were used.

Measuring the surface temperature directly is of great importance in high temperature jet impingement transient cooling as the heat transfer close to the surface is very high and temperature changes rapidly. Kokado et al. [24] reported concerns about direct measurements of surface temperatures due to vapor bubbles sticking on the tip of the surface thermocouples.

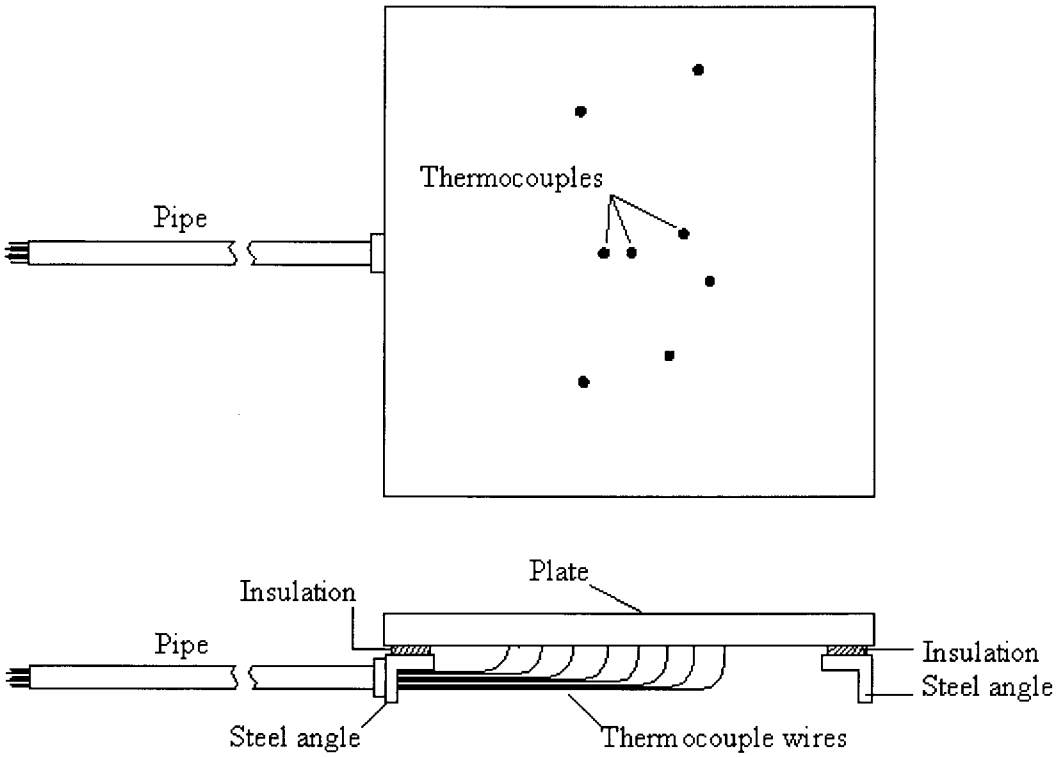

FIGURE 3-5 Schematic view of test plate setup

This is believed to have a negligible effect on measurements in the present study due to high water flow rates and the method of thermocouple installation.

3.3 MEASUREMENT ERRORS

In Table 3-2 the estimated errors associated with the measured quantities are presented. The errors in water flow rate and water temperature measurements were estimated by repeatedly measuring the quantities and from experience working with the equipment.

TABLE 3-2 Measurement errors

Quantity	Error
Temperature [42]	$\pm 2°C$ Temp $\leqq 277°C$ $\pm 0.75\%$ Temp $> 277°C$
Flow rate	± 0.5 l/min
Thermocouple depth	± 0.003 mm
Thermocouple location	± 0.1 mm (relative to center of plate)
Water temperature	$\pm 2°C$

Due to instabilities in the flow from the nozzle exit to the impingement surface the actual location of the stagnation point varied a little bit around the preset location. This variance was observed to be approximately ± 3 mm.

3.4 EXPERIMENTAL PROCEDURE

After instrumenting and attaching the holding pipe to the plate final adjustments were made. The plate assembly was placed under the water jet and its location adjusted so that the jet hits the center of the plate. This preset location ensures that the center of the water jet hits the center of the plate, measurement location number 1, during the cooling process.

The plate was heated in the furnace to a desired temperature, somewhat higher than the desired initial temperature for each test. This was done since the plate cooled down quickly, due to radiation and convection, when moved from the furnace to the nozzle (before the actual water-cooling started). The process of taking the plate out of the furnace took about 10-15 seconds and in that time the temperature of the plate dropped by as much as 50°C. The heating process took approximately 3 hours. The plate was left in the furnace for some time after the final temperature had been reached to ensure that the whole plate was at a uniform temperature. This was monitored by reading the temperature values of the thermocouples while the plate was still in the furnace. The plate was then pulled out of the furnace and positioned at a location directly under the nozzle.

The desired initial temperature for each test was achieved by monitoring the temperature of the plate once it was out of the furnace. Cooling due to radiation and convection (before jet impingement) was slow relative to conductive heat transfer within the plate, hence the temperature gradient in the plate was negligible before the jet impingement. Once the plate was in place, and the desired initial plate temperature was reached the water flow was turned on. When using low flow rates the flow was unstable for a few seconds after being turned on. In those cases an S shaped pipe was used to direct the flow away from the plate until the flow in the nozzle was fully developed. This pipe was then removed and a fully developed water jet hit the plate. Data collection started well before the water was turned on and continued until the plate was fully cooled below normal run out table exit temperatures.

4

DATA PROCESSING

In the literature reviewed for this study the method of measurement was, in all cases, different from that used here. No direct measurement of the the surface temperature and heat flux was done in previous studies. Instead of using an inverse heat conduction model, extrapolation of temperatures or solving the heat transfer equation in a solid for constant heat flux, the test plate was in the current study used as a heat flux sensor. This difference requires a new method of data processing to take full advantage of the new information at hand. In this chapter the methods used to calculate various quantities from the raw temperature data will be described.

4.1 MATERIAL PROPERTIES

The material properties of the test plates are important for calculating the heat flux and hence, the heat transfer coefficient. Some physical properties of steels are highly temperature dependent. The principle property in the present study is the thermal conductivity which varies with temperature.

The properties of the two steel grades used in the study, DQSK steel and SS316 stainless steel, behave quite differently within the temperature range studied. While SS316 is austenite stainless steel having the same phase over the whole temperature range. The DQSK steel experiences phase changes, within the solid phase, while being cooled. DQSK steel is in the austenite phase at elevated temperatures but as the temperature drops, phase transformation takes place and the austenite transforms into ferrite and perlite in proportions dependent on the

cooling rate and temperature of phase change. This is one of the reasons for the importance of controlled cooling in high quality steel making.

Predicting the properties of DQSK steel accurately is difficult since the change in properties varies with temperature within different phases, also the time of phase change is dependent on the thermal history of the material. There is latent heat associated with the exothermic phase change. It is beyond the scope of this study to go into investigations of phase transformation latent heat and its effect on material properties. The properties of the DQSK steel were therefore taken as values given for properties of steels with a similar chemical composition found in handbooks. The SS316 stainless steel is an austenite steel that has no phase changes in the temperature range used. The properties are nonetheless temperature dependent but are more accurately known and well documented.

Thermo-physical properties of the DQSK steel were taken as the values given for plain low carbon steel, AISI 1008, and changes in density and specific heat were considered small and neglected [45]. It should be noted that the properties of the 1008 steel are in good agreement with properties of individual phases of the DQSK steel as presented by Liu [2].

TABLE 4-1 Conductivity of AISI 1008 steel [45].

Temperature [°C]	0	100	200	300	400	500	600	700	800	1000
Conductivity [W / m °C]	59.5	57.8	53.2	49.4	45.6	41.0	36.8	33.1	28.5	27.6

Linear regression for the temperature range in Table 4-1 gave the following correlation with a correlation coefficient of 0.997 and a standard error of 1.000:

Conductivity: $k = 60.571 - 0.03849*T$ [W / m °C]

Density: $\rho = 7800$ kg / m^3

Specific heat: $c_p = 470$ (J / kg / °C)

For austenite stainless steel the properties have the following values for the temperature range on a runout table, changes in density and specific heat are relatively small and are neglected [46]:

TABLE 4-2 Conductivity of austenite stainless steel [46].

Conductivity [W / m °C]	**Temperature [°C]**
k = 10.717 + 0.014955 T	T < 780
k = 12.076 + 0.013273 T	780 < T < 1672

Density: $\rho = 7865 \text{ kg / m}^3$

Specific heat: $c_p = 460 \text{ (J / kg / °C)}$

4.2 HEAT FLUX EVALUATION

To evaluate the heat flux at the surface of the plate one must estimate the temperature gradient, dT/dx, at the surface. Then the heat flux can be evaluated using the heat conduction formula, given by Equation (33).

Estimating the gradient in the first moments of cooling is hard using only two data points since the gradient is highly nonlinear during that period. A measurement was made to investigate how nonlinear the profile was and when, if ever, it could be assumed to be linear. This measurement was done by placing three thermocouples at an equal radial distance from the stagnation point but at varying depths. Assuming symmetric cooling this was equivalent to having three thermocouples, at different depths, at the same location. The results gave indication of the shape of the temperature profile inside the plate when it was being cooled. The results of that measurement are shown in Figure 4-1. The test was conducted on a DQSK steel plate with a water flow rate of 30 L/min and water temperature of 30 °C. Each set of three data points on the graph, connected by a line, are temperatures at the same radial distance but different depths. The sets are drawn with time increments of 0.1 s with the first just before the cooling starts, $t = 0.0$ s, and then step by step with the final set at $t = 0.8$ s, the line furthest to the left. It can be seen that the profile approaches linearity but for the first 0.6 s it is highly nonlin-

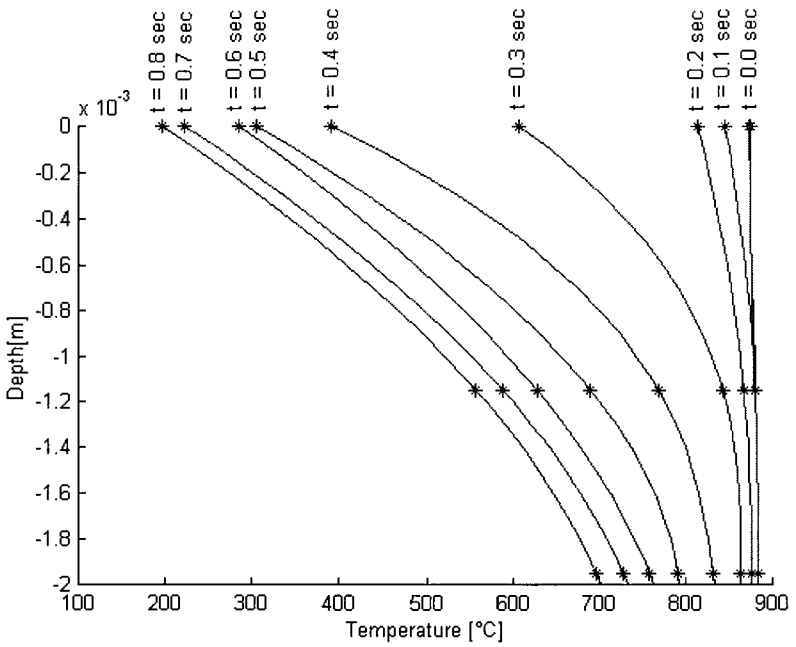

FIGURE 4-1 Temperature measurements at various depths

ear. The line connecting the points is only to indicate which points belong together and is not an accurate representation of the actual profile.

The task at hand was then to find an estimate of the profile, and hence, the gradient at the surface in the first moments of cooling as accurately as possible. This can be done by using numerical equations formulated to solve transient heat conduction problems and using the measured temperatures as boundary conditions.

4.2.1 Finite difference evaluation of the temperature gradient

Crank and Nicolson [43] developed a numerical method to evaluate solutions of partial differential equations of the heat conduction type. Their formulation is a finite difference method and its one dimensional form is given by Equation (34).

$$\frac{T_n^{\,i+1} - T_n^{\,i}}{\alpha \cdot \Delta\tau} = \frac{T_{n+1}^{i} - 2 \cdot T_n^{\,i} + T_{n-1}^{i}}{2 \cdot \Delta x^2} + \frac{T_{n+1}^{i+1} - 2 \cdot T_n^{\,i+1} + T_{n-1}^{i+1}}{2 \cdot \Delta x^2} \qquad (34)$$

Where T_{n-1}, T_n and T_{n+1} are temperatures at grid points inside the plate, α is thermal diffusion, $\Delta\tau$ is the time between measurements and Δx is the distance between temperature values.

Using the measured temperatures and initial plate temperature as boundary conditions and calculating one complete time step at a time it is possible to calculate temperatures at a finite number of points in between the two measured ones for all pairs of data points. This procedure will give calculated temperature values that can be used to estimate the temperature gradient at the surface.

To estimate the temperature gradient at the surface a one-sided second order scheme was used, as given by Equation (35). This scheme uses the measured surface temperature along with two calculated values inside the plate.

$$\frac{dT}{dx} \cong \frac{3 \cdot T_1 - 4 \cdot T_2 + T_3}{2 \cdot \Delta x} \tag{35}$$

Where T_1 is the surface temperature and T_2 and T_3 are calculated temperatures at points inside the plate and Δx is the distance between temperature values.

The finite difference scheme with 20 increments was found to fully converge. Comparison of the temperature gradient at the surface using a linear approximation and the finite difference scheme with 20 or 30 intermediate points, shows that the linear approximation under predicts the gradient dramatically in the first moments of cooling. No difference can be seen between the result when using 20 or 30 intermediate points, the corresponding lines coincide completely. This comparison, for a typical set of data in the impingement zone, is shown in Figure 4-2.

It can be seen that after about 0.7 s the cooling curves for the finite difference scheme and the linear approximation converge thus indicating that the profile can be assumed linear after that time. This initial nonlinearity can also be observed in measurements at locations out-

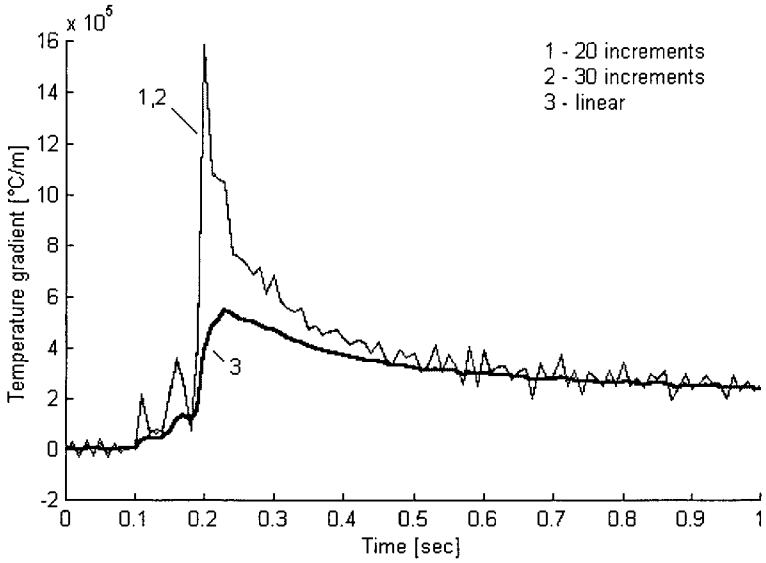

FIGURE 4-2 Temperature gradients using different number of increments in the Crank-Nicolson scheme compared to a linear approximation. Data taken at the stagnation point using water temperature and flow rate of 30°C and 30 l/min respectively and a SS316 steel plate.

side the impingement zone. In those cases the nonlinearity is most apparent at the time when the re-wetting front reaches that location at which point the highest heat flux was observed.

In Figure 4-2 it can be seen that the calculated gradient has a very narrow peak and a lot of fluctuations are created when estimating the gradient, see curves 1 and 2. The reason for this is that small surface temperature fluctuations propagate into large fluctuations in the calculated gradient. Filtering of the measured surface temperature values was thus performed to smooth out these fluctuations and get smoother curves.

The gradient converges with the linear one after the maximum heat flux region. The gradient found using the finite difference method was however used to calculate the heat flux in all cases and at all times for consistency.

One measurement was made with three thermocouples placed at the same radial distance from stagnation, see discussion on page 46 and Figure 4-1. This measurement was

meant to show that the finite difference Crank-Nicolson scheme worked for the highly transient cooling in the current study. In Figure 4-3 the measured intermediate temperature curve and a corresponding calculated temperature curve using Crank-Nicolson are drawn along with measured surface and internal temperatures.

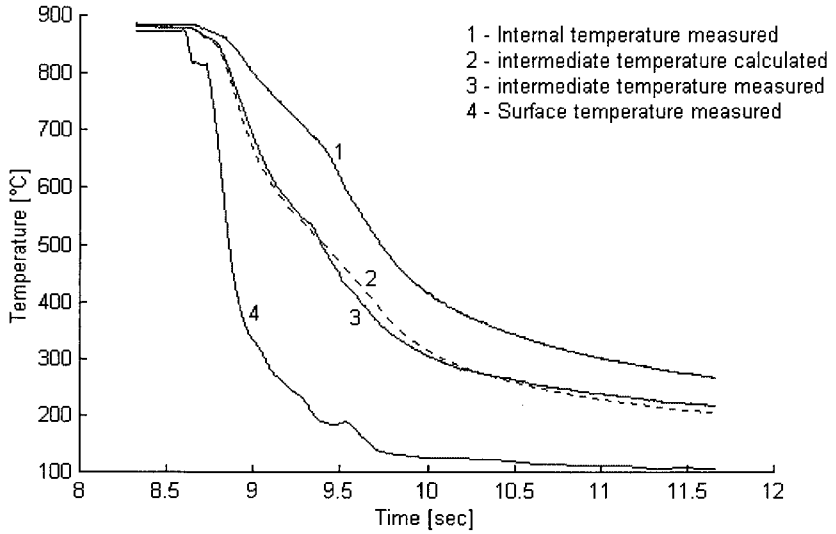

FIGURE 4-3 Comparison between measured and calculated intermediate temperatures. Test done on DQSK steel with flow rate and water temperature of 30 l/min and 30°C respectively.

Relatively good agreement is between the calculated (dashed line) and measured (solid line) curves for the intermediate temperature. It should be noted that the three measurements are not all made at the same location, one on top of the other, but at the same radial distance from stagnation. This fact could explain a part of the small differences seen between the curves.

4.2.2 Filtering of the data

Filtering of surface temperature values was performed using one-dimensional median filtering. The filtration did not lower the maximum peak of the gradient significantly but only helped to smooth out unwanted fluctuations. Such fluctuations are attributable to the larger T

fluctuations within various heat transfer regimes (film, transition and nucleate boiling) as discussed later in Section 5.1.

The filtration was done using the scheme described by Equation (36) through Equation (39). First the average value of n data points around each point, i, was found. Then the residuals were evaluated and smoothed in the same way as the data previously. The final result was then the sum of these two smoothed vectors. In this case filtration was found to be efficient using n = 10 and filtering the data twice.

$$Data'(i) = \frac{Data\left(i-\frac{n-1}{2}\right)+\ldots+Data\left(i+\frac{n-1}{2}\right)}{n} \tag{36}$$

$$Residuals(i) = Data(i)-Data'(i) \tag{37}$$

$$Residuals'(i) = \frac{Residuals\left(i-\frac{n-1}{2}\right)+\ldots+Residuals\left(i+\frac{n-1}{2}\right)}{n} \tag{38}$$

$$Filtered\text{–}data(i) = Data'(i)+Residuals'(i) \tag{39}$$

On Figure 4-4 unfiltered and filtered surface temperature data are compared. On the same graph the calculated temperature gradients found using filtered and unfiltered data are also compared. The dark lines are the data after being filtered while the grey ones are before filtration. From this graph it can clearly be seen how relatively small fluctuations in surface temperature can affect the calculated results. In this case it is the temperature gradient which is used in the heat flux calculations. The fluctuations in surface temperature are likely due to film and transition boiling (see discussion in Section 5.1). A detailed analysis of temperature fluctuations during film and transition boiling is not within the scope of the present study. Hence an average of the data from was recommended. Changes in the maximum value of the temperature gradient and hence the maximum value of the heat flux due to filtration are negligible.

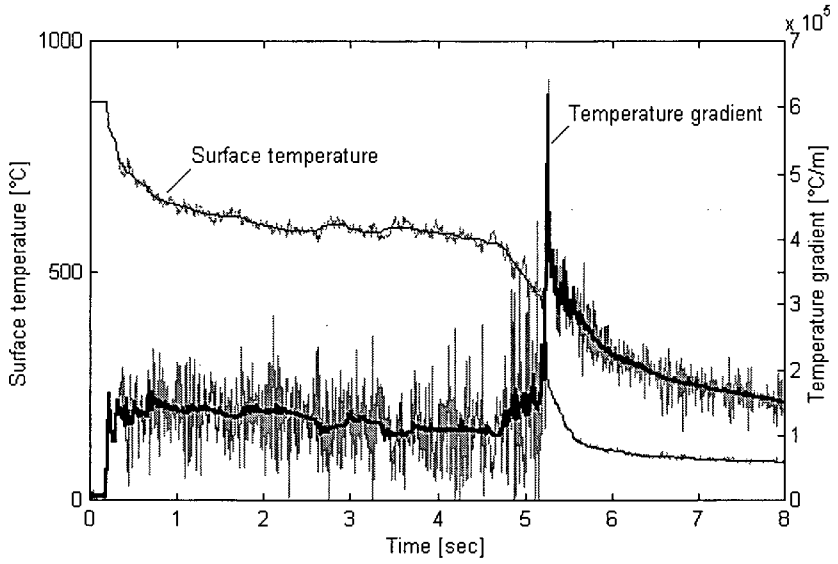

FIGURE 4-4 Comparison of surface temperature (left axis) and temperature gradient (right axis) before and after data filtration.

Figure 4-4 was drawn using data from a test using a SS316 steel plate, with water temperature and flow rate equal to 30°C and 30 l/min respectively. This is a good example of what was typically seen when filtering the data.

4.3 PARAMETERS

4.3.1 Jet velocity and diameter at impingement

Due to the effect of gravity the jet velocity increases from the nozzle exit to the plate surface. The impact velocity of the jet is given by Equation (40).

$$v_{ij} = \sqrt{v_j^2 + 2 \cdot g \cdot H} \tag{40}$$

where v_j is jet exit velocity and H is nozzle to plate height.

The jet diameter decreases according to the conservation of mass as the jet velocity increases. The jet diameter at impingement is hence given by Equation (41).

$$d_{ji} = d_j \cdot \sqrt{\frac{v_j}{v_{ji}}} \tag{41}$$

Where d_j is jet diameter ar nozzle exit.

4.3.2 Wall superheat and subcooling

The saturation temperature of the cooling water depends on pressure. As shown earlier in Figure 2-3, the pressure in the impingement zone varies in the streamwise direction. The pressure in the stagnation region can be expressed with Equation (42) through Equation (32). As presented by Filipovic et al. [44].

$$P_{im}(r) = P_\infty + \frac{1}{2} \cdot \rho_l \cdot V_{im}^2(r) \tag{42}$$

where $P_{im}(r)$ is the pressure and $V_{im}(r)$ is the normal component of the velocity in the impingement zone, both as a function of radial distance from stagnation. P_∞ is the surrounding atmospheric pressure and ρ_l is the density of the water.

$$V_{im}(r) = V_{ij} \cdot \left(\left(\frac{\bar{x}}{1.75} \right)^2 \cdot \left(\frac{2 \cdot \bar{x}}{1.75} - 3 \right) + 1 \right)^{0.5} \tag{43}$$

and V_{ij} is the impact velocity of the jet and the non dimensional distance from the stagnation point is written as

$$\bar{x} = \frac{r \cdot V_{ji}}{V_j \cdot d_j} \tag{44}$$

where d_j is jet diameter. If the non dimensional distance x was larger than 1.75, that is when V_{im} equaled V_{ij} according to Equation (42), the pressure was taken as the surrounding. Hydrostatic pressure was neglected due to the thinness of the film.

The saturation temperature, T_{sat}, was than found using an electronic saturation table database for water.

When the saturation temperature of the water on the plate surface the wall superheat, ΔT_{sat}, and cooling water subcooling, ΔT_{sub}, can be determinate using Equation (45) and Equation (46) respectively.

$$\Delta T_{sat} = T_{surface} - T_{sat} \tag{45}$$

$$\Delta T_{sub} = T_{sat} - T_{water} \tag{46}$$

4.4 IMAGE ANALYSIS

Video recordings of the tests were digitalized using a *DPS Personal Animation Recorder v1.2*. The recordings were processed with a frequency of 30 images a second. The digital images were analyzed using a *MES Ltd. Matrox Inspector v2.0*.

5

RESULTS AND DISCUSSION

In this study the effect of cooling water temperature and flow rate were investigated. The systematic tests done for this research are presented in Table 5-1. Additional tests were also done while developing test procedures and also to take a closer look at thermal profiles. Some duplicates of tests were done to evaluate reproducibility.

TABLE 5-1 Experimental array for DQSK steel and SS316 steel

	Flow rate (V_{ji})	30 °C	40 °C	50 °C
DQSK Steel	15 l/min (5.5 m/sec)	test 5	test 13	test 7
	30 l/min (5.7 m/sec)	tests 3,6	test 12	test 8
	45 l/min (6.0 m/sec)	test 10	test 9	test 11
SS316 Steel	15 l/min (5.5 m/sec)	tests 16,21	Interp.	test 18
	30 l/min (5.7 m/sec)	tests 14,15	Interp.	test 19
	45 l/min (6.0 m/sec)	test 17	Interp.	test 20

Jet velocity and jet diameter at impingement were corrected for the effect of gravity using Equation (40) and Equation (41). The corrected values are listed in Table 5-2.

TABLE 5-2 Jet velocities and diameters at impingement

Flow rate [l/min]	v_{ji} [m/s]	d_{ji} [mm]
15	5.5	7.6
30	5.7	10.6
40	6.0	12.6

Where v_{ji} is jet velocity at impingement and d_{ji} is jet diameter at impingement.

In this chapter the cooling curves (temperature versus time plots) and boiling curves (heat flux versus wall superheat plots) for a particular test are presented. Test #15 was chosen to demonstrate general trends that were observed during all tests. Comparison to correlations

found in the literature is shown and discussed. Visual observations are discussed and the relationship between measured values and visual observations is addressed. Test #3 was chosen to demonstrate what can be seen from first hand observations during tests and from video recordings of those tests. In the final two sections results on the effect of cooling water temperature and flow rate on heat flux are presented.

5.1 COOLING CURVES

Temperatures were measured inside and on the surface of the test plate while it cooled from 850-900°C to a temperature below 100°C. The cooling curves show the surface or internal measured temperature of the plate as a function of time, i.e. the raw data from the tests.

Figure 5-1 shows the surface cooling curves for test #15, which was performed using a SS316 steel plate with a water flow rate and temperature of 30 l/min and 30°C respectively. During the first few seconds, i.e. before the water jet was turned on, all the curves coincided. After the jets first hits the plate the surface temperatures changed rapidly and the cooling curves around the stagnation point dropped.

It can be seen that the curves for surface temperature at stagnation and at 5/8" (15.9 mm) away from the center coincide. This shows that the temperature at these two locations dropped at the same time and, approximately, at the same rate indicating that they are both located in a zone of relatively uniform heat flux. This zone is commonly referred to as the impingement zone but should not be confused with the hydrodynamic impingement zone, defined earlier.

The next location of measurement, at 1 1/4" (31.8 mm) away from the center, cools down a few seconds later putting it outside the strictly defined impingement zone. For this test the impingement zone seems to have a radius somewhat smaller than 31.8 mm or 1.67 times the nozzle diameter but larger than 15.9 mm or 0.84 nozzle diameters. This is a smaller value than reported by Liu [39] for a similar situation, i.e. $1.67 < r/d_j < 2.11$, but larger than reported

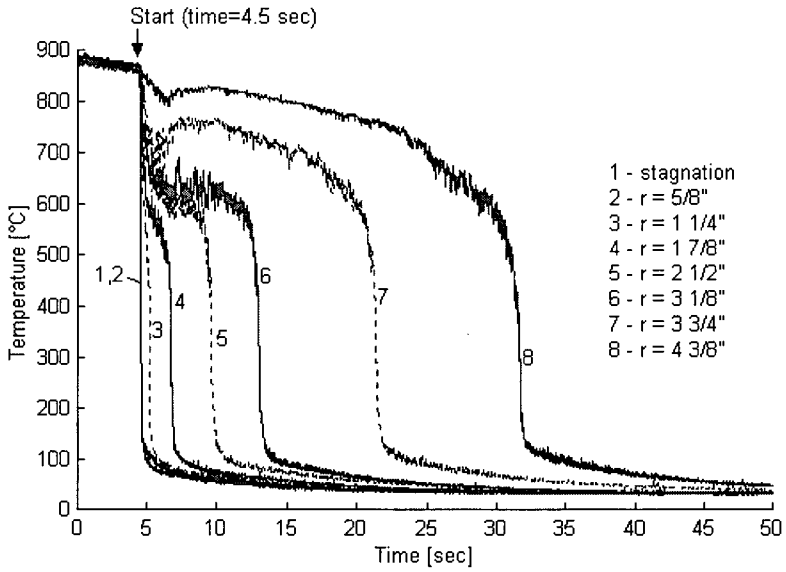

FIGURE 5-1 Measured surface temperature curves for cooling with 30°C water temperature and 30 l/ min flow rate, SS316 steel

by Stevens and Webb [12] for non-boiling heat transfer, i.e. $r/d_j < 0.75$. Liu used a lower sampling rate than is used in the current study and measured temperature inside the plate only. This might have an effect on the estimated size of the impingement zone.

Looking at curves numbered 4, 5 and 6, at distances of 1 7/8" (47.6 mm), 2 1/2" (63.5 mm) and 3 1/8" (79.8 mm) from the center respectively, relatively large temperature fluctuations can be seen. According to Collier [22], Kalinin et al. [5] and Xu et al. [48] fluctuations like these are seen in transition and nucleate boiling. Fluctuations are especially violent in transition boiling when instant wetting of the surface takes place randomly. Temperature measurements at 3 3/4" (95.3 mm) and 4 3/8" (111.1 mm) away from the center are shown by curves 7 and 8 on Figure 5-1 respectively. Surface temperature fluctuations as seen at locations 4, 5 and 6 can also be observed here but start at a later time. The magnitude of the fluctuations associated with each heat transfer mode was similar at all the locations. The fluctuations are small at first but become larger a few seconds before the rapid temperature drop. This behavior can be analyzed as discussed below.

Figure 5-2 shows a graph presented by Xu et al. [48] showing the fluctuations of surface temperature during forced convective subcooled boiling of Freon-113 on a flat stainless steel surface. In Figure 5-3 the surface temperature fluctuations at location 8 are shown for comparison. It can be seen that similar trends are present in the current data as seen in Figure 5-2 but the magnitude of fluctuations is different due to different testing conditions and techniques. The changes in magnitude of fluctuations seen in Figure 5-3 give an indication of the boiling mode over each time interval. Analysis of the temperature fluctuations can be used to help in boiling curves analysis as discussed in the following section. Timing and duration of each heat transfer mode depended on test parameters. Heat transfer modes can also be seen from boiling curves but this is an example of what can be seen directly from the raw data.

At each measurement location two temperatures were obtained, the surface temperature and the internal temperature. Figure 5-4 shows cooling curves for surface and internal temperatures at one location of measurement inside the impingement zone, at r = 5/8", for the same test case as in Figure 5-1. The surface curve on Figure 5-4 is hence the same curve as curve 2 in Figure 5-1 but drawn in a different time scale. The depth of the internal thermocouple was 1.22 mm at this location. By comparing the two curves in the first moments of cooling it can be seen that the surface temperature drops very rapidly but the internal temperature stays relatively constant to begin with and drops much slower than the surface temperature. This indicates that the temperature profile in the plate at this time is highly nonlinear.

In Figure 5-5 the measured temperatures at a distance of 4 3/8" (111.2 mm) from the center are presented, again for the same test case as in Figure 5-1 and Figure 5-4 with water jet temperature and flow rate of 30°C and 30 l/min respectively. The depth of the internal thermocouple was 1.38 mm at this location. Here it can be seen that the difference in temperatures is small at first, indicating low heat flux. Later the difference increases, along with increasing fluctuations, indicating higher heat flux. Again it can be seen that the temperature profile is likely to be nonlinear where the difference in temperature is changing rapidly.

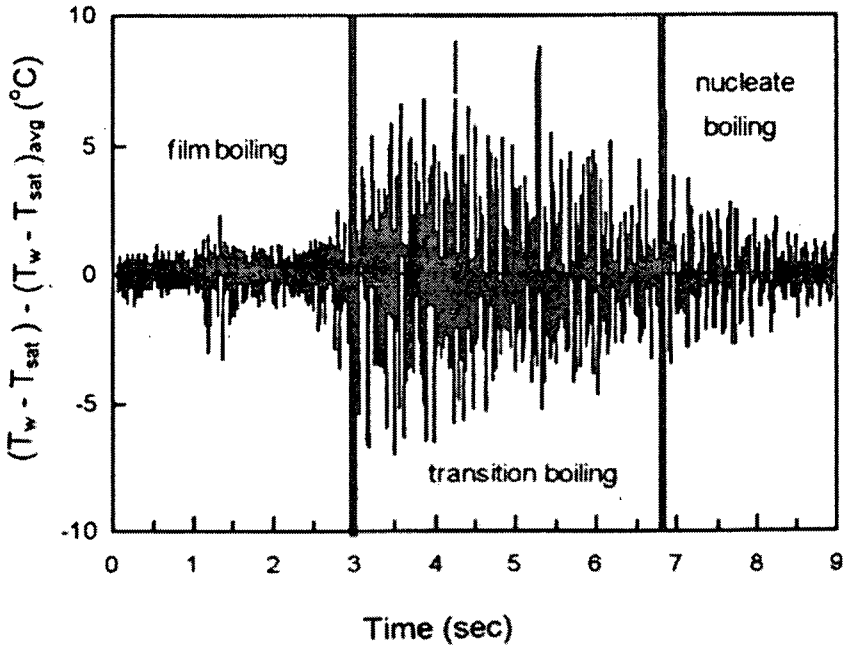

FIGURE 5-2 The magnitude of temperature fluctuations in the three boiling regimes for Freon-113 flowing on a flat stainless steel surface [48]

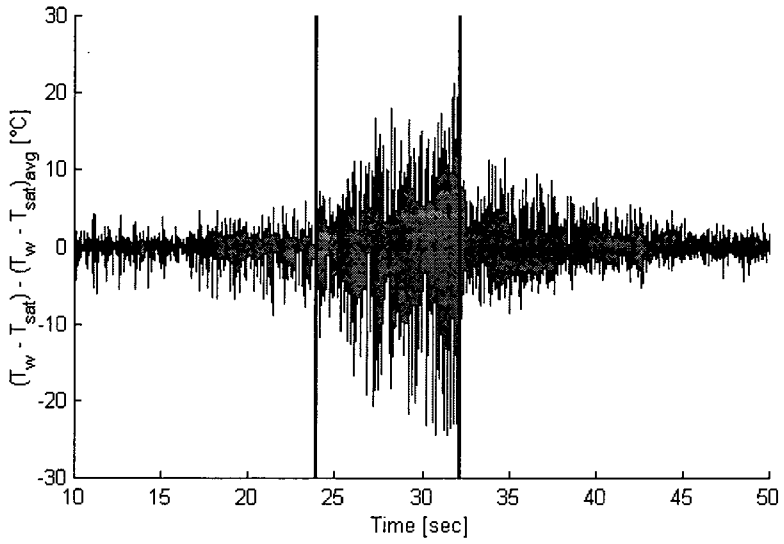

FIGURE 5-3 Magnitude of surface temperature fluctuations at location 8. SS316 plate and flow rate and water temperature of 30 l/min and 30°C respectively

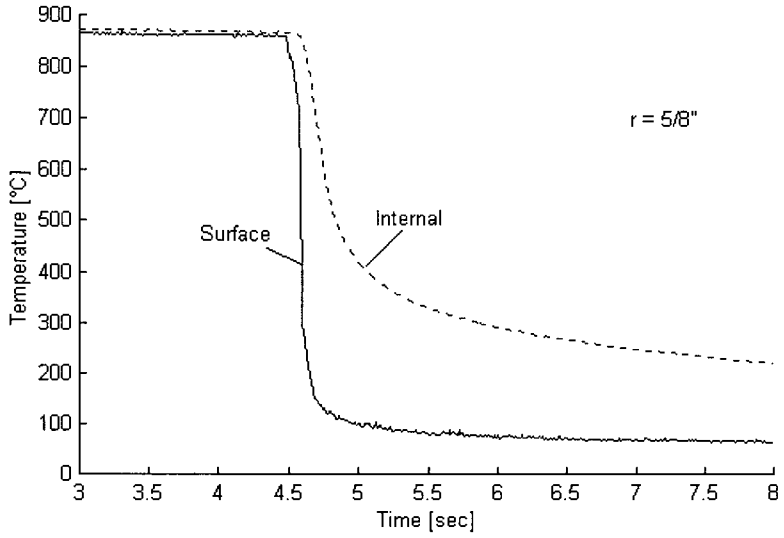

FIGURE 5-4 Surface and internal temperatures inside the impingement zone.

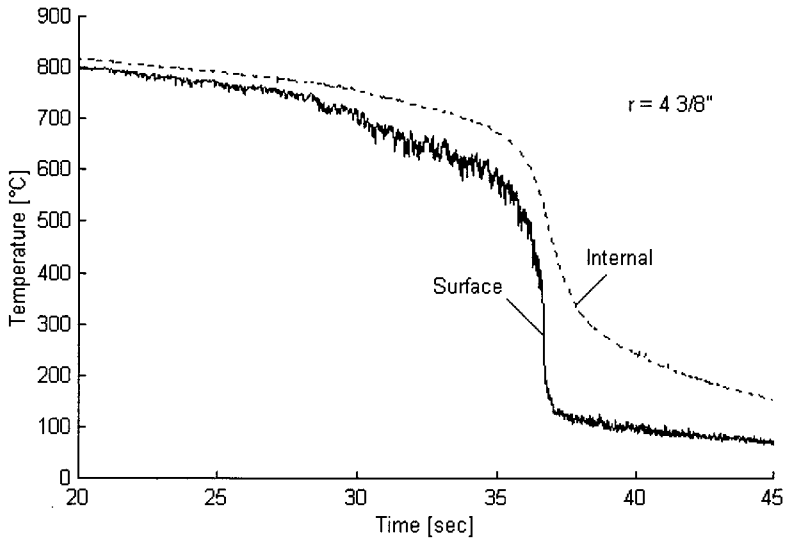

FIGURE 5-5 Surface and internal temperatures at r = 4 3/8" (111.1 mm) from stagnation, outside the impingement zone.

The graphs presented here are just a sample of what can be seen from the raw data taken from all the tests. Similar trends as these were seen in data from all tests.

5.2 BOILING CURVES

Boiling curves are heat flux versus ΔT_{sat} plots that can be drawn for each measurement location in the tests. These curves are useful when comparing heat transfer at various locations within the same test as well as when comparing tests.

Figure 5-6 b) shows boiling curves for various locations on a SS316 test plate cooled using a water temperature and flow rate of 30°C and 30 l/min respectively. On Figure 5-6 a) heat fluxes at all locations for the same test are drawn as a function of time. The boiling curves at locations 1 and 2 are almost identical and the maximum heat flux takes place at the same time for both locations. This shows that in this case the heat transfer is basically the same at these locations. At location 3 the maximum heat flux was only about half of what was seen in the impingement zone. The maximum heat flux was also observed to decrease with increased distance from stagnation at locations 4, 5 and 6 but seems to level out at that point and was approximately constant at locations 6, 7 and 8. The point of maximum heat flux was also observed to shift to a lower ΔT_{sat} value at locations far away from stagnation, from around 450°C at stagnation to around 250°C at location 8 at 111.1 mm radial distance from stagnation.

Data obtained by Kumagai et al. [35], which was presented in Figure 2-7, shows boiling curves at stagnation and various locations away from stagnation. These curves show similar trends as seen in Figure 5-6 b), i.e. decrease in maximum heat flux and the ΔT_{sat} value at the point of maximum heat flux with increasing distance from stagnation. The exact values given by the boiling curves in Figure 2-7 are however not directly comparable with the data from the present study as testing conditions are different.

The data points on Figure 5-6 b) were drawn at a time interval of 0.01 seconds. Noting how far apart the points are at locations close to and at stagnation shows how rapid the cooling

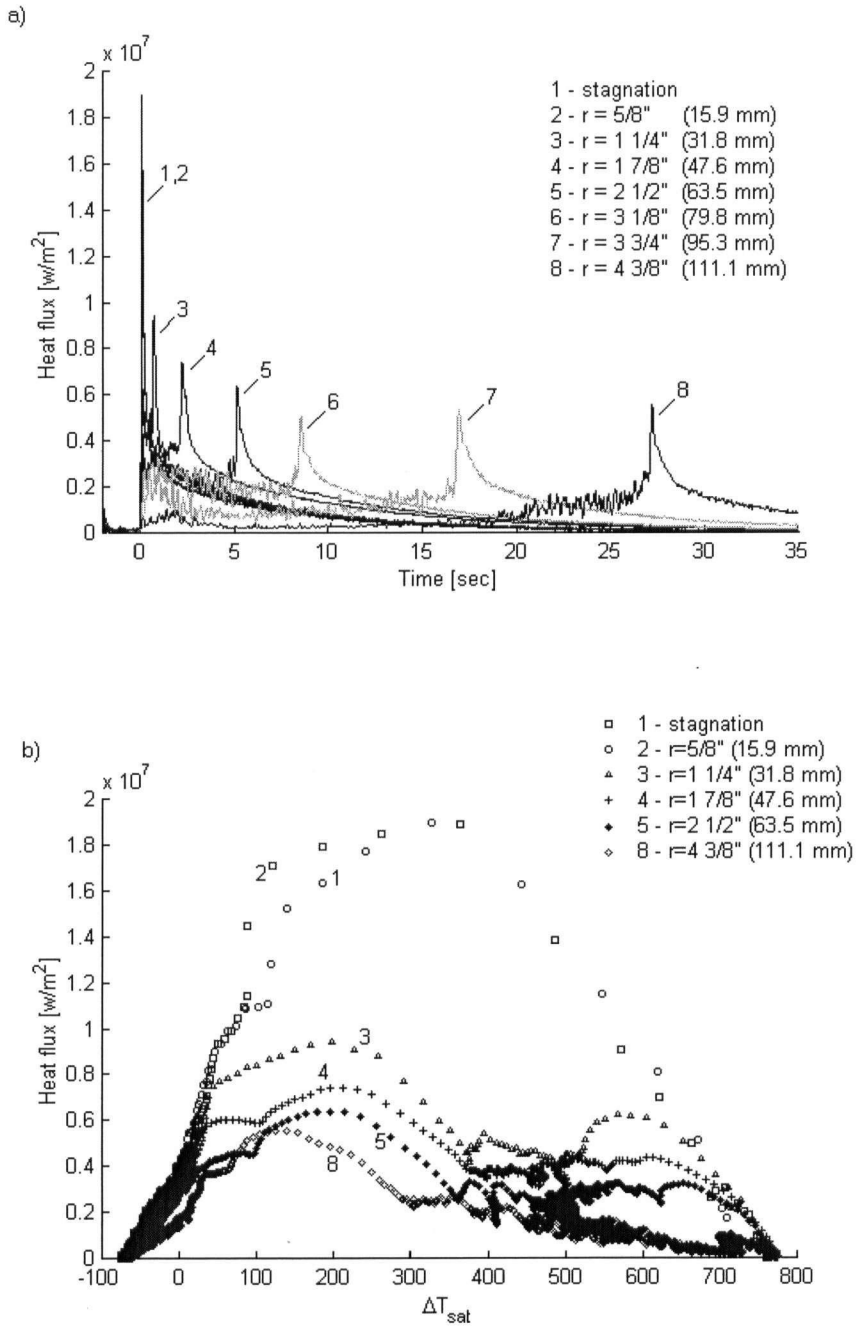

FIGURE 5-6 Test done on a SS316 plate with water temperature and flow rate of 30°C and 30 l/min respectively. a) Heat fluxes at all locations of measurement as a function of time, b) boiling curves for locations 1, 2, 3, 4, 5 and 8.

is at those locations. At locations further away the cooling is slower and the shift in the point of maximum heat flux gradually decreases.

Boiling curves for locations outside the stagnation area, specifically curves marked 3, 4 and 5 in Figure 5-6, show two heat flux peaks, one at around 600°C and another at around 200°C wall superheat. The peak at 200°C is the larger of the two and represents the point of critical heat flux and hence the transition between transition and nucleate boiling, discussed earlier. The behavior in the vicinity of the peak at around 600°C wall superheat is, however, not as clear. From first hand visual observations during the tests, it could be seen that in the first moments after initial impingement, the water flows parallel to the plate radially from the center to the outer edge. During this time, the flowing water was relatively close to, but not in direct contact with, the plate at locations outside the impingement zone. One could speculate that radiation to the surroundings, and forced convection to the air and vapor due to the flowing water, are the governing modes of heat transfer during this time. This would explain the relatively high heat transfer in the first moments of cooling. A few seconds later, depending on test parameters, violent boiling started around the impingement zone, (see discussion in Section 5.4). The bubbles on the surface formed a wedge that directed the water away from the plate so it flowed in an arc rather than parallel to the plate. The water stream was than further away from the surface so the effect of the water flow on the forced convection decreased. This, along with less radiation due to the decreasing temperature difference between the surface and surroundings, could partly explain the decreasing heat flux with decreasing wall superheat in the 600°C to 500°C wall superheat range.

The trends seen here were present in all tests. The maximum heat flux at locations 1 and 2 was considerably higher than elsewhere on the plate in all tests results. The shift in the ΔT_{sat} value at the point of maximum heat flux was also observed in data from all tests as well as the approximately constant maximum heat flux at the outermost locations. The second peak in heat flux at locations outside the impingement zone was consistently seen in all the tests.

To take a closer look at boiling curves outside the stagnation area curve number 8 is extracted from Figure 5-6 b) and shown in Figure 5-7. The vertical lines represent the change from one heat transfer mode to another determined by using the fluctuation analysis shown in Figure 5-3.

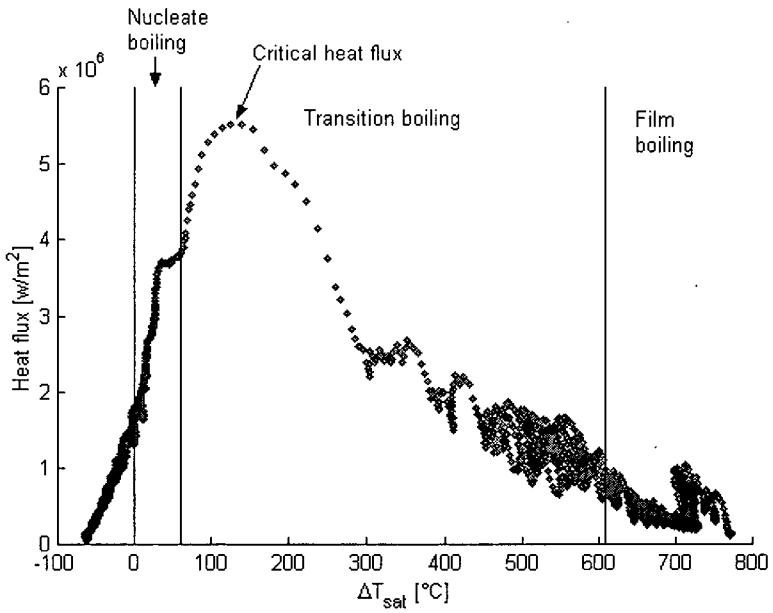

FIGURE 5-7 Boiling curve at 4 3/8" (111 mm) from stagnation. SS316 steel and water temperature and flow rate of 30°C and 30 l/min respectively.

According to the fluctuation analysis the alleged change from transition boiling to nucleate boiling, at a wall superheat of approximately 60°C, coincides with the beginning of the first transition region suggested by Miyasaka et al. [16]. Compared with experimental data it does not overlap with the location on the critical heat flux. One can speculate that it rather points out the onset of significant bubble coalescence. Larger vapor blankets on the right hand side of the transition line (close to the critical heat flux) produce larger temperature fluctuations, as shown in Figure 5-3.

In Figure 5-3 the surface temperature fluctuations do not change as drastically at the transition from film to transition boiling as was observed between transition and nucleate boiling. This makes it more difficult to clearly locate the point of transition from film to transition

boiling. Furthermore this point of transition is commonly seen as a point of minimum heat flux, referred to as the Leidenfrost point. This could not be seen here as the heat flux gradually increased during the transition. This apparent absence of the point of minimum heat flux and stable film boiling is discussed in more detail in Section 5.4.

5.3 COMPARISON WITH CORRELATIONS

In this section two sets of current experimental data will be compared to relevant correlations found in the literature and reviewed in chapter 2. The two test results chosen for comparison represent the two extreme cases found in the testing array. One test performed using the highest flow rate and lowest water temperature, giving the highest heat flux, and the other using the lowest flow rate and highest water temperature, resulting in the lowest heat flux.

5.3.1 Nucleate boiling

Most nucleate boiling correlations found in the literature for jet impingement boiling have the same form, given by Equation (47).

$$q'' = A \cdot \Delta T_{sat}^{\ m} \tag{47}$$

In Figure 5-8 nucleate boiling correlations are presented along with data from the current study. All these correlations were developed using data from steady state experiments and were all shown to fit data obtained during liquid jet impingement. Various values of the constants A and m in Equation (47) have been reported by researchers and are given in Table 5-3. The various studies are reviewed in detail Section 2.2.3.

TABLE 5-3 Nucleate boiling correlations

Correlation	A	m
Monde et al. [11]	450	2
Ishigai et al. [38]	42	3.2
Miyasaka et al. [16]	79	3
Wolf et al. [14]	63.7	2.95
Ruch et al. [6]	4.5*	1.95

*properties at atmospheric pressure

The correlations reported by Monde et al. [11], Ishigai et al. [38] and Miyasaka et al. [16] are given by lines 1, 2 and 3 on Figure 5-8 respectively. These correlations show trends that differ significantly from the current data. Ishigai et al. investigated both steady state and transient cooling and a sample of their data is shown in Figure 2-11 on page 26. Although the current data is not directly comparable to their data due to different test parameters, the same phenomenon can be seen in Figure 5-8 and Figure 2-11, i.e. the steady state results indicate stronger dependence on wall superheat than the transient results. The correlations presented by Wolf et al. [14] and Ruch et al. (see Wolf et al. [6]) for fully developed nucleate boiling during jet impingement are given by lines 4 and 5 respectively. The trends seen here are much closer to what is seen in the current data but the correlations greatly underestimate the heat flux.

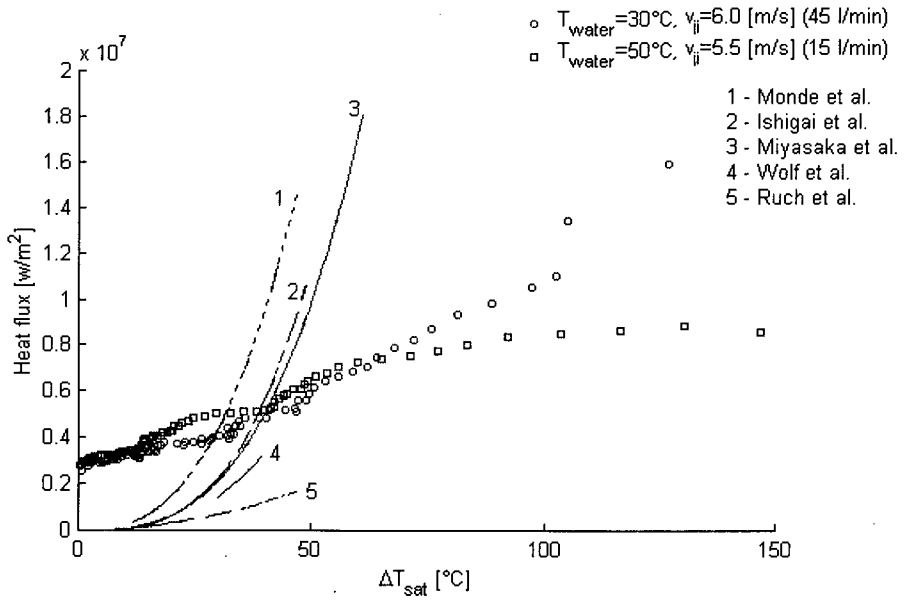

FIGURE 5-8 Comparison between experimental data and correlations in the nucleate boiling region

The current results support what has been reported by various researchers that the wall superheat is the effective driving force of heat flux during fully developed nucleate boiling but the effect of subcooling and jet velocity is relatively small, [6]. The fully developed nucleate

boiling correlations found in the literature are usually valid for wall superheat in the range from 8°C to 60°C.

Chen type correlation for nucleate boiling

The correlation for convective boiling presented by Chen (1966), see Collier [22] and Section 2.2.3, has the general form given by Equation (48).

$$h_{tp} = h_{FC} \cdot F + h_{NB_{pool}} \cdot S \tag{48}$$

Where h_{tp}, h_{FC} and h_{NB} stand for two-phase, forced convective and nucleate boiling heat transfer coefficients, respectively. *F*, always greater than unity, is an enhancement factor accounting for the enhancement of heat transfer due to increased velocities in a two phase flow. *S*, always less than unity, is a suppression factor that accounts for the suppression of the thermal boundary layer (or temperature gradient in the liquid) due to the flow.

A correlation of this type can be adopted to the current situation by adapting appropriate correlations for the forced convective and the nucleate pool boiling parts. The forced convective Dittus-Boelter correlation suggested by Chen (1966) is not suitable for the current case as it is developed for flow in a pipe. The correlation for stagnation point Nusselt number during single phase heat transfer to an impinging jet presented by Vader et al. [33] and given by Equation (5) can be used for the forced convective part in a Chen type correlation. The Forster and Zuber correlation for nucleate pool boiling suggested by Chen (1966) can be applied to the current data. The enhancement factor, *F*, and suppression factor, *S*, were given in graphical form by Chen (1966). The values for *F* and *S* will change if correlations for h_{FC} or h_{NB} are changed.

A Chen type correlation has been developed for the heat flux during nucleate boiling at the stagnation point using the current DQSK steel data. The data was correlated for a wall superheat range from around 8°C to 60°C. These wall superheats have been reported by other researchers to cover the fully developed nucleate boiling range [16]. No clear indications were

seen at the transition from partial nucleate boiling to fully developed nucleate boiling in the current data. A change in slope of the boiling curve in the nucleate boiling region was consistently observed in the current stagnation point data at around 60°C. This is in agreement to the beginning of the first transition region as discussed by Miyasaka et al. [16]. The correlation can be written in the form given by Equation (49).

$$q''_{total} = h_{FC} \cdot (T_{surface} - T_{water}) \cdot F + h_{NB_{pool}} \cdot \Delta T_{sat} \cdot S \tag{49}$$

Where h_{FC} is derived from the stagnation jet impingement Nusselt number correlation presented by Vader et al. [33]

$$h_{FC} = 0.28 \cdot Re_{ji}^{0.58} \cdot Pr^{0.4} \cdot \frac{k_f}{d_{ji}} \tag{50}$$

and h_{NBpool} is found using the Forster and Zuber nucleate pool boiling correlation.

$$h_{NB_{pool}} = 0.00122 \cdot \left(\frac{k_f^{0.79} \cdot c_{p_f}^{0.45} \cdot \rho_f^{0.49}}{\sigma^{0.5} \cdot \mu_f^{0.29} \cdot h_{fg}^{0.24} \cdot \rho_g^{0.24}} \right) \cdot \Delta T_{sat}^{0.24} \cdot \Delta P_{sat}^{0.75} \tag{51}$$

The enhancement factor F is defined as the ratio of the single phase heat transfer coefficients in the two phase flow and in a single phase flow. This ratio can in this case be simplified to a ratio of Reynolds numbers, see Equation (52). The exponent on the Reynolds number ratio, n, depends on the single phase convection used.

$$F = \frac{h_c}{h_{FC}} = \left(\frac{Re_{TP}}{Re_f} \right)^n \tag{52}$$

Where h_c is the convective part of the two phase heat transfer coefficient as defined by Chen (1966) and h_{FC} is the single phase convective heat transfer coefficient. Re_{TP} is the Reynolds number of the enhanced two phase flow and Re_f is the Reynolds number of the flow if it were single phase.

The suppression factor, S, is defined as the ratio of the mean superheat, ΔT_{mean}, to the wall superheat, ΔT_{sat}, see Equation (53). The exponent, n, depends on the correlation used for the pool boiling part of the correlation. Using the Forster and Zuber correlation gives n=0.24.

$$S = \left(\frac{\Delta T_{mean}}{\Delta T_{sat}}\right)^{n} \tag{53}$$

At the stagnation point there is no regular thermal boundary layer developing as the jet impinges the plate vertically. Temperature gradient is nonetheless present in the water and boiling is taking place. In this case the S factor accounts for the suppression of this temperature gradient due the impinging jet.

The procedure used to successfully adopt the above correlation to the current DQSK steel nucleate boiling data was as follows:

1 A set of *S* and *F* factors was found for each test. This was done by minimizing the square error between a correlation of the form given by Equation (49) through Equation (51) and the experimental data by changing *S* and *F*.

2 The effect of jet velocity and subcooling on the factors was analyzed. It was found that jet velocity has a dominating effect on the enhancement factor, *F*, and that subcooling has a dominating effect on the suppression factor, *S*.

3 Correlations of power form were developed for *S* and *F*. A least square error method was used.

The correlated values are given graphically in Figure 5-9 along with the discrete point values of *F* and *S* for individual tests. The power equations that correlate the factors are given by Equation (54) and Equation (55).

$$F = 15.47 \cdot u_j^{-1.22} \tag{54}$$

$$S = 249.8 \cdot \Delta T_{sub}^{-1.597} \tag{55}$$

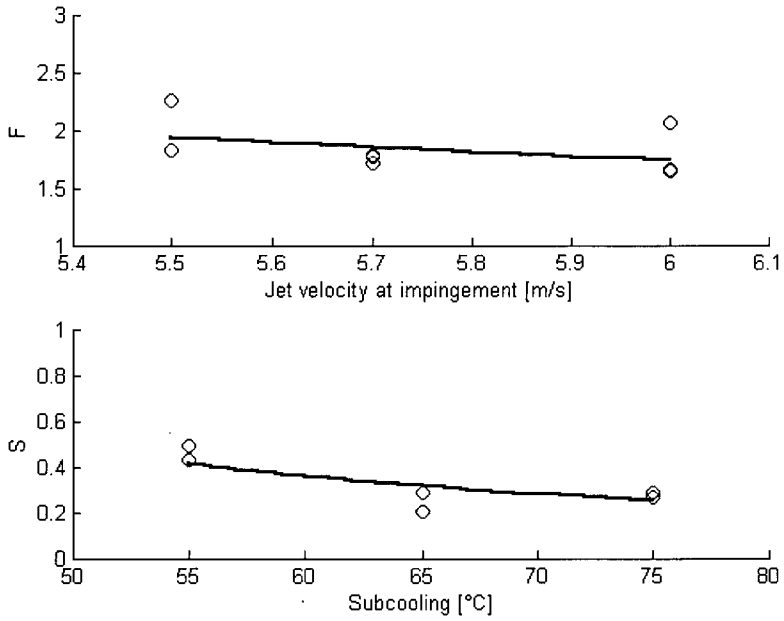

FIGURE 5-9 Enhancement, F, and suppression, S, factors for Chen type correlation of the current data in the nucleate boiling region

On Figure 5-10 the present correlation is compared to a typical set of experimental DQSK steel data. The average error between the experimental data and the correlation was less than 7.3% for all tests and the maximum error for an individual data point was 28%.

Here F is at the order of 2 and n=0.58, see Figure 5-9 and Equation (50). In the Dittus-Boelter correlation commonly used in Chen correlation n=0.8. Using these n values one can find the corresponding F factor in the original Chen correlation to be approximately 2.6. According to Chen's graphical representation of F as a function of Martinelli factor, X_{tt}, this yields a Martinelli factor in the range 0.5 to 1, [22], that again yields steam quality of approximately 2 to 5%.

A similar correlation was not developed for the SS316 steel data as measurements were only made for two different cooling water temperatures of 30°C and 50°C. Therefor the effect of water temperature could not be analyzed in a similar way as described above.

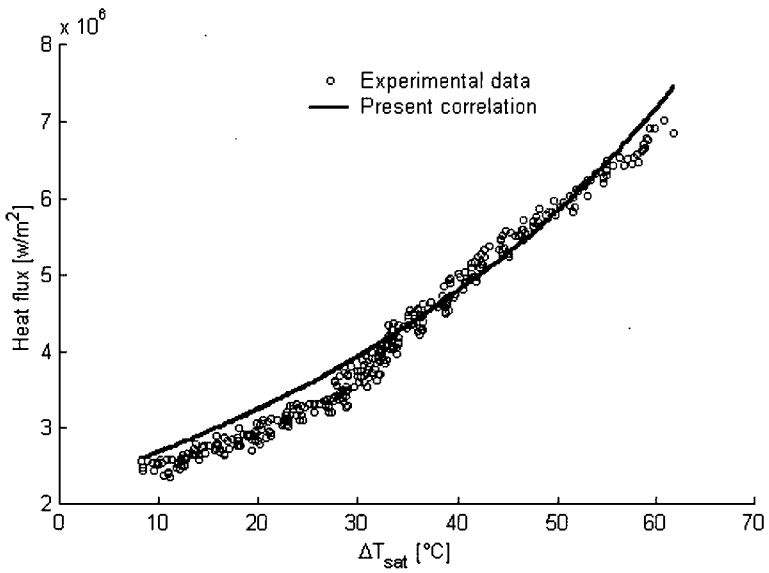

FIGURE 5-10 Comparison between a Chen type correlation and experimental data for DQSK steel and water flow rate and temperature of 30 l/min and 50°C respectively

No applications of Chen type correlations for nucleate boiling were found in the current jet impingement literature. The correlation proposed above was developed to demonstrate that a correlation of this type can be applied to the current problem. It correlates the current data well but further research would be needed to develop a correlation that could be used with confidence at different jet velocities and subcooling.

5.3.2 Critical heat flux

On Figure 5-11 experimental results are plotted along with correlations developed by Miyasaka et al. [16] and Ishigai et al. [19]. The simple critical heat flux correlation for jet impingement at stagnation presented by Ishigai et al. [19] and given by Equation (56) is plotted on Figure 5-11 for the present test conditions as lines marked 4 and 4^*. This correlation correlated their experimental data for a circular water jet impinging on a flat surface. Their research is reviewed in detail in Section 2.2.4. The correlation consistently underestimates the current

data at the point of critical heat flux by about 20% to 40% depending on steel type and test conditions.

$$q''_{CHF} = 0.0142 \cdot 10^6 \cdot \left(\frac{v_{ji}}{d_j}\right)^{0.34} \cdot \Delta T_{sub}^{1.15} \quad (56)$$

Miyasaka et al. [16] elaborated about the existence of two transition regions from fully developed nucleate boiling towards the point of critical heat flux. They presented correlations for heat flux in those boiling regions at stagnation during subcooled water jet impingement given earlier by Equation (21) through Equation (25). These correlations are plotted on Figure 5-11 and can be observed to consistently overestimate the heat flux. The trends given by the correlations are, however, similar to the trends seen in the experimental data for the same wall superheat. Miyasaka et al. [16] also presented a correlation for the critical heat flux during jet impingement, shown as lines marked 3' and 3* on Figure 5-11. They defined the critical heat flux in an unconventional way as the heat flux at departure from fully developed nucleate boiling but not as the maximum heat flux. Due to this definition the value given by the correlation is not comparable to the experimentally found maximum heat flux.

5.3.3 Transition boiling

As noted earlier transition boiling is the least understood of all boiling regimes. It is a combination of unstable nucleate boiling and unstable film boiling. One could speculate that an efficient way to correlate transition boiling data would be to use the general form given by Equation (57) i.e. an addition of heat flux at solid vapor contact and heat flux at liquid solid contact. This form has been used by authors in the transition pool boiling literature [40]. No correlations for heat flux during transition boiling were found in the jet impingement literature reviewed.

$$q'' = C_1 \cdot q_f'' + C_2 \cdot q_g'' \quad (57)$$

Where q''_f and q''_g are heat fluxes at liquid and vapor contact respectively.

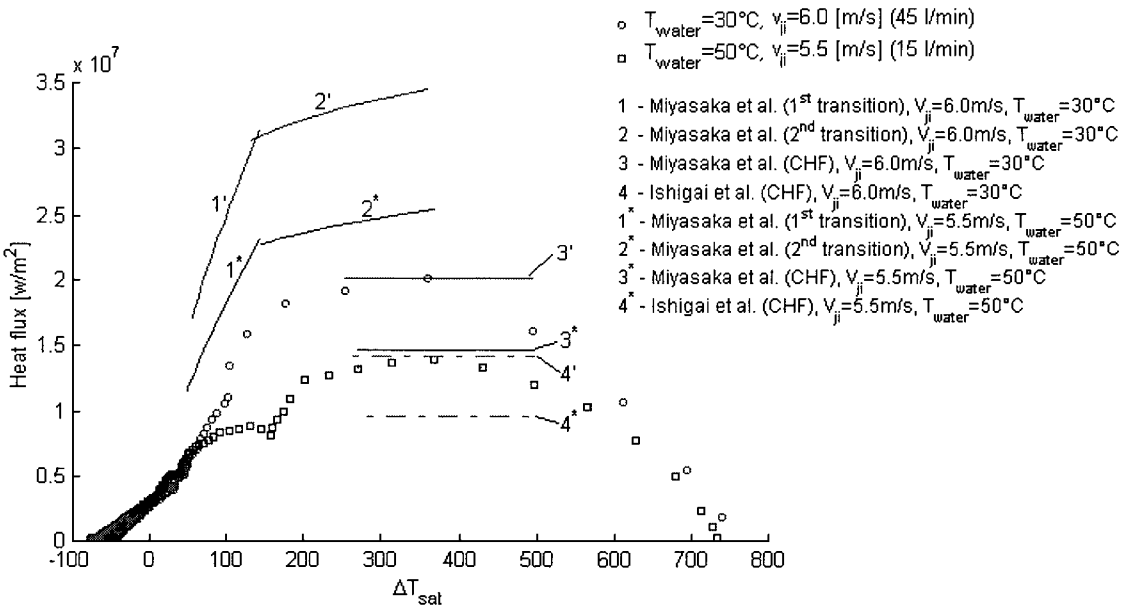

FIGURE 5-11 Comparison between experimental data and correlations for critical heat flux and the first and second transition region

In Figure 5-12 experimental data is compared to a correlation for transition pool boiling presented by Kandlikar et al. [40] having the general form given by Equation (57). The correlation is given in detail and discussed in Section 2.2.5. This correlation requires that the value of the minimum heat flux at stagnation is known. The minimum heat flux value at stagnation could not be obtained from the current data. The correlation for minimum heat flux at stagnation presented by Ochi et al. [9] was used instead (see Equation (31)). The correlation does not reflect the anticipated behavior in the transition boiling region.

It is beyond the scope of the current study to analyze the mechanism of transition boiling and no attempt will be made to develop a correlation for the heat flux during transition boiling. The author, however, believes that a correlation of the form given by Equation (57) would be a good starting point in development of a correlation due to the nature of transition boiling as discussed earlier.

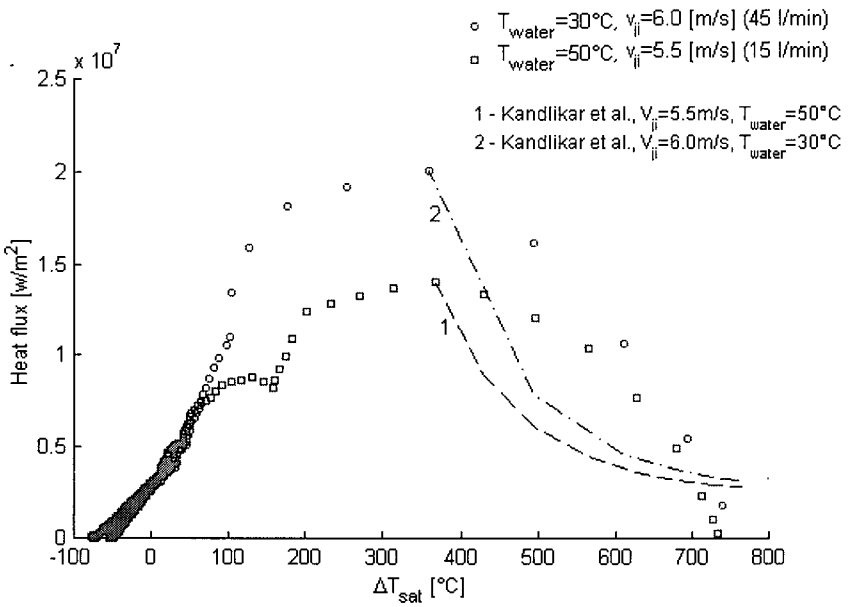

FIGURE 5-12 Comparison between experimental data and correlations for transition boiling.

5.4 VISUAL OBSERVATIONS

The cooling process for each test was video-recorded and those recordings along with first hand observations during the tests were used for data evaluation.

When the plate was removed from the furnace it was bright red in color and at a temperature of approximately 920°C. In the time it took to move the plate from the furnace and position it under the nozzle, no color change of the plate was visible. The temperature drop of the plate was of the order 50°C during the move. When the impinging water jet hit the plate it darkened around the stagnation point immediately, i.e. it turned gray. One can speculate that the gray color indicates the presence of vapor bubbles on the solid surface. Outside the darkened zone the plate was still red hot. This indicates that there was very limited or no direct liquid solid contact in that area as even small droplet reaching the surface have been observed to result in small dark spots on the surface. Considerable evaporation of the cooling water occurred and vapor could be seen rising from the plate.

Shortly after the start of cooling the gray area around the impingement zone began to turn black and progress radially outwards. The progression of the black zone was very rapid inside the initially gray zone. As the black zone was growing inside the gray zone the gray zone was also growing but considerably slower. When the size of the black zone got close to the size of the gray zone the two zones grew at approximately the same rate. Hence, while the plate was being cooled there was a circular black zone around the center of the plate, a relatively small grey circle around the black zone and then finally a bright red zone outside the gray zone.

Because of the violent boiling in the grey zone the water was observed to be diverted off the plate approximately where the gray and red zones met. The rest of the plate therefore seemed to be in little or no direct contact with the cooling water. In this context it is interesting to look at cooling curve number 8 in Figure 5-1. There it can be seen that the slope of the cooling curve before and after the start of impingement is essentially the same. Ignoring the relatively small temperature drop in the first few seconds of cooling the cooling curve from 10 to 24 seconds is basically an extension of the curve before impingement. This indicates that the water has only a limited effect on the heat transfer at the location furthest away from stagnation during this time and the modes of heat transfer were the same as before impingement, radiation and free convection to air.

Figure 5-13 through Figure 5-17 on the following pages show the connection between the black, gray and red zones, observed on the plate during cooling, and the surface temperature and heat flux at different times and locations in the zones. On Figure 5-13 the temperatures and heat fluxes for locations 1, 3 and 4 are shown for the first 7 seconds of cooling. On Figure 5-14 through Figure 5-17 the temperature and heat flux at all locations, except number 7 which did not work in this test, along with a picture of the plate at a given time are shown. The times at which the pictures are taken are shown as vertical lines on Figure 5-13 along with a vertical line showing the time of initial impingement, at time = 0 s.

Figure 5-14 shows the conditions at 0.16 s after the start of impingement. At this time location 3 is approximately at the boundary between the gray zone and the red zone. A rapid temperature drop is seen at the location and a steep rise in heat flux associated with it. At this time no black zone is seen, only a relatively large gray zone reaching all the way to location 3 (at approximately 32 mm from stagnation). Figure 5-15 shows the conditions at 2.10 s after the start of impingement. Now location 4 is approximately at the boundary between the gray and red zones. A similar effect can be seen here as was seen earlier for location 3 but of lower magnitude. Figure 5-16 and Figure 5-17 show conditions at 2.63 s and 6.10 s respectively. At 2.63 s location 3 was observed to be at the boundary of the gray and black zones and at 6.10 s location 4 was observed to be at the same boundary. From these figures it can be seen that ΔT_{sat} at the boundary of the gray and red zones was around 500°C, whereas ΔT_{sat} at the boundary between the gray and black zones can be observed to be around 40°C.

From these graphs, and from further observations of pictures and data not presented here, one can see that no dramatic changes in ΔT_{sat} or heat flux are seen as the point of measurement goes from the gray to the black zone. Furthermore it is apparent that some boiling is taking place in the black zone, (as $\Delta T_{sat} > 0$), and that the point of maximum heat flux is located somewhere in the gray zone, not necessarily on its boundaries. This indicates that the mode of heat transfer in the gray zone was possibly film boiling at the outer edge of the zone and then transition boiling and finally fully developed nucleate boiling at the inner edge. Transition to partial nucleate boiling is likely taking place in the black zone close to the boundary. The location of the critical heat flux could not be clearly located visually in the gray zone. Singlephase convection takes over somewhat later during the test. On Figure 5-17, at 6.10 seconds, ΔT_{sat} at location 3 is decreasing to below 0°C and from the figure it can be seen that the point of measurement is well inside the black zone. No change in appearance of the black zone was observed with the naked eye following the change to single phase convection.

It should be noted that the progression of the black and gray fronts and their relative size depends on testing conditions, but the same phenomenons and fundamental behavior as discussed here was seen consistently in the tests.

In the zone close to stagnation the velocity gradient of the flow is evident and the narrowing of the water jet from the nozzle exit to the point of impingement is also noticeable with the naked eye. This narrowing of the water jet is due to gravitation. At high flow rates violent turbulent behavior was apparent in the flow from the nozzle exit towards the plate. Due to instability in the flow the point of impingement to vary a little bit around the preset location. The variation is small, of the order of a few millimeters on the surface of the plate for the highest flow rate used, i.e. 45 l/min. This slight variation will be ignored in processing the data and the point of stagnation will be taken as the center of the plate, i.e. measurement location 1.

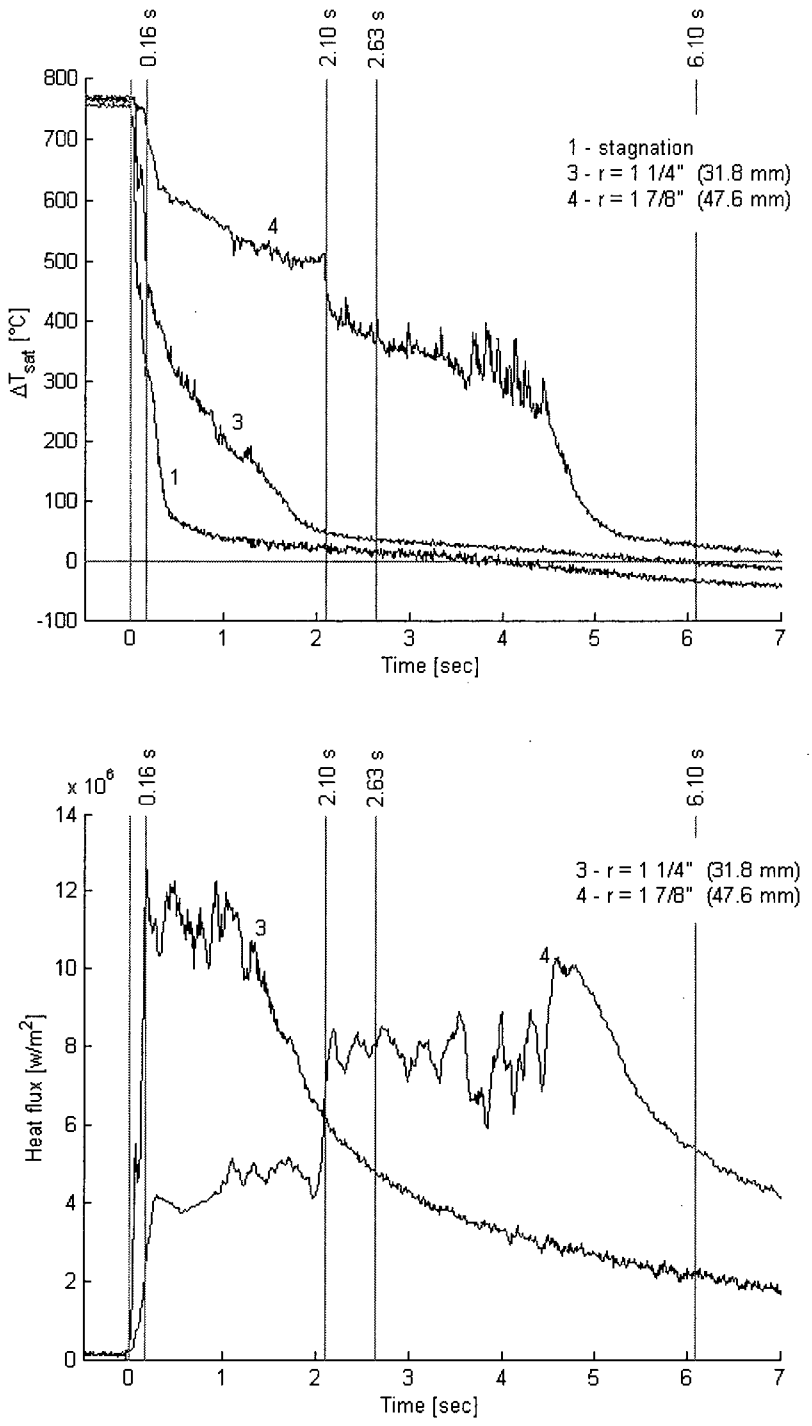

FIGURE 5-13 Cooling curves and heat flux curves at locations 1, 3 and 4 for a DQSK steel plate. Flow rate and water temperature of 30 L/min and 30°C respectively (test #3)

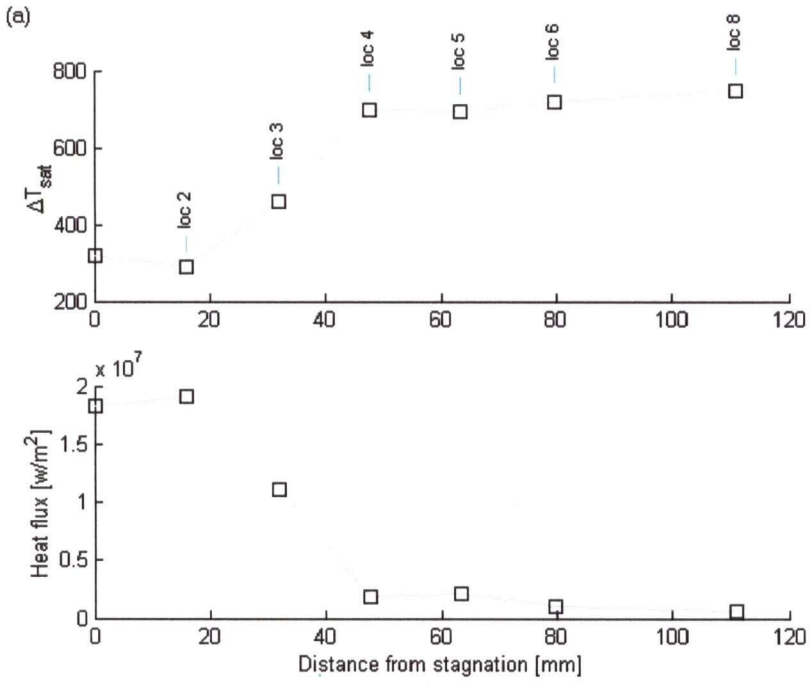

(b)

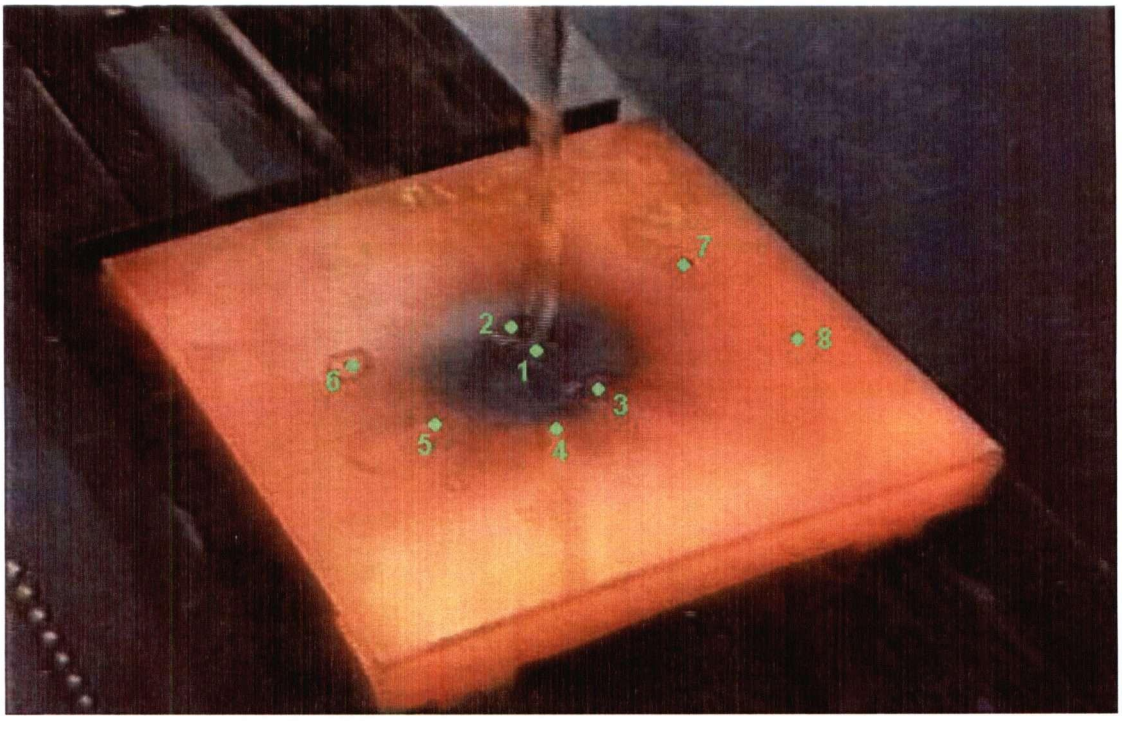

FIGURE 5-14 Conditions at 0.16 seconds from start of impingement. (a) Temperature and heat flux at locations of measurement (b) test plate at time 0.16 s. Test performed using a DQSK steel plate and flow rate and water temperature of 30 L/min and 30°C respectively (test #3)

(a)

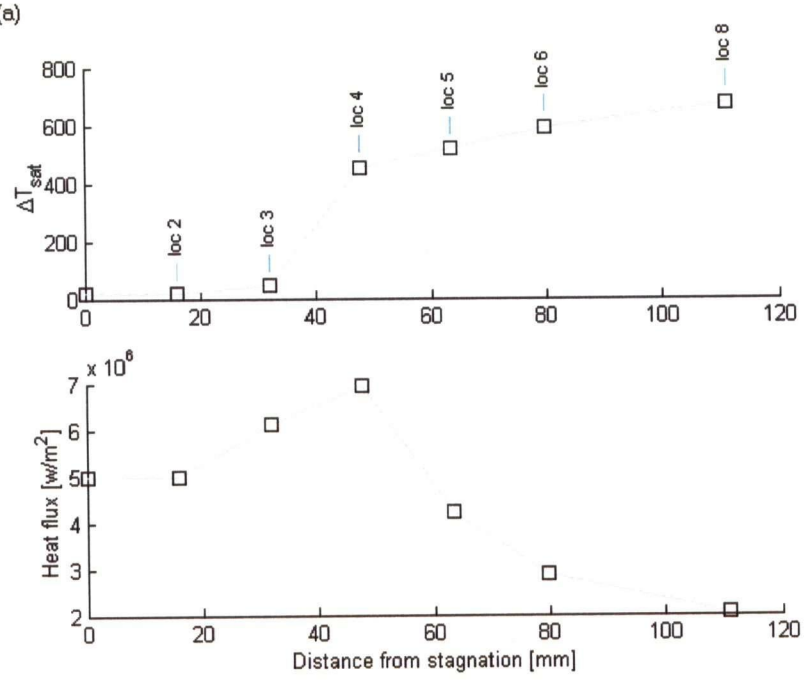

(b)

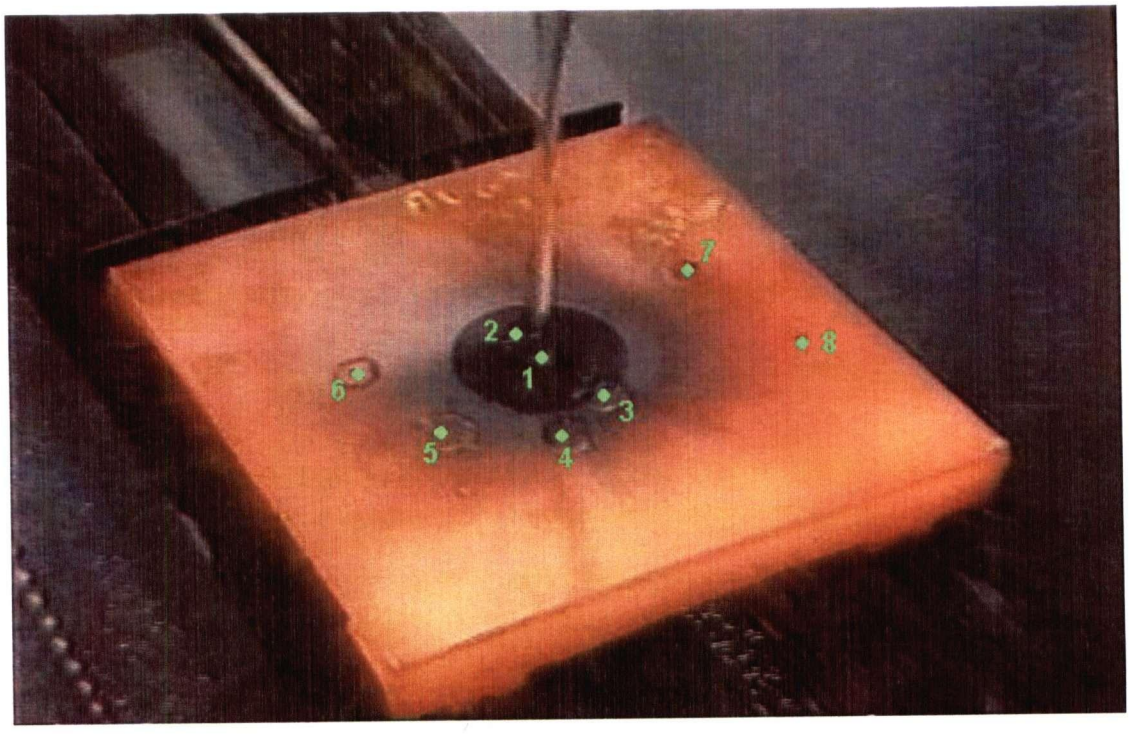

FIGURE 5-15 Conditions at 2.10 seconds from start of impingement. (a) Temperature and heat flux at locations of measurement (b) test plate at time 2.10 s. Test performed using a DQSK steel plate and flow rate and water temperature of 30 L/min and 30°C respectively (test #3)

(a)

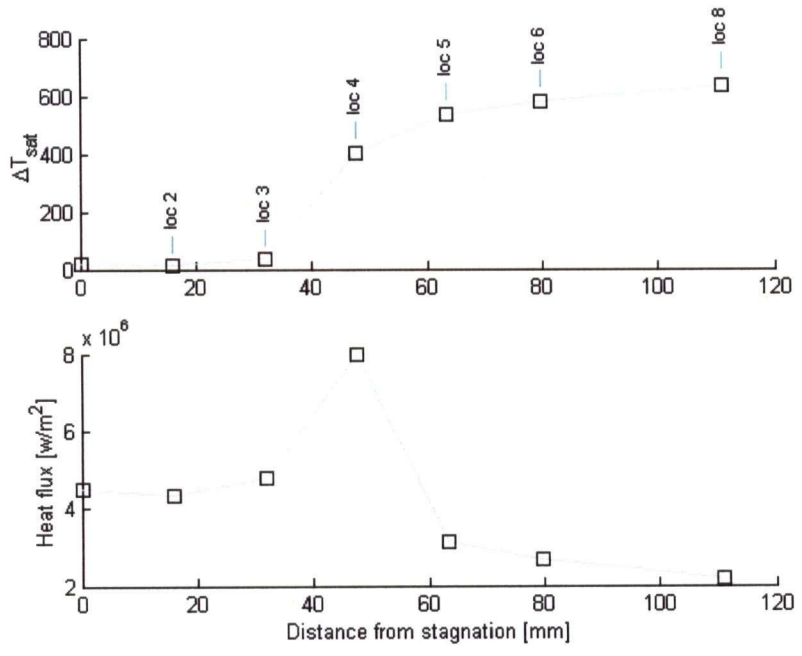

(b)

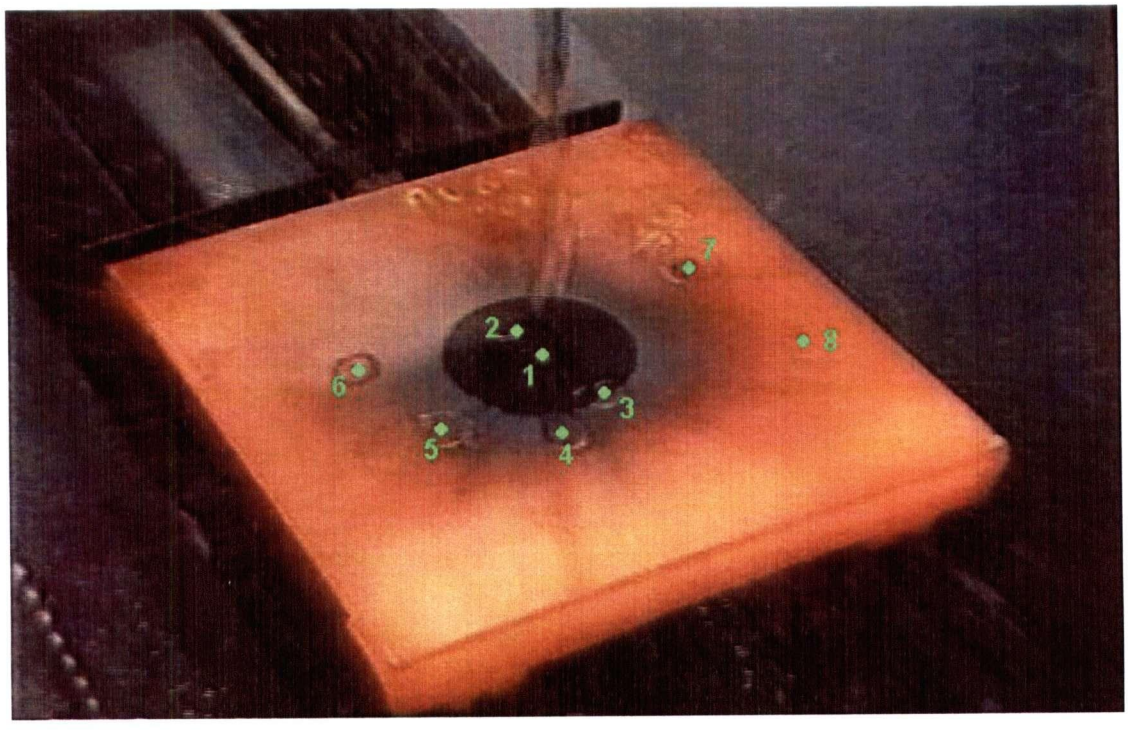

FIGURE 5-16 Conditions at 2.63 seconds from start of impingement. (a) Temperature and heat flux at locations of measurement (b) test plate at time 2.63 s. Test performed using a DQSK steel plate and flow rate and water temperature of 30 L/min and 30°C respectively (test #3)

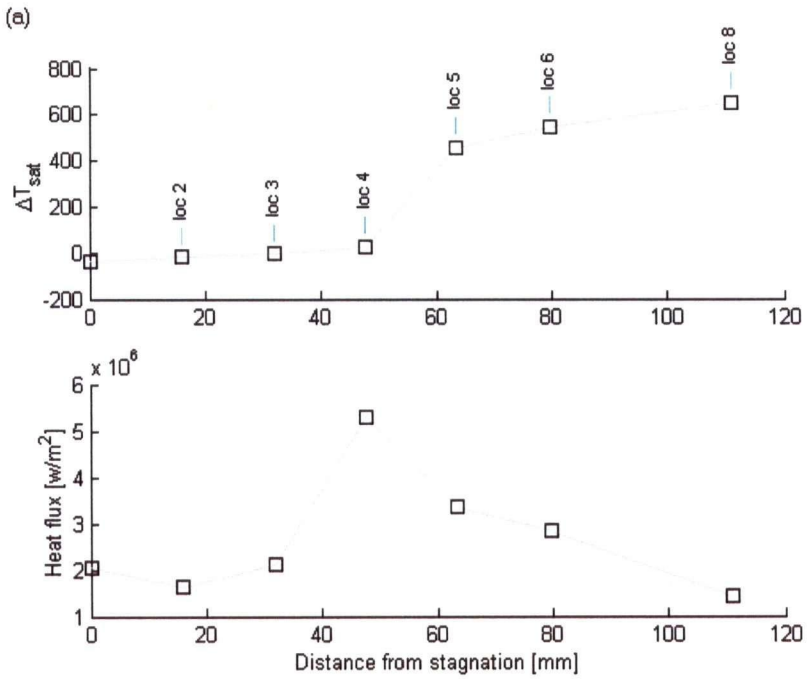

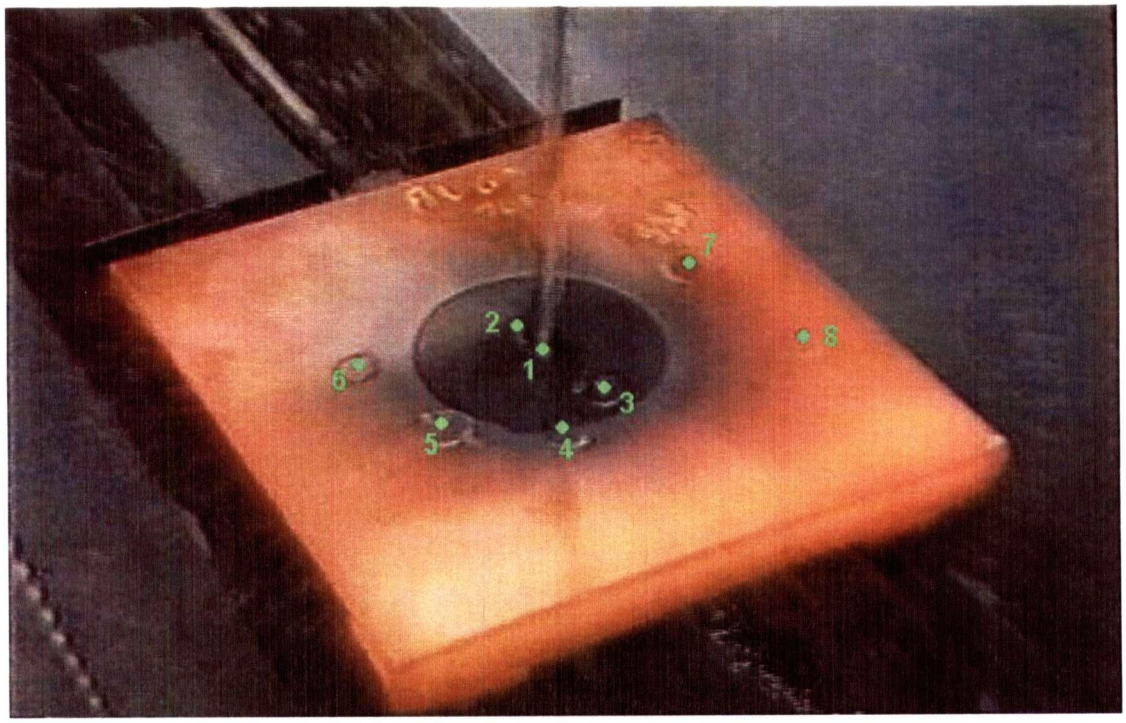

FIGURE 5-17 Conditions at 6.10 seconds from start of impingement. (a) Temperature and heat flux at locations of measurement (b) test plate at time 6.10 s. Test performed using a DQSK steel plate and flow rate and water temperature of 30 L/min and 30°C respectively (test #3)

5.5 EFFECT OF COOLING WATER TEMPERATURE

The temperature of the water jet was varied from 30°C to 50°C in the current research. In this section the effect of water temperature on heat flux at various locations on the test plates is shown and discussed.

On Figure 5-18 the maximum heat flux at all locations of measurement for a fixed flow rate of 30 l/min and varying water temperature is shown. Heat fluxes for both DQSK and SS316 plates are shown. The maximum heat flux is essentially the same at locations 1 and 2 but falls rapidly at location 3 in all tests shown. As discussed earlier the maximum heat flux is relatively constant at locations far away from stagnation.

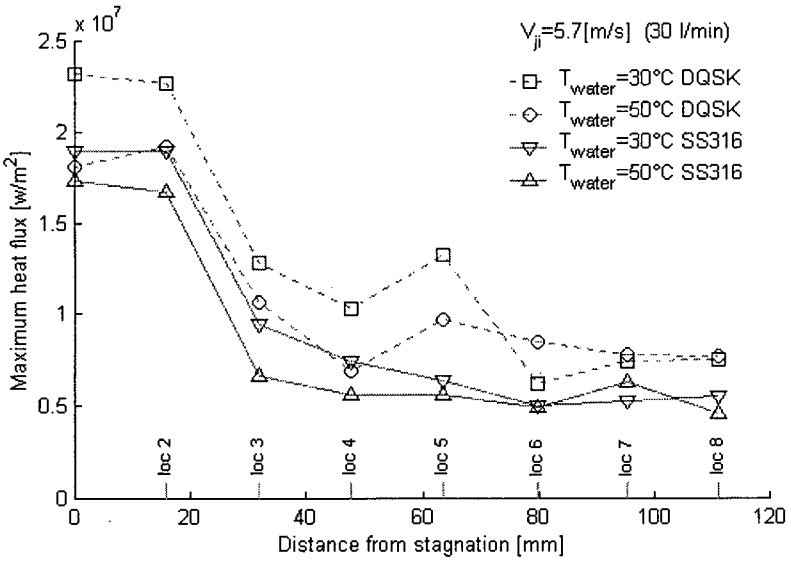

FIGURE 5-18 Maximum heat flux at all locations of measurement for SS316 and DQSK steels with varying water temperature and fixed flow rate.

The effect of cooling water temperature on the maximum heat flux is clear close to stagnation with higher heat flux when using lower water temperature. This effect decreases though as the distance from stagnation increases and the two curves finally converge. Same effects of varying water temperature were seen at other flow rates.

A considerable difference is between maximum heat fluxes for DQSK and SS316 test plates at virtually all locations. The DQSK steel experiences higher maximum heat flux than the SS316 steel at same cooling water temperature and flow rate. Possible causes for this difference include lack of accurate physical properties for the DQSK steel and different surface roughness as both steels were in the as-rolled condition but not polished to the same standard. It is beyond the scope of the current research to speculate further about possible causes for this difference.

On Figure 5-19 the times at which the maximum heat flux occurs at various locations is plotted for the same set of tests as are plotted in Figure 5-18. The slope of the lines on this graph is a measure of the velocity of the maximum heat flux front where a steeper line indicates a lower velocity. From this graph along with Figure 5-18 interesting things about the locations close to stagnation can be observed. The curves on Figure 5-19, for tests performed using 30°C cooling water temperature show, that the maximum heat flux at the first three locations occurs at virtually the same time. On the other hand the value of the maximum heat flux at locations 1 and 2 is approximately the same in all the tests but the heat flux at location 3 is considerably lower, see Figure 5-18. During visual observations of the tests, see Section 5.4, the initially gray area around stagnation could be seen to cover the first three locations almost instantly after the start of impingement. This indicates that outside the thermodynamic impingement zone, a zone of relatively constant heat flux around stagnation, there is another zone, second impingement zone, that is covered with liquid almost instantly after impingement but experiences a lower maximum heat flux. When cooling water temperature of 50°C was used the maximum heat flux at location 3 occurred a little later than at locations 1 and 2. This suggests that the cooling water temperature has an effect on the size of the second impingement zone. The effect of cooling water temperature on the size of the impingement zone itself, however, is not apparent from these results. The first two locations were within the impingement zone for all temperatures tested at a flow rate of 30 L/min and 45 L/min. The only exception to this was tests done on DQSK steel at 15 L/min, see discussion in the following section.

Another phenomenon seen in Figure 5-19 is that the velocity of the maximum heat flux front decreases as it progresses from stagnation towards the edge of the plate. This is consistent with what was seen during visual observations as well as the relatively steep drop in velocity around 80 mm from stagnation, at location 6. The velocity drop was associated with the sizes of the black and gray zones getting close to each other, see discussion in Section 5.4.

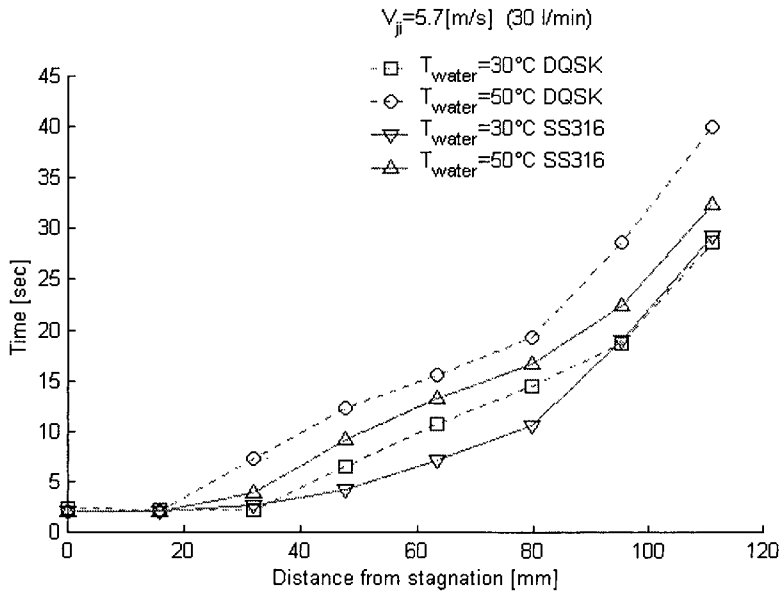

FIGURE 5-19 Time of maximum heat flux at various locations, fixed flow rate

Figure 5-20 shows boiling curves at stagnation for two tests using different water temperatures but same flow rate of 45 L/min. Both test were performed using SS316 steel plates. In the transition boiling region the two curves coincide but begin to separate around the point of critical heat flux. The critical heat flux is lower at higher water temperature, like seen in Figure 5-18 for a different set of tests.

For comparison correlations for nucleate boiling and the two regions of transition observed by Miyasaka et al. [16] are plotted on Figure 5-20. Line 1 is a correlation developed by Wolf et al. [14], Equation (9). This correlation correlated nucleate boiling data obtained by Wolf et al. using a rectangular nozzle and water temperature of 50°C. Line 2, Equation (21),

and line 3, Equation (22), are lines that correlated data presented by Miyasaka et al. [16] for pool boiling at ΔT_{sub} = 85°C. Miyasaka et al. found that the jet impingement boiling curve was an extension of the pool boiling curve, see Figure 2-8. The shape of the curves given by the correlations is in good agreement with the shape of the boiling curves obtained from the current data. The exact heat flux values given by the correlations are however not directly comparable with the data from the present study as test parameters are different.

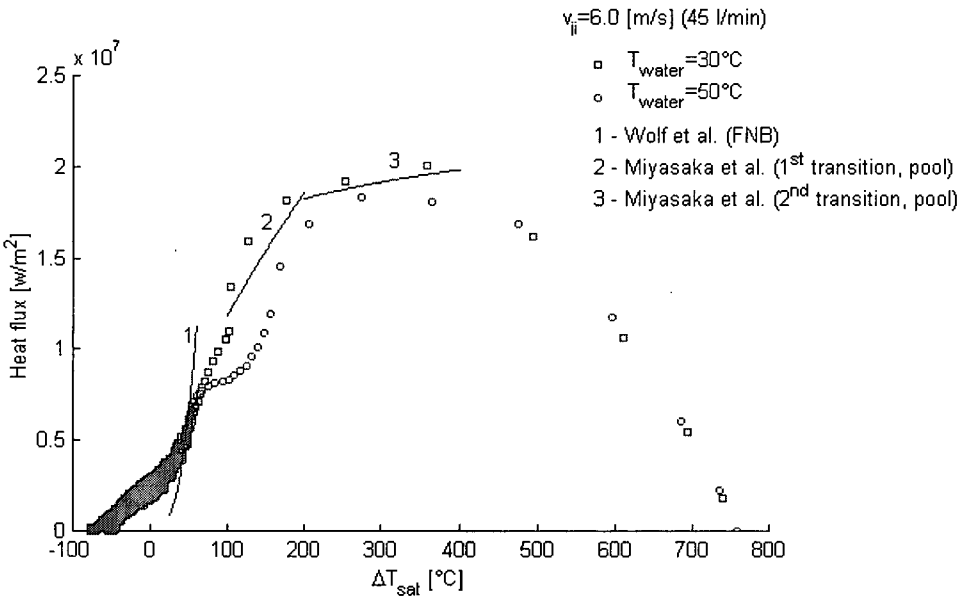

FIGURE 5-20 Boiling curves at stagnation, fixed flow rate and varying cooling water temperature, SS316 steel.

Boiling curves presented by Ishigai et al. [38], see Figure 2-5 and Figure 2-11, show their data for jet impingement boiling at stagnation. They used ΔT_{sub} as high as 55°C, comparable to the 50°C water temperature used here but lower jet velocities and higher initial surface temperature than used in the current study. The shoulder they saw in the transition boiling region was not seen in the current stagnation point data. However the overall shape of the curves at ΔT_{sub}=55°C seen in Figure 2-5 is similar to the current data. The exact values can not be compared as testing parameters are different. Comparison with boiling curves at stagnation presented by Ochi et al. [9], see Figure 2-9, yields similar findings. The shoulders seen there

are not seen in the current data and the exact values are not comparable as the jet velocity in the current study is considerably higher than used by Ochi et al..

Correlations for maximum heat flux found in literature were found to under predict the value of maximum heat flux considerably. The definition of critical heat flux used by Miyasaka et al. [16], see Equation (17) and discussion on page 19, differs from the common definition and is hence not comparable to current results. Ishigai et al. [19] presented a correlation for critical heat flux valid for the range of sub cooling and jet velocities used in the current research, Equation (20). The value of their correlation for a water temperature of 30°C and flow rate of 30 L/min under predicts the maximum heat flux values presented here by approximately 30% for DQSK steel and 20% for the SS316 steel. For flow rate and water temperature of 30 L/min and 50°C respectively the correlation under predicts the values by approximately 40% for DQSK steel and 20% for SS316.

No significant difference between the boiling curves in the transition boiling region at T_{water}=50°C and 30°C was seen in the current data. Data from both Ishigai et al. and Ochi et al. show on the other hand a significant increase in heat flux in the transition boiling region with increased sub cooling.

5.6 EFFECT OF WATER FLOW RATE

The cooling water flow rate was varied from 15 L/min to 45 L/min in the current study. In this section the effect of water flow rate on heat flux at various locations will be shown and discussed.

On Figure 5-21 the maximum heat flux at all locations of measurement for flow rates of 15 and 30 L/min is shown for a constant cooling water temperature of 30°C. Results for both DQSK and SS316 steel test plates are presented for comparison. Thermocouple at location 4 in the 15 L/min SS316 steel test did not work properly so the point will be ignored.

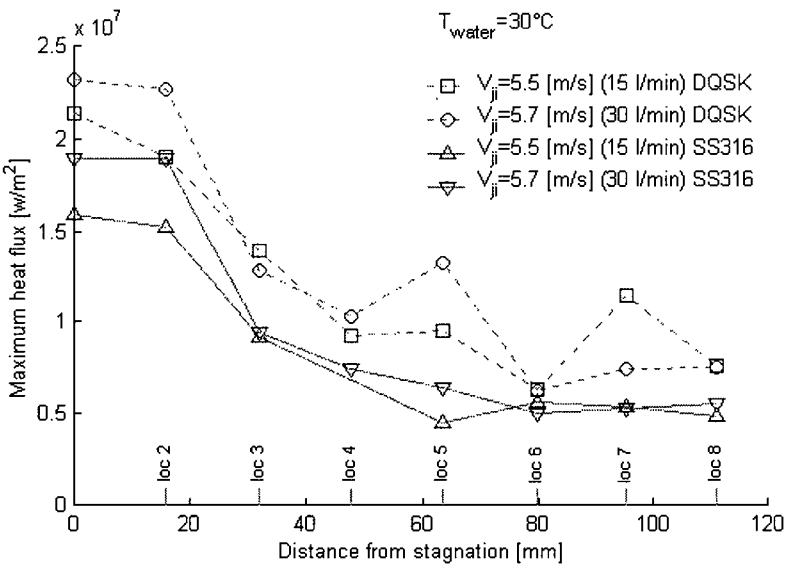

FIGURE 5-21 Maximum heat flux at all locations of measurement for SS316 and DQSK steels with varying flow rate and fixed water temperature.

Like shown earlier on Figure 5-18 the value of the maximum heat flux for the DQSK steel plates is higher than for the SS316 steel for the same test conditions. The curves for both steel types behave much in the same way. The heat flux at stagnation and location 2 is essentially the same for all the tests except for the lower flow rate, 15 L/min, on the DQSK steel plate. This drop of maximum heat flux at location 2 relative to location 1 was observed in all tests performed on DQSK steel at 15 L/min but was not observed to the same extent in test done on SS316 steel using the same test parameters. This indicates that the zone of constant heat flux, the thermodynamic impingement zone, is smaller for lower flow rates as well as smaller for DQSK steel than SS316 steel.

The effect of flow rate on the maximum heat flux is clear at the first two locations of measurement but at location 3 the effect is no longer seen. At locations 4 through 8 the effect of flow rate is not clear, the values are somewhat scattered, especially at the lower flow rate and for DQSK steel. Possible reason for this scattering of maximum heat flux values is that at low flow rate any surface imperfections, which are prone to be existent on a plate in the as

rolled condition, affect the flow more. When the flow is somehow affected the otherwise circular progression of the re-wetting front can become asymmetric and the velocity of the front, when it passes a point of measurement, can change.

On Figure 5-22 the times at which the maximum heat flux occurs at various locations is plotted for the same set of tests as are plotted in Figure 5-21. Like shown earlier on Figure 5-19 and discussed on page 84 the point of maximum heat flux for tests performed using 30°C water temperature and 30 L/min flow rate occurs virtually at the same time at the first three locations of measurement. At the lower flow rate of 15 L/min, however, this is not the case and the maximum heat flux at location 3 takes place a few seconds later. This indicates that the flow rate has an effect on the size of the previously discussed second impingement zone with its size decreasing with decreased flow rate, see page 84. An interesting point is that despite the fact that the 15 L/min DQSK steel tests had a drop in the value of maximum heat flux between locations 1 and 2 the point of maximum heat flux took place at the same time. This strongly suggests that location 2 was in the second impingement zone.

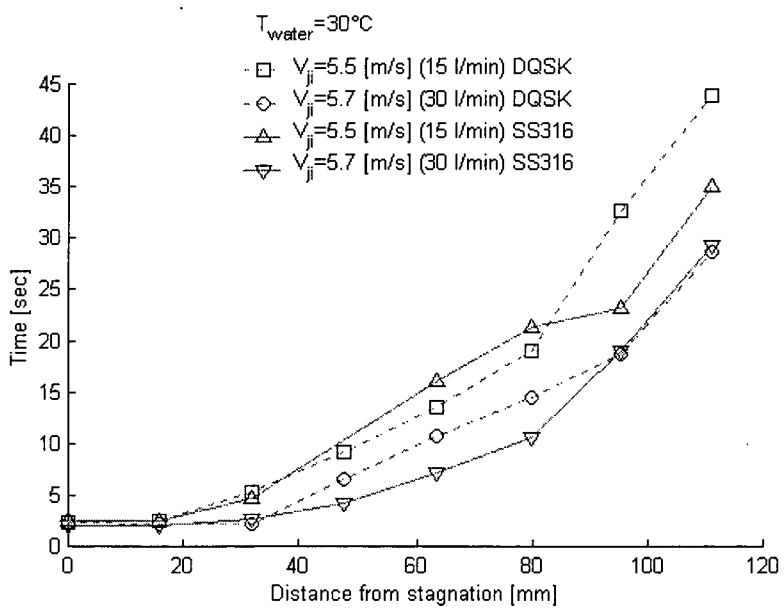

FIGURE 5-22 Time of maximum heat flux at various locations, fixed water temperature

As seen in Figure 5-19 the velocity of the maximum heat flux front decreases as it progresses from stagnation outwards. The drop in velocity at around 80 mm away from stagnation, as discussed on page 85, is also seen here with the exception of the 15 L/min SS316 steel test. There the maximum heat flux seems to take place later than expected at locations 5 and 6. This is likely due to some asymmetry in the progression of cooling as locations 5 and 6 are opposite to locations 7 and 8 on the plate, see Figure 3-4.

On Figure 5-23 boiling curves at stagnation for a fixed cooling water temperature of 50°C and various flow rates are plotted. The effect of flow rate is clear around the point of maximum heat flux with higher heat flux at a higher flow rate. This effect seems to be decreasing as the flow rate is increased but further investigation would be needed to verify that. In the beginning of the transition boiling region little or no effect of flow rate is seen and the same applies for the lower part of the nucleate boiling.

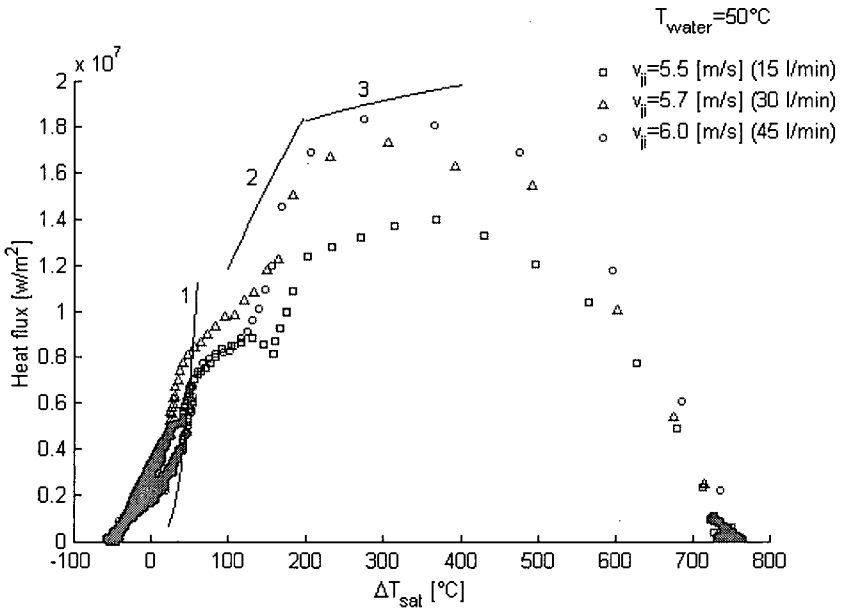

FIGURE 5-23 Boiling curves at stagnation along with some correlations. Varying flow rate and fixed temperature at 50°C. SS316 steel.

Lines 1, 2 and 3 are correlations for nucleate boiling and the first and second transition region and are the same as plotted on Figure 5-20 and discussed on page 85. The boiling

curves have a similar slope as the nucleate boiling correlation, line 1, over a narrow range of ΔT_{sat} much like what can be seen in Figure 5-20. The values of the correlations for the first and second transition regions, lines 1 and 2, are not directly comparable to the current data as test conditions are different. The shape of the curve follows the correlations quite well which indicates that the current data for jet impingement boiling at stagnation is an extension of the the pool boiling curve as observed by Miyasaka et al. [16].

6

CONCLUSIONS AND FUTURE WORK

An experimental procedure and novel method of instrumentation were developed to measure surface and internal temperatures of a steel plate being cooled with an impinging water jet. Intrinsic thermocouples with no time delay were used for direct temperature measurements on the surface and inside the test plates. The current method of measurement, based on direct measurement of surface temperature as well as temperature inside the plate, provides an improvement over the inverse heat conduction method commonly used in similar research. The systematic collection of data at stagnation and at various radial distances from stagnation gives a basis for ongoing research.

- First hand visual observations and video recordings were used to evaluate the symmetry of tests as well as to follow the cooling pattern on the test plates. Interesting observations include the fact that two re-wetting fronts are seen during cooling of the plate. As the plate is being cooled a gray circular zone, centered at stagnation, progresses outward. Inside the gray zone another black zone is progressing outward. Furthermore, a zone significantly larger than the impingement zone, was observed to turn gray almost instantly after initial impingement. At all points of measurement in this zone the maximum heat flux took place at the same time but the value of the maximum heat flux decreases significantly with increasing distance from stagnation.

- A numerical finite difference model, based on the Crank-Nicolson scheme, was used to calculate the the temperature gradient in the plate and hence the surface heat flux during the cooling process. The predictions from the model were found to fit experimental data well.

- Effect of varying the cooling water temperature in the range of 30°C to 50°C on heat transfer from the test plate was investigated. The effect on the maximum heat flux was clear close to stagnation with higher heat flux when using lower water temperature. This effect decreases as the distance from stagnation increases and is no longer seen at around 4 nozzle diameters from stagnation. Cooling water temperature was also found to affect the size of the instantly cooled zone around stagnation and the progression of the re-wetting front. The size of the instantly cooled zone decreased and the re-wetting front progressed slower with increased water temperature.

- Effect of flow rate in the range of 15 L/min to 45 L/min on heat transfer from the test plate was investigated. The effect on the maximum heat flux close to stagnation was significant but decreased rapidly and was no longer seen at a distance of approximately 1.5 nozzle diameters from stagnation. Similarly to cooling water temperature, flow rate was also found to affect the size of the instantly cooled zone around stagnation and progression of the re-wetting front. The size of the zone decreased and the progression of the front was slower at lower flow rates.

- The boiling curves were analyzed. It can be concluded that the boiling modes seen at stagnation are transition and nucleate boiling. At locations outside the impingement zone some evidence of film boiling were observed but primary boiling modes were transition and nucleate boiling. The point of maximum heat flux was observed to

shift to a lower wall superheat and lower heat flux value with increased distance from stagnation.

- Comparison with existing models shows that no models found in literature successfully correlate the current data. It also shows that a considerable variance is between the existing models and their use is restricted to specific conditions. A Chen type correlation for nucleate boiling at the stagnation point was developed. It correlated the current DQSK steel data well with an average error of less than 7.3% for wall superheat in the range of 8°C to 60°C.

6.1 RECOMMENDATIONS FOR FUTURE WORK

Research is ongoing in the field of jet impingement boiling heat transfer in relation to steel mill runout table applications. The results from the current research indicate that the boiling heat transfer behavior in runout table jet impingement is extremely complicated and that a number of factors can influence this behavior. Suggestions for future work include:

- Further testing needs to be done with increased number of measurements in the vicinity of the stagnation point to investigate the size of the instantly cooled zones around stagnation, i.e. the thermodynamic impingement zone and its surrounding second impingement zone. The size of the thermodynamic impingement zone is of great interest as it has a significant meaning in a practical application on a runout table. The second impingement zone is also of interest since it reaches its maximum heat flux at the same time as the impingement zone itself.

- Measurements of the actual jet diameter and jet velocity at impingement as well as changes in experimental setup to accurately locate the stagnation point need to be done. This would be very helpful in investigating the size of the impingement zone and its relation to jet diameter and velocity.

- Further testing using a wider range of water temperatures and flow rates could yield interesting findings about the boiling modes present. Data from those tests would, along with data gathered during the current research, create a good database for jet impingement cooling. The Chen type correlation developed for the current data indicates that a correlation of that form could be developed for a wider range of water temperatures and flow rates. A larger data base would also enable the development of correlations for the whole boiling curve that could be used as boundary conditions in finite element models that are currently under development.

- Testing performed with a plunging jet, i.e. with a layer of water flowing on top of the hot plate while cooling it with an impinging jet, needs to be performed. Effects of water layer thickness and velocity need to be investigated. This is of great importance in practical runout table applications as much of the steel strip is covered with water separated from the strip by a vapor layer.

REFERENCES

1. D.T. Blazevic: "Comparison of cooling methods: sprays, water curtains, laminar tubes and aspirated sprays", 35th MWSP Conf. Proc., Vol.XXXI, ISS-AIME, 1994, pp297-310
2. Z. Liu: "Experiments and mathematical modelling of controlled runout table cooling in a hot rolling mill", Ph.D. Thesis, MMAT, UBC, 2001
3. I.V. Samasakera, D.Q.Jin, J.K.Brimacombe: "Critical challenges in the prediction of mechanical properties of hot-rolled steel strip", THERMEC'97, TMS, 1997, (ed. By T. Chandra and T.Sakai), pp57-66
4. E.K.Kalinin, I.I.Berlin, V.V.Kostiouk: "Film boiling heat transfer", in Advances in heat transfer, Vol. 11, 1975, pp51-197
5. E.K.Kalinin, I.I.Berlin, V.V.Kostiouk: "Transition boiling heat transfer", in Advances in heat transfer, Vol. 18, 1987, pp241-323
6. D.H.Wolf, F.P.Incropera, R.Viskanta: "Jet impingement boiling", in Advances in heat transfer, Vol. 23, 1993, pp1-131
7. B.W.Webb, C.F.Ma: "Single-phase liquid jet impingement heat tranfer", in Advances in heat transfer, Vol. 26, 1995, pp105-217
8. X. Liu, V.J.H. Lienhard and J.S. Lombara: "Convective heat transfer by impingement of circular liquid jets", J. Heat Transfer, 113, 1991, pp571-582
9. T.Ochi, S.Nakanishi, M.Kaji and S.Ishigai: "Cooling of a hot plate with an impinging circular water jet", Muliphase Flow and Heat transfer III: Part A: Fundamentals, ed. By T.N.Veziroglu et al, Elsevier Science Publishers, B.V., Amsterdam, 1984, pp671-681
10. Y. Katto and M. Monde: "Study of mechanism of burn-out in a high heat flux boiling system with an impinging jet", Proc. 5th Int. Heat Transfer Conf., B6.2, 1974, pp245-249
11. M. Monde: "Burnout heat flux in saturated forced convection boiling with an impinging jet", Heat Transfer Japanese Res., 9(1), 1980, pp31-41
12. J.Stevens and B.W.Webb: "Local heat transfer coefficients under an axisymmetric, single-phase liquid jet", J. Heat Transfer, Vol 113, 1991, pp71-78
13. M. Monde and Y. Furukawa: "Critical heat flux in saturated forced convective boiling with an impinging jet coexistence of pool and forced convective boiling", Heat Transfer Japanese Res., 17(5), 1988, pp31-91
14. D.H.Wolf, F.P.Incropera and R.Viskanta: "Local jet impingement boiling heat transfer", Int. J. Heat and Mass Transfer, Vol 39, No. 7, 1996, pp105-1406
15. D.H.Wolf, R.Viskanta and F.P. Incorporeal: "Turbulence dissipation in a free-surface jet of water and its effect on local impingement heat transfer from a heated surface: Part 2 - local heat transfer", J. Heat Transfer, Vol 117, 1995, pp95-103

16.Y.Miyasaka, S.Inada and Y.Owase: "Critical heat flux and subcooled nucleate boiling in transient region between a two-dimensional water jet and a heater surface", Journal of Chemical Engineering of Japan, Vol. 13, No.1, 1980, pp29-28

17.Y. Katto and M. Kunihiro: "Study of the mechanism of burn-out in boiling system of high burn-out heat flux", Bull. JSME, 16, 1973, pp1357-1366

18.R.J. Copeland: "Boiling heat transfer to a water jet impinging on a flat surface", Ph.D. Thesis, Southern Methodist University, Dallas TX, 1970

19.S. Ishigai and M. Mizuno: "Boiling heat transfer with an impinging water jet (about the critical heat flux)", Preprint of JSME, No. 740-16, 1974, pp139-142

20.A.Sakurai and M.Shiotsu: "Temperature controlled pool boiling heat transfer", Proceedings of the 5th International Heat Transfer Conference, 1986, pp2031-2036

21.J.C.Chen, K.K.Hsu, "Heat transfer during liquid contact on a superheated surface", Proceedings of the pool and external flow boiling conference, ASME, 1992, pp257-261

22.J.G.Collier: Convective boiling and condensation, McGraw-Hill Book Company (UK) Limited, 1972, pp106-173

23.R.Viskanta, F.P.Incropera: "Quenching with liquid jet impingement", Heat and Mass Transfer in Materials Processing, Hokkaido, Japan, 28-31, Oct., 1990, Hemisphere Publishing Corporation (USA), 1992, pp455-476

24.J.Kokado, N.Hatta, H.Takuda, J.Harada, N.Yasuhira: "An analysis of film boiling phenomena of subcooled water spreading radially on a hot steel plate", Arch. Eisenhuttenwes (steel research), 55, Nr. 3, pp113-118, 1984

25.S.Lee, J.Lee and D.Lee: "Local heat transfer measurements from an elliptic jet impinging on a flat plate using liquid crystal", Int. J. Heat and Mass Transfer, 37-6, 1994, pp967-976

26.L.Huang and M.S.El-Genk: "Heat transfer of an impinging jet on a flat surface", Int. J. Heat and Mass Transfer, 37-13, 1994, pp1915-1923

27.C.Pan, J.Y.Hwang and T.L.Lin: "The mechanism of heat transfer in transition boiling", Int. J. Heat and Mass Transfer, 32-7, 1989, pp1357-1349

28.H.Fujimoto, H.Takuda, N.Hatta and R.Viskanta: "Numerical simulation of transient cooling of a hot solid by an impinging free surface jet", Numerical Heat Transfer, Part A, Vol. 36, 1999, pp767-780

29.J.Filipovic, R.Viskanta, F.P.Incropera and T.A.Veslocki: "Thermal behavior of a moving steel strip cooled by an array of planar water jets", Steel Research (Germany), vol. 63, no. 10, 1992, pp438-446

30.N.Hatta, Y.Tanaka, H.Takuda and J.Kokado: "A numerical study on cooling process of hot steel plates by a water curtain", ISJI International, Vol. 29, No. 8, 1989, pp673-679

31.N.Hatta and H.Osakabe: "Numerical modeling for cooling process of a moving hot plate by a laminar water curtain", ISJI International, Vol. 29, No. 11, 1989, pp919-925

32.K.Oliphant, B.W.Webb and M.Q.McQuay: "An experimental comparison of liquid jet array and spray impingement cooling in the non-boiling regime", Experimental Thermal and Fluid Science, Vol. 18, 1998, pp1-10

33.D.T.Vader, F.P.Incropera and R.Viskanta: "Local convective heat transfer from a heated surface to an impinging, planar jet of water", Int. J. Heat and Mass Transfer, 34-3, 1991, pp611-623

34.M.Monde, Y.Katto: "Burnout in a high heat flux boiling system with an impinging jet", Int. J. Heat and Mass Transfer, 21-3, 1978, pp295-305

35.S.Kumagai, S.Suzuki, Y.Sano and M.Kawazoe: "Transient Cooling of a Hot Metal Slap by an Impinging Jet with Boiling Heat Transfer", Proceedings of the ASME JSME Thermal Engineering Joint Conference 1995, Lahaina, Maui, Hawaii, March 19-24, 1995, Part 2, pp347-352

36.S.Olek, Y.Zvirin and E.Elias: "A simple correlation for the minimum film boiling temperature", J. Heat Transfer, Vol. 113, 1991, pp263-264

37.Z.Liu and J.Wang: "Study on film boiling heat transfer for water jet impingement on high temperature flat plate", Int. J. Heat and Mass Transfer, 44, 2001, pp2475-2481

38.S.Ishigai, S.Nakanishi and T.Ochi: "Boiling heat transfer for a plane water jet impinging on a hot surface", Heat Transfer - 1978, Hemisphere, Vol. 1, Washington DC, 1978, pp445-450

39.Z.Liu, D.Fraser and I.Samarasekera: "Experimental study of boiling heat transfer of steel plates during runout table operation in a hot strip mill", Proceedings of NHTC'01, 36th National Heat Transfer Conference, Anaheim, California, june 10-12, 2001

40.S.G.Kandlikar, M.Shoji and V.K.Dhir: Handbook of phase change: boiling and condensation, Taylor & Francis (USA), 1999, pp167-196

41.Y.Pan and B.W.Webb: "Heat transfer characteristics of arrays of free-surface liquid jets", J. Heat Transfer, Vol. 117, 1995, pp878-883

42.M.S.Loveday, M.F.Day and B.F.Dyson: Measurement of high temperature mechanical properties of materials, Her Majesty's stationary office (UK), 1982, pp58-82

43.J.Crank and P.Nicolson: "A practical method for numerical evaluation of solutions of partial differential equations of the heat conduction type", Proceedings of the Cambridge Philosophical society, England, 43, 1947, pp50-67

44.J.Filipovic, R.Viskanta, F.P.Incropera and T.A.Velocki: "Thermal behaviour of a moving steel strip cooled by an array of planar water jets", Steel Research (Germany), vol. 63, no. 10, 1992, pp438-446

45.H.E.Boyer and T.L.Gall: Metals handbook desk edition, American society of metals, 1995

46.C.Y.Ho and T.K.Chu: "Cindas report", AISI, september 1977

47.D.A.Zumbrunnen, R.Viskanta and F.P. Incropera: "The effect of surface motion on forced convective film boiling heat transfer", J. Heat Transfer, Vol 111, 1989, pp760-766

48.J.J.Xu, K. Adham-Khodaparast and M. Kawaji: "Study of transition boiling heat transfer in quenching of flat surface using surface temperature and heat flux microsensors", Proceedings of Convective flow boiling, USA, 1995, pp237-242